ECOLE
POLYTECHNIQUE
DE BRUXELLES

ULB

UNIVERSITÉ LIBRE DE BRUXELLES, UNIVERSITÉ D'EUROPE

Experimental study of the influence of an electric field on the shape of a droplet

Mémoire présenté en vue de l'obtention du diplôme
d'Ingénieur Industriel

Núria Romero Herreros

Directeur
Pierre Colinet

Co-promoteur
Pierre Lambert

Superviseur
Sam Dehaeck

Service
Transferts, Interfaces et Procédés (TIPs) – Fluid Physics Unit

Année académique
2014-2015

Contents

Acknowledgements **3**

Abstract **4**

List of Figures **7**

Introduction **9**

Chapter I: Literature review **11**

1.1. Electrowetting configuration 11

1.1.1. Wetting fundamentals 11

1.1.2. Theoretical background of electrowetting 12

1.1.3. Material properties 17

1.1.4. Contact Angle 21

1.1.5. AC and DC electrowetting 24

1.1.6. Applications of electrowetting 28

1.2. Taylor cone configuration 32

1.2.1. External electric field review 32

1.2.2. Applications of Taylor cone 35

1.3. Objectives of the present work 37

Chapter II: Experimental Methods and Materials **38**

2.1. Two ways to establish the electric field 38

2.1.1. Features of the Electrowetting configuration 39

2.1.2. Design of the Taylor cone configuration 40

2.2. Liquid: HFE-7500 47

2.3. Digital interferometry methodology 47

Chapter III: Experimental results on Electrowetting configuration **50**

3.1. Experiment I: Comparison between three different cases 50

3.1.1. Analysis of Contact Angle 50

3.1.2. Analysis of Evaporation Rate 53

3.2. Experiment II: Electric Field On and Off on the same drop 53

3.2.1. Small Drop 53

3.2.2. Large Drop 56

3.3. Experiment III: Frequency dependence 59

3.4. Experiment IV: DC voltage 63

3.5. Conclusions 65

Chapter IV: Experimental results on Taylor cone configuration 66

4.1. Experiment I: HFE-7500 – Two parallel plates 66

4.2. Experiment II: Water – Two parallel plates 67

4.2.1. Water Drop – 13000 V 67

4.2.2. Water Drop – 14000 V 68

4.3. Experiment III: HFE-7500 – Metal Ring 69

4.4. Experiment IV: HFE-7500 – Needle 71

4.5. Conclusions 73

Chapter V: Conclusions and Outlook 75

Appendices 77

A. Processing 77

B. Radius as a function of Time (*2.1.1. Experiment I: Comparison between three different cases*) 78

C. Volume as a function of Time (*2.1.2. Experiment II: Electric Field On and Off on the same drop*) 78

D. Blurred images (*2.1.3. Experiment III: AC frequency dependence*) 79

E. Contact angle results (*2.1.3. Experiment III: AC frequency dependence*) 79

F. Design – Parallel plates (*2.2.2. Parallel discs design*) 80

G. Electric field – Conductive droplets[153] 82

Bibliography 83

Acknowledgements

I would first like to express my gratitude to my promoters, Professors Pierre Colinet and Pierre Lambert for giving me the opportunity to study at the ULB and for their guidance in obtaining my Master's Thesis.

Also, I would like to thank my advisor, Dr. Sam Dehaeck, who helped me and spent countless hours assisting me in this research, both in theoretical and experimental work. His effort in support of this thesis is testament to his true dedication to his students.

My sincere appreciation goes to Dr Massimo Mastrangeli and Hervé Baudine who helped me with the design and setup of the experimentation.

My thanks go also to my family, especially to my brother Alberto, for his support and encouragement.

Finally, I would like to thank Astrid and Jonas for helping me with the translations and also thanks to Júlia, for sharing with me this unforgettable experience in Brussels.

Abstract

English

The electrowetting effect has emerged as an important research topic in recent years. Manipulation of droplets by electric fields has been extensively studied employing different setups, the most common being the configuration in which the electric field is created inside the droplet. However, such a configuration has been mostly employed using conductive liquids, whereas non-conductive droplets have been barely tested under the effect of an electric field using this setup. On the other hand, the influence of an electric field on the shape of a droplet has also been of considerable interest using an alternative configuration in which the electric field is applied between two electrodes with no contact with the drop – the Taylor cone configuration. However, the effects observed employing this last setup are rather different to those obtained using the aforementioned design. While the most important effect in those experiments in which the electric field is created inside the drop is the reduction of the contact angle, the main effect found using the second configuration is the droplet elongation in the electric field direction. In order to demonstrate if dielectric and almost perfectly wetting liquid droplets are affected in the same way as other fluids already tested, the effect of an electric field on the shape of an HFE-7500 droplet has been examined under two different experimental setups by means of interferometric techniques.

For the setup where the internal electric field is created, no statistically relevant reduction was measured. Nevertheless, shape deviations have been found at a certain distance of the wire through which the electric field is applied. Moreover, the existence of such deviations depends strongly on the AC frequency.

Regarding the second design, it should be mentioned that the initial parallel plate design was working correctly for water+salt droplets. However, no remarkable effects were observed applying strong electric fields of up to 10 kV/cm on HFE-7500 droplets. With the goal of increasing the field strength, two improvised configurations of a metal ring and a needle as a counter-electrodes have also been implemented. In these cases, a strong non-uniform electric field was created which did lead to shape changes of the droplets.

Nederlands

Het electrowetting effect is de voorbije jaren een belangrijk research onderwerp geworden. De manipulatie van druppels onder elektrische controle is uitgebreid onderzocht geweest onder verschillende opstellingen, waarbij de meest gebruikelijke deze is waarbij het elektrische veld gecreëerd wordt binnenin de druppel. Bij deze opstelling wordt er echter meestal gebruik gemaakt van geleidende vloeistoffen, maar niet-geleidende druppels zijn zelden getest onder het effect van een elektrisch veld met deze opstelling. Aan de andere kant is de invloed van een elektrisch veld op de vorm van een druppel van aanzienlijk belang. Hiervoor wordt gebruik gemaakt van een alternatieve configuratie waarbij het elektrische veld wordt toegepast tussen twee elektroden zonder contact met de druppel – de Taylor kegel configuratie. De effecten die met deze opstelling worden geobserveerd zijn tamelijk verschillend van deze van de eerder genoemde opstelling. Terwijl het belangrijkste effect in de experimenten waarin het elektrisch veld gecreëerd wordt in de druppel de verkleining van de contacthoek is, is het voornaamste effect in de tweede configuratie de verlenging van de druppel in de richting van het elektrisch veld. Om aan te tonen of diëlectrische en bijna perfect bevochtigde vloeibare druppels op dezelfde manier veranderen als andere vloeistoffen die al getest zijn, is het effect van een elektrisch veld op de vorm van een HFE-7500 druppel getest onder deze twee verschillende experimentele opstellingen met interferometrie-technieken.

Voor de eerste opstelling werd de contacthoek niet significant verkleind. Wel werden er vormveranderingen vastgesteld op een zekere afstand van de draad waardoor het elektrische veld werd gecreëerd. Het bestaan van zulke afwijkingen hangt sterk af van de AC frequentie.

Voor de tweede opstelling dient opgemerkt te worden dat de initiële opzet met parallelle plaat correct werkte voor water + zout druppels. Er werden echter geen noemenswaardige effecten vastgesteld wanneer sterke elektrische velden tot 10kV/cm werden getest op de HFE-7500 druppels. Met als doel de veldsterkte te vergroten, werden twee geïmproviseerde configuraties geïmplementeerd met een metalen ring and een naald als tegenelektroden. In deze opstellingen werd een sterk non-uniform electrisch veld gecreëerd die wel leidde to vormveranderingen van de druppels.

Français

L'effet électromouillage a donné lieu à de nombreuses recherches ces dernières années. La manipulation de gouttes sous contrôle électrique a été rigoureusement étudiée par divers moyens, le plus répandu étant la configuration dans laquelle le champ électrique a été créé à l'intérieur de la goutte. Cependant, cette configuration a surtout été employée en utilisant des liquides conducteurs, alors qu'il n'y a que rarement eu des expérimentations dans cette configuration avec des gouttes non-conductrices sous un champ électrique. D'autre part, l'influence d'un champ électrique sur la forme de la goutte a aussi fait l'objet de nombreuses études où on utilise une configuration alternative avec un champ électrique appliqué entre deux électrodes sans contact avec la goutte (configuration Taylor Cone). Cependant, les effets observés durant cette expérimentation sont de nature différente de ceux observés dans l'expérimentation mentionnée précédemment. Ainsi, dans le premier type d'expérimentation où le champ électrique est créé à l'intérieur de la goutte, l'effet obtenu est la réduction de l'angle de contact, alors que dans le second type d'expérimentation, on observe une dilatation de la goutte dans le sens du champ électrique. Dans l'optique de voir si les gouttes liquides diélectriques réagissent de la même façon que d'autres liquides déjà testés, l'effet d'un champ électrique sur la forme d'une goutte HFE-7500 a été examiné dans deux expérimentations à l'aide de techniques d'interférométrie digitale.

Dans la première configuration, l'angle de contact HFE-7500 n'a pas été réduit de manière statistiquement signifiante suite à l'application d'une tension électrique de 300 V. Pourtant, on a observé des déviations de forme à une certaine distance du câble par lequel on a appliqué la tension électrique. De plus, notons que l'existence de telles déviations dépend fortement de la fréquence AC.

En ce qui concerne la seconde expérimentation, mentionnons que le montage initial fonctionnait correctement pour des gouttes formées d'eau et de sel. Cependant, aucun effet remarquable n'a été observé suite à l'application de forts champs électriques allant jusqu'à 10 kV/cm sur des gouttes HFE-7500. Dans l'optique d'accroître la tension du champ, deux expérimentations improvisées avec un anneau métallique et une épingle agissant comme électrode ont aussi été mises en place. Ceci a créé des champs non-uniformes forts qui ont été capable de déformer la goutte.

List of Figures

Fig. 1: Schematic of two different ways to establish the electric field.....9

Fig. 2: Sketch of a drop deposited on a solid substrate in equilibrium.....11

Fig. 3: Shape of a droplet placed on hydrophobic or hydrophilic surfaces.....12

Fig. 4: Sketch of a Lippmann-type capillary electrometer, taken from J. Lyklema[1].....13

Fig. 5: Schematic EWOD setup. Solid line: zero voltage. Dashed line: finite voltage.....14

Fig. 6: Lippmann-Young relation between contact angle and applied.....15

Fig. 7: Hydrophobic layer is placed on top, in contact with the drop and the insulating layer.19

Fig. 8: Contact angle of a 10^{-4}M KNO_3 solution as a function of the applied potential.....20

Fig. 9: A sketch of a droplet on a window that illustrates the hysteresis phenomenon.....21

Fig. 10: Schematic of the contact angle hysteresis - electrowetting experimental setup.....22

Fig. 11: Plot that shows the saturation effect.....23

Fig. 12: Equivalent circuit which represents the AC electrowetting behaviour.....25

Fig. 13: Contact angle dependence on the rms voltage.....26

Fig. 14: (a) Flow patterns at low (b) between low and high and (c) high frequency.....27

Fig. 15: Patterns of drop oscillation at 60 V for different frequencies (Oh et al.[2]).....27

Fig. 16: Images that that prove what EW based fluid lens are capable.....29

Fig. 17: Proof of electrowetting on various flexible substrates.....30

Fig. 18: EW array on a flexible plastic substrate (Taken from Steckl et al.[3]).....30

Fig. 19: (A) Top and (B) side views of a typical lab-on-a-chip setup.....31

Fig. 20: Water droplet deformed by the electric field using the second setup.....32

Fig. 21: Electrospray schematic depicting the Taylor cone.....33

Fig. 22: Electrospinning representation from Ref. Li et al[4].....35

Fig. 23: Electrospray picture taken from www.newobjective.com.....36

Fig. 24: Schematic of two different ways to establish the electric field.....38

Fig. 25: Glass plate covered with ITO and Parylene-C placed on his protective case.....38

Fig. 26: Pictures of the first (A) and second setup (B).....39

Fig. 27: Schematic representing the electrowetting experimental setup.....40

Fig. 28: Second setup design (Solid Works).....42

Fig. 29: Breakdown voltage of Parylene C and N vs Polymer film thickness.....43

Fig. 30: (A) Schematic of a simplication of the second setup and its (B) Equivalent circuit.....43

Fig. 31: Side view of the Mach – Zehnder interferometer, Taken from Tsoumpas[5]……48

Fig. 32: (A) Fringe pattern for an HFE-7500 droplet and its (B) local slope map ……49

Fig. 33: Interferogram (A) Case A, (B) Case B and (C) Case C……51

Fig. 34: Apparent contact angle versus radius for A (EF), B (No EF) and C (No needle)……52

Fig. 35: Evaporation rate versus radius for A (EF), B (No EF) and C (No needle)……53

Fig. 36: Fringe patterns (A) Off, (A) first image On, (C) after several images we detect On……54

Fig. 37: Apparent contact angle versus time for a small HFE-7500 drop……55

Fig. 38: Histogram of all the contact angles values obtained along the periphery……55

Fig. 39: Height and local angle profiles regarding two different states: On and Off……56

Fig. 40: Fringe pattern obtained when (A) no voltage is applied and (B) the electric field is applied……57

Fig. 41: Apparent contact angle as a function of time for a small HFE-7500 droplet……57

Fig. 42: Histogram of all the contact angles values obtained along the periphery……58

Fig. 43: Height and local angle profiles regarding two different states: On and Off……58

Fig. 44: Apparent contact angle versus radius for different frequencies……60

Fig. 45: Height profiles for different frequencies……60

Fig. 46: Local angle profiles for different frequencies……61

Fig. 47: Height and local angle profiles regarding two different states: On and Off……62

Fig. 48: (A) Contact angle for different DC voltages. (B) Evaporation rate as a function of radius……64

Fig. 49: Height and local angle profile for different DC voltages……64

Fig. 50: Picture of the upper plate after its breakdown……67

Fig. 51: Water droplet fringes……68

Fig. 52: Height and Local angle profiles sessile water drop……68

Fig. 53: Height and Local angle profiles sessile water drop……68

Fig. 54: Metal ring……69

Fig. 55: Metal ring configuration (A) side view and (B) upper view……69

Fig. 56: HFE-7500 droplet fringes using the ring setup variation……70

Fig. 57: Local angle of HFE-7500 droplets using the ring setup variation……70

Fig. 58: HFE-7500 droplet ejecting liquid in the field direction……71

Fig. 59: Needle configuration……72

Fig. 60: HFE-7500 droplet fringes using the needle setup variation……72

Fig. 61: Local angles of HFE-7500 using the needle setup variation……73

Introduction

The experimental study described in this paper is related to the so-called electrowetting effect. This is the effect where the apparent contact angle of liquid droplets is reduced upon application of an external voltage. There has been considerable interest in digital microfluidics and the different methods for liquid actuation by thermal, chemical and electrical means. Electric fields are extensively used as a tool to manipulate liquids on small scales for use in applications such as variable focus lenses, display technology, fiber optics and lab-on-a-chip devices.

In this report we will investigate the influence of an electric field on the shape of an HFE-7500 droplet. Liquids that belong to the Hydrofluoropolymer's (HFE) family are dielectric fluids in which dielectrophoretic and electrostrictive forces rule the phenomenon excluding free charge migration from the system. Although most of the available literature has focused on electrowetting using conductive liquids, recently several authors have been interested in non-conductive liquids as well. Usually, these reports have been based on liquids with relatively high contact angle. Unlike those latter liquids, HFE-7500 has a very low contact angle and therefore it will be proved if non-conductive and almost perfectly wetting liquid droplets are affected in the same way.

In order to achieve such goals, two different setups have been used with the aim to test the droplet under various configurations. Mainly, the effect of an electric field on the shape of a liquid droplet will be examined in two different setups which we will denote: Electrowetting and Taylor cone configurations.

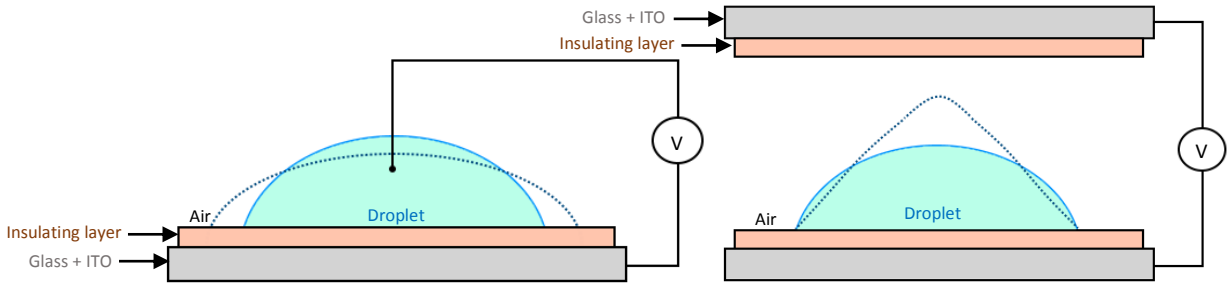

Figure 1 Schematic of two different ways to establish the electric field. The figure on the left shows how to establish the electric field inside the droplet and the one on the right represents the setup where the electric field is applied outside the drop.

The first experiments were carried out employing the conventional setup for electrowetting, in which the base material of the substrate was ITO-coated glass – ground electrode – and a very thin Parylene-C layer was deposited on the electrode surface as an insulating layer. On top of that, an HFE-7500 droplet was placed by means of a syringe onto the substrate and the positive electrode was a thin wire immersed into the liquid. An AC power supply was used in these first

experiments where the applied potential between the two electrodes was of 300 V. Using this configuration we expect a decrease of the contact angle with the application of the electric field.

In the second setup, the electric field was established between two parallel plate electrodes with the same characteristics described above, but in this case there was no drop-electrode contact – the droplet is deposited onto the bottom plate and the upper plate is placed at a certain distance. Here, a DC source was used. This setup, which is less common than the first one, requires high voltages that are in the range of several kV. In this configuration, we rather anticipate a so-called Taylor cone which refers to the behaviour of liquid droplets under strong electric fields where the drop elongates in the electric field direction and at a certain threshold voltage the tip starts to emit a jet of liquid. The whole experimental measurements are obtained by means of digital interferometry.

This thesis is divided into five main chapters. First of all, an overview from the basics to the most recent developments in electrowetting will be presented. Also, in this first section, the Taylor cone phenomenon is introduced as well as its main applications. In the end of this chapter the objectives of the present study are briefly summarized. Chapter 2 is devoted to the experimental methods and materials. In this section, we will present the two aforementioned setups and we will discuss their designs. Also, HFE-7500 properties and the digital interferometry methodology are introduced therein. Chapter 3 and 4 deals with the experimental results using the electrowetting and Taylor cone configurations respectively. Finally, in chapter 5 we will conclude our study and possible future investigations will be mentioned.

Chapter I: Literature review

1.1. Electrowetting configuration

This chapter will begin with an introduction of the fundamental science behind wetting and contact angle phenomena, followed by a description of the electrowetting effect from the basics to the most recent experiments. Different approaches have been proposed in order to explain the contact angle decrease caused by the electric field; a brief overview of them will be presented. In the following paragraph will be detailed the materials mainly used in electrowetting and which properties they must fulfil. Furthermore, a short introduction about the contact angle hysteresis and the contact angle saturation phenomenon will be described. The difference between using AC or DC voltage has also a considerable influence on electrowetting, for this reason, we will also present a summary of the recent observations about this topic. Lastly, since this phenomenon is used in a wide range of applications, some of them will be recapitulated in the last paragraph of this chapter.

1.1.1. Wetting fundamentals

The fundamental problem of wettability has been widely investigated together with its practical point of view as it plays an important role in industry (such as liquid coating processes[6], printing[7,8], 'lab-on-a-chip' devices for DNA and protein analysis[9–12], adaptive optical lenses[13–16] and electronic display technology[17–19]).

The term of wettability is used to describe the chemical-physical properties when a solid and liquid interact. When a liquid droplet is placed in contact with a solid surface, the drop spreads on the surface in order to minimize the free energy of the system[20]. The degree of wetting is usually characterized by the measurement of the contact angle (θ_Y) of the droplet[20,21].

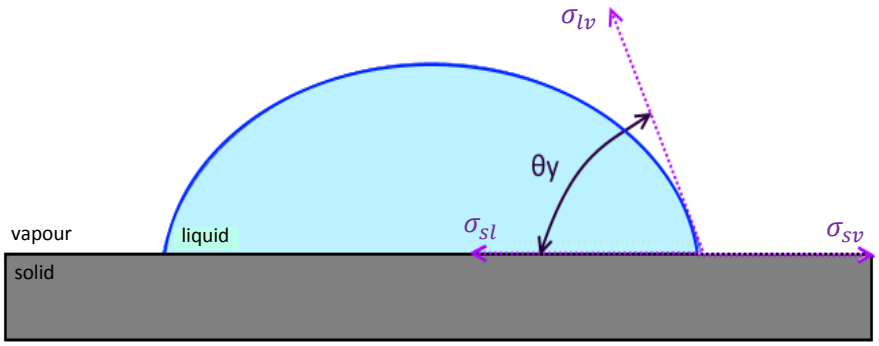

Figure 2 Sketch of a drop deposited on a solid substrate in equilibrium

In order to maintain the droplet in equilibrium with a certain contact angle, the three interfacial tensions operate together at the triple line. There are two necessary conditions that any equilibrium liquid morphology has to fulfil:

- *Laplace equation: Pressure difference across an interface of a certain curvature*[22]

$$\Delta p = \sigma_{lv} \cdot \left(\frac{1}{r_1} + \frac{1}{r_2}\right) = \sigma_{lv} \cdot K \quad (1)$$

Taking the vapour as the ambient phase, σ_{lv} is the solid-vapour interfacial energy, r_1 and r_2 are the two principal radii of curvature of the surface and K is the constant mean curvature.

- *Young's equation: Relation between the three interfacial tensions at a state of mechanical equilibrium*

$$\cos\theta_Y = \frac{\sigma_{sv} - \sigma_{sl}}{\sigma_{lv}} \quad (2)$$

Where θ_Y is the contact angle in equilibrium and σ_{sv},σ_{sl}, σ_{lv} are the three interfacial energies.

When $\sigma_{sv} = \sigma_{sl}$, the liquid and vapour have the same surface tension with the solid surface, thus $\theta_Y = 90°$. When the surface tension of the liquid-solid interface is lower, $\sigma_{sv} > \sigma_{sl}$, $\theta_Y > 90°$ and the inverse when the surface tension is larger. For water, a surface is called hydrophobic when $\theta_Y > 90°$ and hydrophilic when $\theta_Y < 90°$.

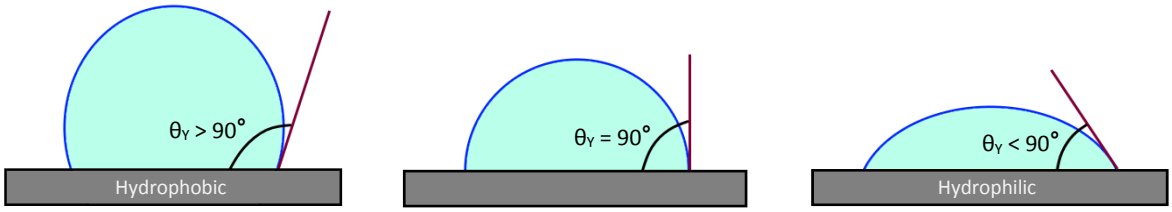

Figure 3 Shape of a droplet placed on hydrophobic or hydrophilic surfaces

Many chemical or physical methods have been developed to control the wettability of surfaces[21]. Lyophilic, superlyophilic, lyophobic and superlyophobic surfaces can be fabricated[23]; such surfaces maintain their wetting properties over some time, but the main disadvantage is their static nature, which prevents active control of liquids after being manufactured[20,21]. Although there was substantial improvement in these type of surfaces, the real-time actuation, the switching speed, the long term reliability and the compatibility with variable environments remain not suitable for most practical applications. Other approaches to control the contact angles have been developed, among them the electrostatic method is the most popular one as it has proven very successful in all these respects previously mentioned[21,24].

1.1.2. Theoretical background of electrowetting

Electrowetting is used to describe the electrically induced spreading of a liquid onto a solid and the observed contact angle reduction[25]. Contact angle of sessile droplets has been investigated under the influence of the electric field for a long time; the physicist Gabriel Lippmann, more

than one century ago, found that capillary forces can be controlled by external electrostatic forces[26]. In 1875, a detailed description of the basis of electrocapillarity (first foundations of electrowetting) was reported by Lippmann. His works using mercury in contact with aqueous electrolytes and applying a voltage between them, showed that we are able to control the contact angle of interfaces[21,26].

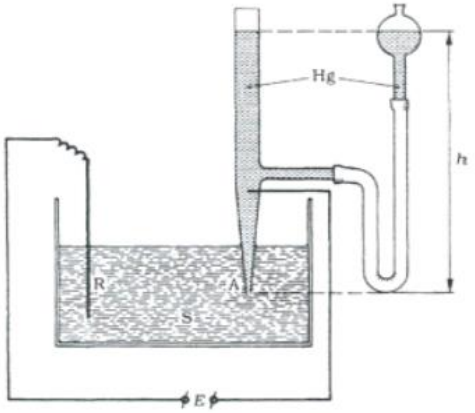

Figure 4 Sketch of a Lippmann-type capillary electrometer, taken from J. Lyklema[1]

The mercury-solution interface is situated in the slightly conical capillary *A* in which a certain height *h* is chosen at which the measurements are carried out. The potential is externally applied: in Lippmann's experiments the electrode was connected to the solution *S* via a salt bridge[1]. The interfacial tensions between mercury and the solution was obtained from the height *h*[1].

Upon applying an elementary electric field, an elementary potential difference builds up at the interface and an electric double layer forms in the liquid at the contact of the surface, which acts as a small capacitor.

Similar works of those who followed Lippmann, as also had been stated by himself before, found that the surface tension decreased by applying an electric field and in consequence the decrease of the contact angle due to this change of interfacial energy[20].

- *Lippmann's equation: Decrease in surface tension with applied potential related to the charge accumulated at the interface*

$$\sigma_{sl}(\phi) = \sigma_{sl}(0) - \frac{1}{2}C\phi^2 \qquad (3)$$

Where C is the capacitance and ϕ is the potential at the interface, i.e. the potential difference ϕ = U - U_{pzc} (U → Potential applied, U_{pzc} → Potential of Zero Charge, the voltage required to

[1] In electrochemistry, a salt bridge is a laboratory device that allows to maintain electrical neutrality within the internal circuit. If no salt bridge were present, the solution in one half cell would accumulate negative charge and the solution in other half cell would accumulate positive charge as the reaction proceeded.

compensate for a spontaneous charging that is created when a material like mercury is immersed into electrolyte solutions)[20].

Electrowetting has been studied by researchers from various fields, consequently different approaches have been used to describe this phenomenon.

- *Thermodynamic and electrochemical approach*

The classical Lippmann's experiments were performed directly in mercury surfaces. In most recent experiments of electrowetting the liquid is separated from the electrode by an insulating layer due to the electrolytic decomposition of water upon applying voltages beyond a few hundred millivolts. The use of this dielectric film was initiated by Berge (early 1990s)[27] in order to eliminate the problem of electrolysis. Moreover, insulators guard working fluids from electrodes and allow a much higher applied electric field (i.e stronger electrowetting effect), before an electrical leakage or breakdown[25]. This configuration is known as electrowetting on dielectric (EWOD).

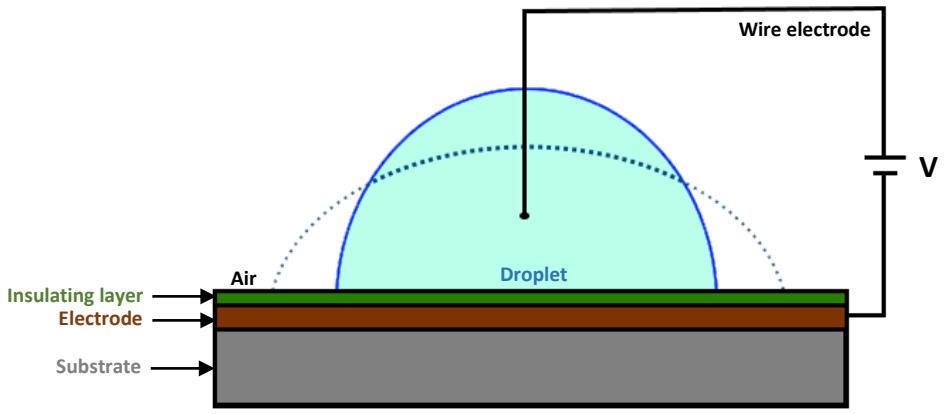

Figure 5 Schematic EWOD setup. Solid line: zero voltage. Dashed line: finite voltage.

Following first the original Lippmann's tests, contact angle for an electrolyte droplet deposited directly on an electrode surface (Lippmann-Young's equation) is determined by the expression[20]:

$$\cos\theta = \cos\theta_Y + \frac{\varepsilon_0 \cdot \varepsilon_1}{2 \cdot d_H \cdot \sigma_{lv}} \cdot \left(U - U_{pzc}\right)^2 \qquad (4)$$

Where θ is the contact angle that results after applying the electric field, ε_1 is the dielectric constant of the liquid, d_H the distance from the surface where the counter-ions (charges created on the liquid side of interface) are located, U_{pzc}[20] is the potential of zero charge and U is the voltage applied.

As mentioned already, the EWOD configuration has more practical applications nowadays. In the case of dielectric coatings thicker than 0.1 μm, the capacitance is mainly determined by the

capacitance of the insulator film. Thus, the total capacitance is only dependent on the thickness of the coating and its dielectric constant[28].

Therefore, contact angle for an electrolyte droplet deposited on a dielectric film underlying the electrode surface (Lippmann-Young's law for EWOD) is formulated as[20]:

$$\cos\theta = \cos\theta_Y + \frac{\varepsilon_0 \cdot \varepsilon_d}{2 \cdot d \cdot \sigma_{lv}} \cdot U^2 = \cos\theta_Y + \eta \qquad (5)$$

Where ε_d is the dielectric constant of the insulator film and d is the insulator thickness. The dimensionless electrowetting number, η, measures the strength of the electrostatic energy compared to surface tension[20]. The potential at no charge, U_{pzc}, has been neglected assuming that the insulating layer does not give rise to spontaneous adsorption of charge.

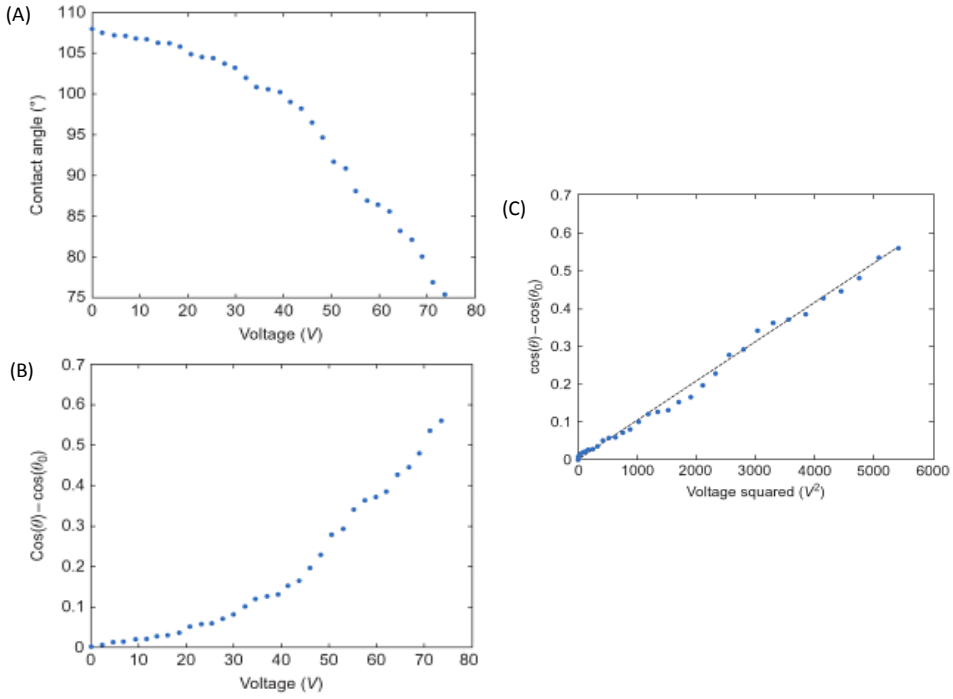

Figure 6 Lippmann-Young relation between contact angle and applied voltage (From Ref. O. Raccurt[30], CEA/LETI). (A) Contact Angle versus Voltage, (B) cos θ − cos θ$_Y$ versus Voltage, (C) Linear dependency between cos θ − cos θ$_Y$ and V².

After applying a certain voltage, the contact angle will decrease to reach a new equilibrium value as Lippmann claimed. It has been verified, for small to medium voltages, that the relation between the contact angle and the applied voltage follows indeed the Lippmann-Young's law. The plot of *Figure 6 (B)* shows the quadratic dependency of $\cos\theta - \cos\theta_Y$ versus the voltage U; if we plot $\cos\theta - \cos\theta_Y$ versus U^2, the curve is well fit by a straight line, according to Lippmann-Young's equation (see *Figure 6 (C)*)[29,30].

- *Energy minimization approach*

The electrowetting equation can be derived simultaneously by minimizing the surface energies and the electrostatic energy, leading directly to Lippmann-Young's equation. This method, first derived by Berge[27], considers that the free energy of a droplet contains both interfacial and electrostatic components (for further explanation see indeed[20,29]).

This interpretation, like the thermodynamic approach, does not provide a physical picture of how the contact angle is reduced in mechanical terms. When electrowetting dynamics needs to be scrutinized, the actual force at the contact line must be captured and the energy minimization approach cannot be used[29].

- *Electromechanical approach*

Considering the forces exerted on the liquid by the electric field, as Jones *et al*. proposed[31,32], the reduction of the contact angle can be explained by the forces near the contact line. In the case of simple liquids, one of the most widely accepted formulations is the Korteweg-Helmholtz body force density[33]:

$$\vec{f_k} = \sigma_f \vec{E} - \frac{\varepsilon_0}{2} E^2 \nabla \varepsilon_f + \nabla \left[\frac{\varepsilon_0}{2} E^2 \frac{\partial \varepsilon_f}{\partial \rho} \rho \right] \quad (6)$$

Where σ_f is the electric charges, ε_f is the permittivity of the liquid and ρ is the mass density of the liquid. The first term represents the body force due to the interaction of the free charges in the fluid with the electric field. The second term encompass dielectrophoresis[31], and the third term describes electrostriction. The last one usually can be neglected as the mass density of the liquid remains constant. By a volume integration over the equation formulated above (neglecting the electrostriction), we can obtain the net force acting on a volume element of the fluid.

The later experimental observations and theoretical studies show electromechanical model is more accurate than the thermodynamic interpretation. Several authors claim that contact angle change is only apparent; at scales of the order of dielectric thickness (d), contact angle is unchanged by applying voltage. Most recently, Mugele and Buehrle[34] observed that the microscopic contact angle remains at Young's angle and the interfacial tensions do not actually change with voltage. These aspects were confirmed by their experiments. Despite the remarkable difference between the apparent contact angle and the local one at the contact line, the calculations would be incorrect only within a very small region; therefore, the models that have been described before the electromechanical approach are sufficient as long as the phenomena of interest occur on a length scale larger than d[20,34].

1.1.3. Material properties

1.1.3.1. Liquid properties

The liquids used typically in electrowetting are aqueous salt solutions and they are treated as perfect conductors. For these electrolyte solutions the conductivity depends on either the salt concentration or frequency. As will be shown below, at low frequency (f<1kHz), even demineralized water shows substantial decrease in the contact angle[35,36]. Kumar *et al*.[37] determined by varying the conductivity and the frequency of the applied AC voltage, the range of the validity of the perfect conductor assumption. They found that the contact angle decrease is dramatically reduced at high frequency and low salt concentration due to Ohmic losses with the liquid.

Although water still remains the most extensively and commonly studied electrowetting liquid, there are some reports with alternate fluids. To give just one example, Chevalliot *et al*.[38] selected some fluids such as acetonyl acetone, propylene glycol or diacetone alcohol, among others.

1.1.3.1.1. Influence of the electric field in conducting and non-conducting liquid drops

Different experiments have been conducted by several researchers over the years in order to improve the physical understanding of this phenomenon. In so doing, a wide range of liquids have also been used. An overview about the use of conducting and non-conducting liquids will be shown below.

The study of the action of an electric field on a sessile drop have been studied by numerous researchers as we have been seeing throughout this study. Bateni et al.[39] studied the equilibrium of a droplet under the action of an electric field. This study, however, was limited to the case of a conducting fluid, where Coulombic forces are dominant. Most recently, Di Marco and co-workers[40] presented a study that concerns ethanol – dielectric polar fluid with high relative electric permittivity - as insulating liquid, in which dielectrophoretic and electrostrictive forces rule the phenomenon and exclude free charge migration from the system. Both works have been studied the effect on contact angle when the electric field is established outside the droplet (between two parallel plates), which is not as commonly used as the configuration where the electric field is established inside the droplet.

Electrowetting has been extensively studied as a tool to actuate and control conducting droplets. On the other hand, electrical actuation of insulating liquids has been also explored using other configurations. Many industries are based on electrospinning and electrospraying[2] which use dielectric fluids. Dielectric liquids are also found in Dielectrophoresis (DEP), which is a phenomenon where an electrical force is exerted on a dielectric particle when it is subjected

[2] Such effects will be presented in paragraph 1.2.2.

to a non-uniform electric field. However, the classical analyses of the electrowetting are based on the premise of the droplet being a perfect electrical conductor, as we have already seen before. Nevertheless, experimentation has shown that even low electrical conducting liquids and even perfectly insulating liquids can be actuated by electrical means. Microelectronics applications which involve direct contact of the liquid with an electronic component necessarily require the use of electrically insulating liquids. Also, insulating liquids are typically much less corrosive than the electrically conducting alternatives[41].

Many of the liquids used by Chatterjee et al.[42], such as organic solvents or surfactant solutions, had very low electrical conductivities and therefore cannot be considered perfectly conducting fluids.

The actuation forces on conducting and dielectric droplets have a common electromechanical origin[43] and the principle of energy minimization can be used in order to analysed it. This means that much of the knowledge of electrowetting on conducting droplets can also be applied to the study of dielectric droplets.

The energy-minimization framework developed by Bahadur and Garimella[44] for conducting droplets is used also by them and Kumari[41] for insulating droplets. However, the treatment of a dielectric droplet is significantly different because of the capacitive energy stored in the droplet itself. In the dielectric case, this capacitive energy is significant and needs to be accounted for in the energy minimization framework.

1.1.3.2. Properties of the insulating layer

Although the liquid properties have certain influence on the electrowetting phenomenon, the properties of the insulating film which separate the electrode from the liquid are much more critical. The materials used must be chemically inert and stable to ensure reproducibility and a long lifetime.

With the aim of minimizing the voltage required for contact angle reduction, some experiments to optimize the properties of these layers were carried out. There are two main goals to achieve: In terms of practical applications a wide contact angle range is wanted, there is thus a need to obtain at zero voltage a contact angle as large as possible. Furthermore, the insulating film should be as thin as possible[20]. In order to achieve the first target set, hydrophobic insulator may be used. However, more frequently, the problem is fixed by covering hydrophilic insulators with a very thin hydrophobic top coating[45].

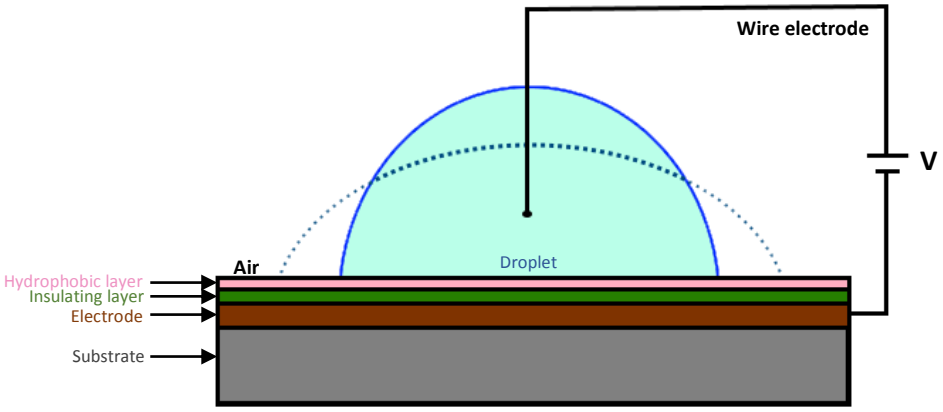

Figure 7 The hydrophobic layer is placed on the top, in contact with the drop and the insulating layer.

Usually, the most common material used for this coating process is Teflon AF[28,46,47] which is chemically inert and provides very small contact angle hysteresis. Others fluoropolymers[45] are also used, as for example Fluoropel[48] or Cytop[46].

Talking about the second goal that should be achieved, the insulator layer must be thick enough in order to avoid the dielectric breakdown. Parylene C[12] and silicon dioxide (SiO_2)[12] have been the most frequently used materials for EWOD experiments. The threshold voltages for 800nm Parylene C (with 60nm Teflon as hydrophobic layer) have been reported to be 60~80V and 25V for 100nm silicon dioxide (with 20nm Teflon)[49]. Comparing these two materials to Teflon AF (as an insulator, not as hydrophobic coatings), Parylene C and SiO_2 offer a higher dielectric constant, which means a further reduction of the operating voltage.

Cahill *et al.*[50] tested the relation between electrowetting and dielectric breakdown by measuring the contact angle of a droplet of water placed on dielectric coatings such as Silicon Dioxide, Silicon Nitride and Parylene.

Raj *et al.*[51] achieved electrowetting operation at voltages below 12V through implementation of composite dielectrics and surfactants. $A_{12}O_3$ and Si_3N_4 covered by a thin film of hydrophobic Cytop fluoropolymer exhibit higher capacitance and therefore lower voltage electrowetting operation. Surfactants were also explored to lower the water-oil interfacial surface tension and thereby further reduce the voltage required for electrowetting.

Welters *et al.*[28], performed some experiments with Parylene C and polyimide as insulators (both with a very thin Teflon coating) with different thickness in order to observe the contact angle of a 10^{-4} KNO^3 solution as a function of the applied potential and the coating thickness. They found experimentally that, for thinner layers with higher dielectric constants, the voltage needed is lower to affect the same decrease in contact angle.

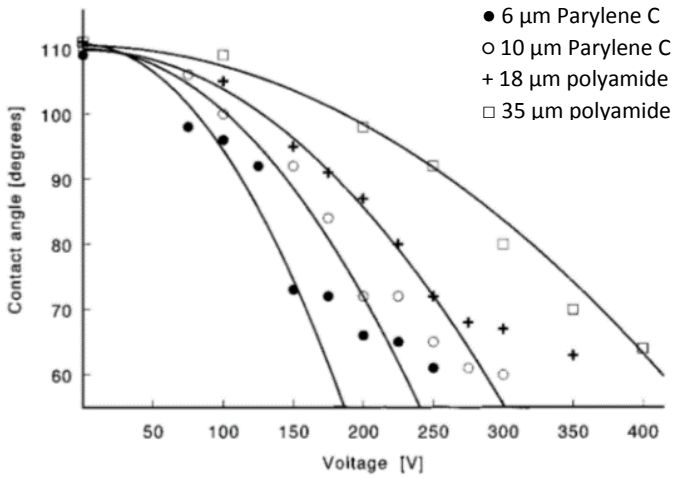

Figure 8 Welters et al[28]. results: Contact angle of a 10^{-4}M KNO_3 solution as a function of the applied potential and coating thickness. The lines give the theoretical contact angles based on the coating thickness and dielectric constant.

Recently, Choi *et al*.[52] reported the improvement in the breakdown properties using a mixture of poly(acrylic acid) (PAA) polyelectrolyte and a surfactant (Tween 80, TW80). They compared breakdown characteristics of large-molecule ionic solution with those of conventional electrolytes (Na_2SO_4). They demonstrated that defects in dielectric and hydrophobic layers are less vulnerable to larger ionic molecules.

Early studies have shown that the polarity of the applied voltage can also affect the electrowetting phenomenon depending on the material of the insulating layer[21]. When Parylene is used as an insulator film, the decrease of the contact angle is independent of polarity[24,28,53]. However this is not the case when Teflon is used; a strong deviation from the theory has been reported by several researchers when a positive voltage is applied[46]. Several studies have recognized that polarity effects in electrowetting are most probably due to molecular processes near the liquid-solid interface (for a more detailed explanation consult[21] and also[54–56]).

1.1.3.3. Ambient properties

Electrowetting experiments have been performed in air or liquid medium. Olive oil[57] and Fomblin vacuum oil[58], as a surrounding liquid, have been reported with the outcome of reducing the contact angle hysteresis. Brassard *et al*.[59] conducted experiments with water droplets in air and in silicone oil; for the water droplets in air, the contact angle was seen to decrease from 118° to about 80° (when the voltage applied was from 0 to 120V respectively). In a silicone oil medium, the contact angle changed from 167° to 60°. As it had been seen in other works, they also found that by varying the voltage back and forth from 0 to 120V, a rather complex hysteresis pattern in air while almost no hysteresis is seen in oil.

In lab-on-a-chip applications, the evaporation of the droplet is a critical issue. The thermal treatments that are required for some biochemical assays call for additional measures against

evaporation. This is the reason why lab-on-a-chip devices are frequently operated with oil as the surrounding medium[60].

Although the presence of an oil medium prevents droplets evaporation, minimizes the contamination of the devices and transporting the droplets requires lower operation voltages than in air, it also increases the viscous drag, complicates the fabrication and handling of the devices, and prevents the use of some on-chip detection or analysis techniques[61]. Moon *et al.*[62], carried out for the first time proteomic reagents using EWOD in an air (as opposed to oil) environment because the use of oil media is not compatible with many potential applications.

1.1.4. Contact Angle

In this section, after having seen at the beginning of this chapter the basis of wetting and electrowetting and therefore having determined the theoretical principles of the contact angle, we enter the contact angle hysteresis description, which is mainly caused by inhomogeneous substrates. Then, we explore the contact angle saturation, whose physical origins have not yet been explained successfully.

1.1.4.1. Contact Angle Hysteresis (CAH)

Contact angle hysteresis is another important element in electrowetting[63–65]. Looking at a drop on a window we can see how gravity pulls on the drop to move down while hysteresis keeps the drop in its place. Hysteresis (H) refers to the difference in contact angles between the advancing (θ_a) and receding (θ_r) ends of sessile drops when the drop reaches a certain size and slides down in an asymmetric shape[45].

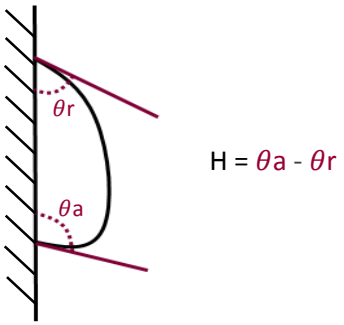

Figure 9 A sketch of a droplet on a window that illustrates the hysteresis phenomenon

This phenomenon is strongly influenced by the surface morphology and by the presence of chemical and physical heterogeneities on the surface. Solutes in the liquid (surfactants, polymers, etc.) may deposit a film on the solid surface, and the presence or absence of the film can, in some cases, lead also to hysteresis effects[66].

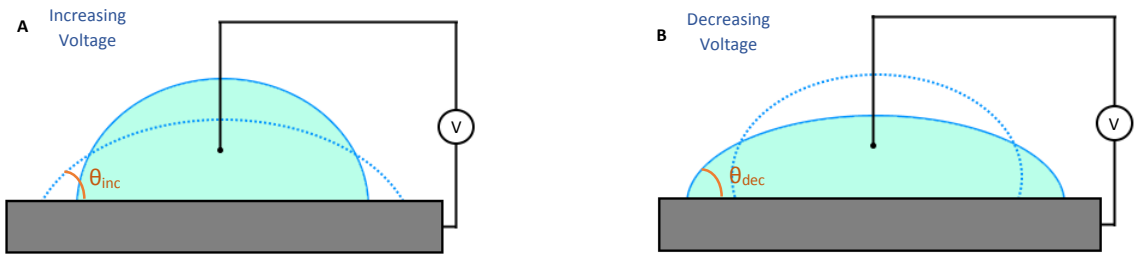

Figure 10 Schematic of the contact angle hysteresis employing electrowetting experimental setup

There are two main effects that hysteresis causes[21]: first, electrowetting can start only when the applied voltage is larger than a threshold value U_{th}[54,55]. Second, depending if the voltage is increasing or decreasing, different angles can be measured with the same applied voltage (known as irreversibility or hysteresis of electrowetting)[63,69]. Given a finite potential applied, the electrowetting hysteresis is defined as the difference between the apparent contact angles measured when the potential is increasing (*Figure 10 A*) and decreasing (*Figure 10 B*).

Despite the fact that it is not determined yet how smooth a solid surface must be for surface roughness not to have an important impact on the contact angle, there are some recommendations: the solid surface should be prepared as smooth as possible and as inert to the liquids of interest as possible[70]. In general, contact angle hysteresis should be sufficiently small, i.e. less than 5°, in order to characterize a surface adequately clean and smooth[5].

Gupta *et al.*[71] characterized the electrowetting response of materials with CAH ranging from 1 to 30° to investigate the effect of the hysteresis on the spreading of a liquid drop with applied potential. They demonstrated that even a small amount of CAH (5°) alters the electrowetting performance, exhibiting deviations from the electrowetting equation.

As we have stated before, oil as surrounding medium helps to reduce the CAH. Verheijen *et al.*[72] used an insulator layer coated with a highly fluorinated layer impregnated with oil providing a contact angle hysteresis lower than 2°.

Yang *et al.*[73] showed that advancing contact angle is found to be intrinsically higher than the receding one, regardless of the surface heterogeneity. This suggests even perfectly smooth and homogeneous surface (although experimentally impossible) would have a contact angle hysteresis due to its dependence on the amount of energy dissipated in the process of wetting and dewetting.

1.1.4.2. Contact Angle Saturation (CAS)

By increasing the applied voltage, according to the basic electrowetting theory, the contact angle should reach zero degrees. However, in practice, the effect of contact angle saturation has always been observed to limit the contact angle modulation. The parabolic relation between the observed contact angle and the applied voltage was shown experimentally to hold at low voltage[20], but above a certain voltage (U_s) the cosine of the contact angle deviates from the parabolic behaviour. Additionally, saturation can also be experimentally interpreted when the contact angle ceases to respond to voltage - it plateaus – or even begins to reverse.

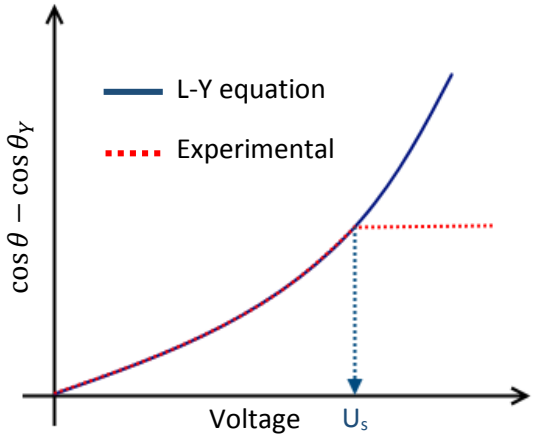

Figure 11 Plot that shows the saturation effect.

The origins of this failure of the electrowetting equation have not yet been explained unequivocally. Recently, several scientists have suggested different hypotheses and their works indicate that a variety of distinct physical effects are responsible for the saturation phenomenon[48].

Below is a summary of several existing hypothesis for saturation:

- *Zero interfacial tension*

Some researchers have suggested that saturation is due to a thermodynamic limit of stability. Interfacial tensions between liquid-solid has to remain positive for the interface to be stable[74]. However, this theory is in conflict with widely accepted electromechanical effect of electrowetting and with experimental observation that Young's angle never actually changes microscopically[34,75].

- *Dielectric Charging (Breakdown)*

The electric field diverges close to the triple contact line and its strength is expected to reach significantly high values (hundreds of volts per micrometre). It has been suggested by Drygiannakis *et al.*[76] that this field enhancement can exceed the electrical insulation ability of

the dielectric and charges are then trapped in or on the dielectric. The diverging field was thought to lead to saturation through local breakdown of the dielectric. However, Chevalliot et al.[48] have reported with experimental results on DC electrowetting and they showed that the saturation contact angle is invariant with respect to a number experimental parameters, among which are the electric field strength, contact line profile, interfacial tension, choice of non-polar insulating liquid, type of polar conductive fluid or ionic content and the type of dielectric used[21].

- *Gas ionization/Insulating Fluid Charging*

Another possible cause that might be responsible of CAS is the air ionization around the contact line for voltages larger than the saturation voltage[77]. Chevalliot et al.[48] suggested that for liquid-liquid-solid interfaces, this effect could be caused by charging the insulating fluid due to ejection of charges or satellite drops from the conducting drop into the oil.

- *Other Hypotheses*

Some observations have been reported related with AC electrowetting, such as instabilities of the contact line close to the critical (saturation) voltage, or hydrodynamic flows which develop inside the drop within a certain frequency range. However, apart from requiring much more rigorous tests, these models fail to explain the contact angle saturation of DC electrowetting.

Most recently, another explanation has emerged; Chevalliot *et al.*[48], according to their experimental results, state that Taylor cone phenomena could be related to the CAS. This, in any case, remains to be proved.

1.1.5. AC and DC electrowetting

- AC - DC comparison

The use of DC or AC electrical voltages is another notable feature of the available research which electrowetting phenomena also involves. Although DC voltage has been the most used over the years on the majority of the experiments, recently the research on the influence of AC voltage on the actuation of liquid droplets is increasing due to the benefits AC provides. Below, we present a brief summary which sets out the main differences between the use of AC and DC voltage.

The contact angle hysteresis exists in DC electrowetting due to pinning effects[63–65]. This causes, as we mentioned before, that electrowetting can start only when the applied voltage is larger than a threshold value U_{th}[49,67,68,78]. The equilibrium contact angle is situated between the receding and the advancing contact angle values, e.g. $\theta_R < \theta_{eq} < \theta_A$. When we apply the electric field, the electrostatic force tries to reduce the contact angle but the contact line will move only if the electrostatic force exceeds the pinning force[63,64]. The use of AC voltage perturbs the force

balance at the contact line and leads the depinning of the contact line from the surface[79], consequently, the contact angle hysteresis is smaller in AC than in DC electrowetting[64,79]. This should reduce the threshold voltage for AC actuation.

Many experimental results showed that the contact angle saturation occurs at a smaller contact angle for AC electrowetting in both systems: liquid-solid-air[48,80] and liquid-liquid-solid[81–83]. Chevalliot et al.[48] found that the contact angle saturation lowered from 60° to about 45° for the AC case (using NaCl aqueous solution electrowetted on glass/ITO/Parylene/Fluoropel substrate). They stated that it may be cause of the quickly changing polarity that removes injected or adsorbed charges, but the observed results could also be due to less pinning of the contact line when using AC voltage.

Another aspect associated with AC electrowetting is the edge instability. Instabilities occur only in the AC case and especially at very low electrolyte concentrations[84]; tiny satellite droplets are disintegrated from the mother drop[84,85]. A simple theory dealing with electrostatic phenomena at the line perimeter accounts for the order of magnitude of the voltage where this instability occurs; it explains the experimentally-observed size-dependence of the expelled droplets with the insulator thickness[77].

1.1.5.1. Frequency dependence

The Lippmann-Young's equation is correct as long as the basic assumptions are not violated. The assumption that the liquid is treated as a perfect conductor breaks down upon increasing the frequency. Far below a certain critical frequency, f_c, the liquid behaves as a perfect conductor; far above, it behaves as a dielectric (electric field-induced actuation of liquids beyond f_c is still possible, but in this case these forces are dielectric body forces)[20]. The critical frequency is related to the physical properties of the liquid as well as to the geometry of the insulating layer.

The general AC electrowetting behaviour can be represented by the analogy with an equivalent circuit, as shown by Mugele and Baret[20].

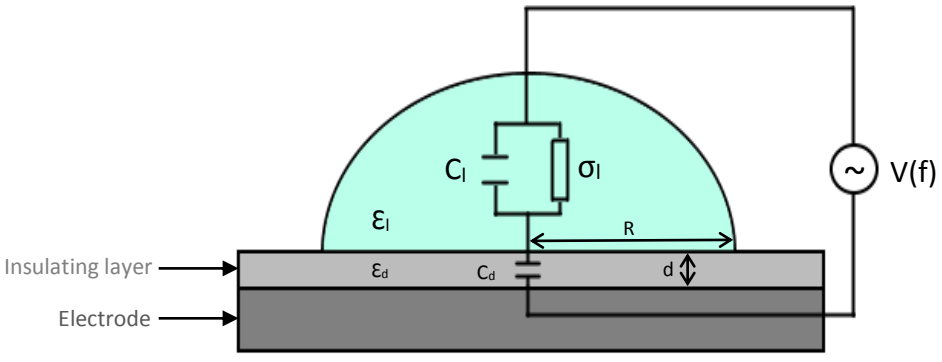

Figure 12 Equivalent circuit which represents the AC electrowetting behaviour.

- *Critical frequency by Mugele and Baret[20]:*

$$f_c \sim \frac{\sigma_d + \sigma_l \frac{d}{R}}{\varepsilon_0 \left(\varepsilon_d + \varepsilon_l \frac{d}{R}\right)} \tag{7}$$

Where σ_d and σ_l are the conductivities of the dielectric layer and ε_d and ε_l are the permittivity of the insulating layer and the liquid, respectively. $\frac{d}{R}$ represents the size ratio of the dielectric layer and the drop[21]. For deionized water, f_c is typically few kHz, which matches with experimental observations (see[32,35,79]).

The electrical current is generally composed of two contributions: the Ohmic current and the displacement current. For a time-periodic signal, the Ohmic current is proportional to σE while the displacement current is proportional to jƐωE, where σ and Ɛ are the electrical conductivity and permittivity of solution and ω is the angular frequency[86].

$$\omega = 2\pi \cdot f_c \tag{8}$$

Here, $j = \sqrt{-1}$ means that there is a phase difference of π/2 between the two currents. Since the displacement current is proportional to the AC frequency, the Ohmic current dominates over the displacement current at very low frequencies, but this is reversed at an extremely high frequency. As a result, the droplet behaves more like a conductor at a very low frequency and like a perfect dielectric at a high frequencies[32,35].

1.1.5.2. Flow patterns and oscillations

Flows in electrowetting can be beneficially used to improve mixing of fluids[87,88] and could be used as a countermeasure against the troublesome adsorption of DNAs and polymers[89,90]. In the preliminary experiments of Ko and co-workers, they showed that the flow has a considerable effect on contact angle too[86]. In *Figure 13* one can observe that the solid line, which represents the Lippmann-Young's equation, fits to the DC case.

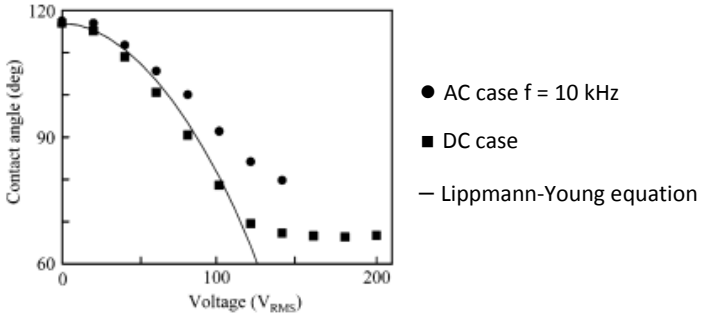

Figure 13 Contact angle dependence on the rms voltage for an electrolyte concentration of 10-3M (Taken from Ko et al.[86])

Ko et al.[86] focused their investigation on characterizing the general features of the hydrodynamic flows to try to determine its origin. Experimental results revealed that two distinctive flow patterns exist, one of them in low-frequency and the other in high-frequency.

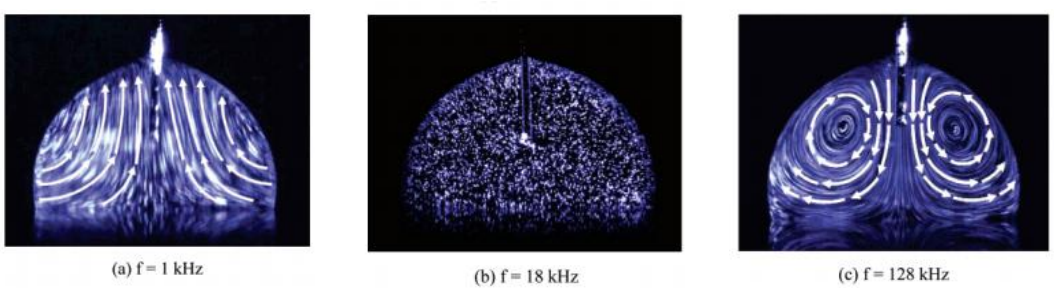

Figure 14 (a) Flow patterns at low-frequency, (b) between low and high-frequency, (c) high-frequency (Images taken from Ko et al.[86])

In the low frequency range (typically from 1 to 15 kHz), the flow forms two axisymmetric toroidal vortexes whose centre is not visible[86,91] (*Figure 14 (a)*). Then, only negligible fluid motion is observed between about 15 and 35 kHz (see *Figure 14 (b)*). In the high frequency range (in *Figure 14* (c) f = 128 kHz), the flow is highly stable and the vortex centre is always located around the counter-electrode[86].

Ko et al.[86] also found that the low-frequency flow is almost independent of conductivity as they expected. However, the high-frequency flow is significantly affected when the electrolyte concentration changes.

The high-frequency flow is originated by the electrothermal effects[92,93]. The liquid behaves as insulator at high frequencies, which implies that there is not enough time to charge completely the capacitor of the insulating layer[84], leading to Joule heating of the liquid. This gives rise to a gradient in conductivity and permittivity[92,93] generating an electric body force resulting in an internal flow. The low frequency flow is mainly driven by the oscillations of the contact line of the drop[86] resulting in a hydrodynamic viscous streaming inside the drop. However, some studies[91,94,95] point out that some additional mechanisms may influence the hydrodynamics.

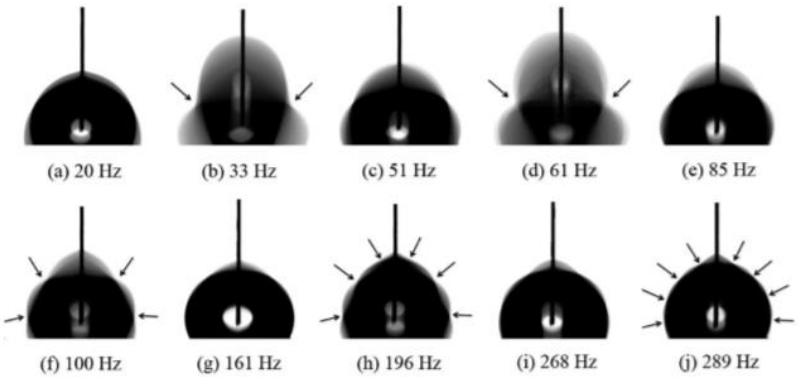

Figure 15 Patterns of drop oscillation at 60 V for different frequencies (Taken from Oh et al.[2])

Apart from these flow patterns, a sessile drop also oscillates when an AC voltage is applied as a result of the time varying electrical force concentrated on the three-phase contact line[2]. The change in wetting tension in AC electrowetting can be decomposed into steady and time-harmonic parts: the steady part is responsible for the time-average change in the apparent contact angle which can be described by the Lippmann-Young's equation, and the time-harmonic part is expected to be closely related to the advantages mentioned before of AC electrowetting. Some authors reported the existence of oscillations in AC electrowetting[2,88,96], Ko et al.[86] suggested that the hydrodynamic flows in AC electrowetting could be caused by those shape oscillations of the drop surface. Oh et al.[2] developed a theoretical model to analyse the oscillation which revealed that the resonance occurs at certain frequencies and the oscillation pattern is highly dependent on the applied AC frequencies. Their theoretical results were compared with experimental results with qualitative agreement.

Most recently, Li et al.[97] presented a numerical method for drop oscillation in AC electrowetting which was validated against the experiment and the results showed that the predicted resonance frequencies for different oscillation modes agree reasonably well with the experimental tests. Furthermore, Mampallil et al.[98] reported azimuthal oscillations of sandwiched between two substrates by periodically modulating the contact line via AC electrowetting.

In practical terms, the nature of the oscillation should be understood in order to optimize the mixing efficiency in drop-based microfluidics. Moreover, a precise change in the meniscus shape from one state to another is need in electrowetting-based liquid lenses[99,100] and reflective displays[19].

1.1.6. Applications of electrowetting

As we have seen at the beginning of this chapter, electrowetting has been not only a scientific phenomenon, but is also a practical technology[101–103]. Over the last 10 years, a wide number of interesting applications have been developed or are currently flourishing. EWOD applications have shown their strong competitiveness in different fields and they are based on the fact that it is possible to control the movement or quick change (hundredths of a second) of different states of a system by using an external electric field, setting aside mechanical tools. It also allows the important fact that systems can be miniaturized to scales of less than a millimetre and still be controlled with great precision.

A brief description of recent applications of EWOD is listed below:

- *Liquid Lenses*

Liquid lenses is a typical example of EWOD implementation[15,104–107]. Variable-focus lenses have a wide range of applications in cameras as well as in consumer electronics or medical instruments. Berge et al.[104] used electrocapillarity in order to change the contact angle of a transparent drop, thus realizing a lens of variable focal length. The quality and reversibility of the lens was surprisingly good. The optical power variation can be 5 to 10 times the one of the human eye.

A new configuration of adjustable focal liquid lens based on EWOD was presented by Kang et al.[108]; their experimental results showed that at a 40 V power supply, the liquid lens is able to focus on objects away from 2.5 cm up to infinity with a good imaging quality.

Figure 16 Images that that prove what EW based fluid lens are capable. The letters 'IM' are situated closer to the lens than the doll. When the voltage applied is changed, the focal plane is moved from near to far, and this way the letters 'IM' and the doll are sequentially focalized (Taken from Kang et al.[108])

Adhesion force changes by electrowetting on a polymer microlens were reported by Im et al[109]. It has been shown that a larger difference in the adhesion force by electrowetting can be achieved on the fabricated microlens array than on a flat Teflon surface.

- *Electronic paper*

EWOD can also be used in electronic display technology such as electronic paper (e-paper)[19,110–113]. E-paper is a display surface very similar to a paper in terms of the reader's sensation; these display surfaces are unique in the fact that they reflect light as oppose to displays which emit light like television or computer screens. A light-reflecting display - more similar to looking at a regular printed paper - is less tiring for the eye. E-paper has the potential to serve in the future a variety of display needs, and perhaps even to replace computer and television screens in use today. Researchers have succeeded in developing very thin displays surfaces for use as display

screens for small electronic devices such as mobile phones or Pocket PCs, but much more additional work is required before it will be possible to replace a computer screen[102].

Prototypes of flexible electrowetting arrays on plastic substrates are demonstrated to switch reversibly by applying a low voltage difference (20 V). These results indicate the promise of flexible electrowetting devices for mobile and other devices, including video rate flexible e-paper. Steckl et al.[3] are currently developing flexible displays that utilize electrowetting technology on substrates made of flexible materials such as paper or plastic; of course paper is an attractive substrate material for many device application (very low cost, light weight, flexible and biodegradable).

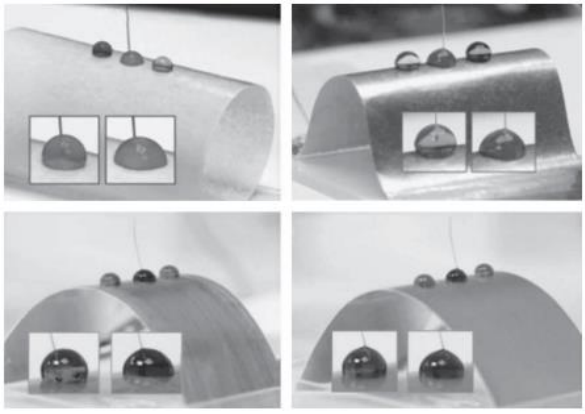

Figure 17 Proof of electrowetting on various flexible substrates. When the voltage is applied, the contact angle of the drop is apparently shifted. (Taken from Steckl et al.[3])

Figure 17 shows a flexible EW display array on a flexible plastic material (PET) substrate whose specifications are 45x21 array with 300x900 μm2 pixels. The left and right photographs show the array at zero voltage (OFF state – oil covering pixels) and -20 V voltage (ON state – oil displaced), respectively[3].

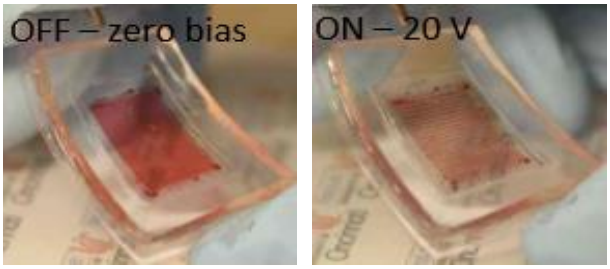

Figure 18 EW array on a flexible plastic substrate (Taken from Steckl et al.[3])

- *Lab-on-a-chip*

Besides, EWOD is commonly used in biomedical[60,68,90,114] and chemical[115,116] devices due to rapid and repeatable droplet manipulation and transportation. Different operations such as mixing, translation, merging and splitting can be carried out using static electrowetting schemes.

The typical scheme of a lab-on-a-chip system is to provide a substrate with a series – preferentially an array – of individually addressable electrodes that allow for moving droplets around along arbitrary paths.

For the practical realization of such a device, several aspects have to be taken into account: first, the usual procedure of immersing wires into the droplets is not practicable for lab-on-a-chip applications. Instead of using this configuration, a sandwich design consisting of two parallel substrates with liquid confined in between has become standard (see Figure 19).

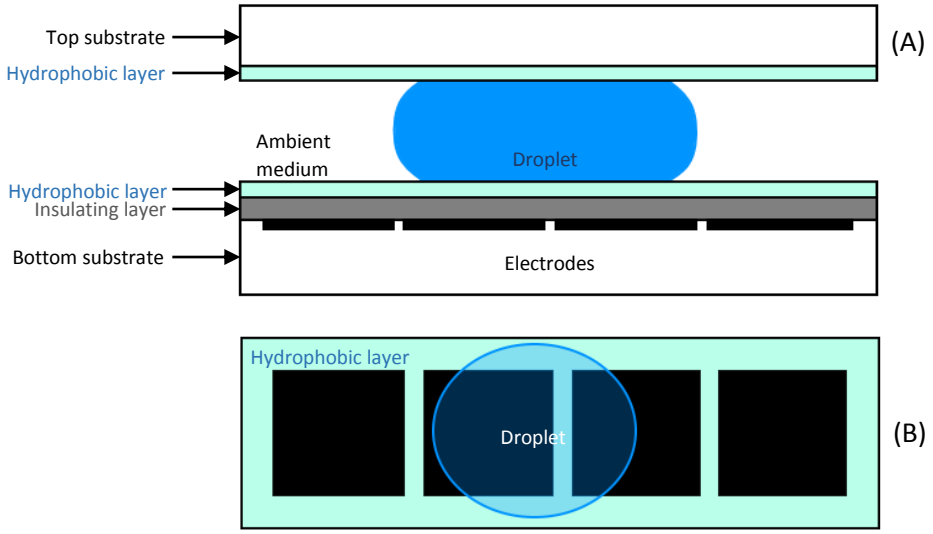

Figure 19 (A) Top and (B) side views of a typical lab-on-a-chip setup

Second, in order to allow for reliable droplet actuation, droplet edges must overlap with at least two adjacent electrodes. Third, some measures against evaporation must be taken; the problem is somewhat reduced by the two-plate sandwich design, but it is also frequently the use of oil as a surrounding medium to diminish this effect.

Yoon et al.[90] also found that biomolecular adsorption seems to be suppressed more efficiently by using an oil phase as the ambient medium instead of air. Srinivasan et al.[60] confirmed that electrowetting actuation can be carried out succesfully on physiological fluids such as whole blood, saliva, sweat, plasma and urine. However, biocompatibility issues particularly the problem of protein adsorption was discussed and it was found that a thin oil film wetting the hydrophobic substrate to avoid direct liquid-surface contact led to suppression of the undesirable adsorption effects.

Most recently, Zhou et al.[117] utilized nanostructured ZnO based superhydrophobic high dielectric constant surface to fabricate digital microfluidic device. Tian et al.[118] also applied the EWOD technology in biomedicine experiments; they built a micro-polymerase chain reaction (μPCR) chip utilizing EWOD to control the temperature uniformity in the microchamber.

Lately, an application of electrowetting for cooling of processor units was developed by Cheng et al.[119]. A EWOD-based microfluidic technique for active and adaptive thermal management of on-chip hot spots. Without the need of external pumps and valves, the droplets were precisely delivered to cooling target.

1.2. Taylor cone configuration

1.2.1. External electric field review

In the following paragraphs we will focus on the second setup. As introduced previously, the Taylor cone configuration leads to a different effect on the liquid droplet. A brief review of the literature regarding the effect of the electric field established between two parallel electrodes will be presented below. Herein, the influence of the electric field on the contact angle, the drop shape and the evaporation rate will be described[120].

- *Influence on the shape and contact angle of a drop*

When the electric field is established outside the drop, unlike in the other setup, typically it tends to elongate the drop along the field direction as we can see in *Figure 20*.

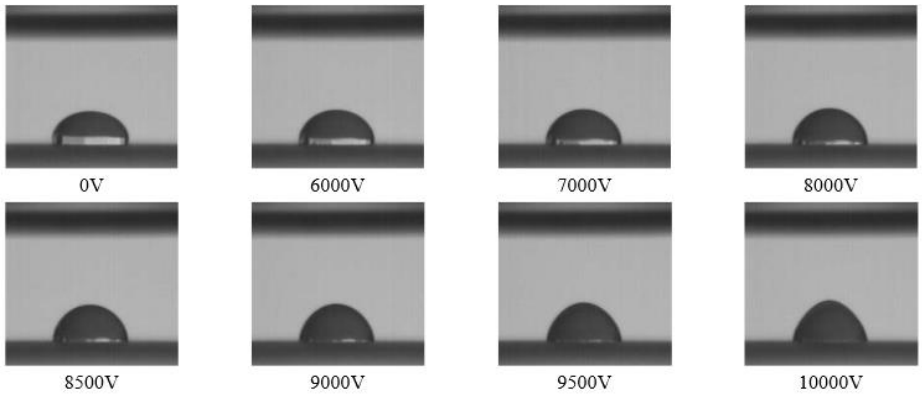

Figure 20 Water droplet deformed by the electric field using the second setup with the electrode spacing of 10mm[133].

Lord Rayleigh (1882), pioneered a study of the interaction of charges and electric fields on liquid droplets. He theoretically derived the critical amount of charges required to destabilise an isolated, surface-charged, spherical drop[121]. His work represents the beginning of electrohydrodynamics[122].

The disintegration of conductive drops in strong electric fields has been more intensively studied over the past 50 years by several researchers. However, Zeleny (1917) had already showed experimentally how drops held at the end of capillary tubes and raised to a high potential. In his experiments the voltage was applied to two bare electrodes, one immersed in the fluid and the other placed at a certain distance away from the fluid. He also measured at which potential the drops disintegrated and start jetting little droplets from a pointed end.

Several decades later, Taylor (1964) showed in his works the instability of a drop under electric fields and how its tip develops obtuse-angled conical points from which axial jets are projected. It has been presented in his work[123] that a conical interface between two fluids can exist in equilibrium in an electric field, but exclusively when the cone has a semi-vertical angle of 49.3° (see *Figure 21*).

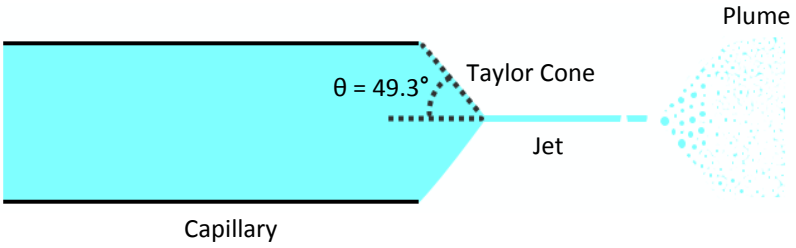

Figure 21 Electrospray schematic depicting the Taylor cone

Sessile and pendant droplets of polymer solutions have been used to perform experiments by Yarin et al.[124]. They demonstrated that the Taylor cone corresponds essentially to a specific self-similar solution, whereas there exist nonself-similar solutions which do not tend toward a Taylor cone.

The formulation that Taylor[125] used to explain the conical shape of the droplet before the jet issued had a mathematical singularity at the tip of the cone where the jet begins. Yarin et al.[124] represented the shape as a hyperboloid, instead a parabolic shape, which asymptotically approached a cone. This new shape approximation removed this singularity and also allowed calculations to be made of the equipotential lines very close to tips with very high curvature. The hyperboloidal shape led to a smaller value for the half angle of the cone than Taylor's formulation produced.

The average electric field in the absence of a jet is sometimes reported as the electrical potential difference divided by the gap between the plates, which is a good approximation near the collector. However, the electric field within a distance commensurate with the radius of curvature of the top of a Taylor cone before the jet appeared, was much higher. After a jet was stablished, the electric field at the location of any typical segment was modified, by the electrical charge carried by all parts of the jet, in a time varying was that depended on the complicated instantaneous path of the entire jet, as Reneker and Yarin explained in their paper[126].

In the last ten years, several authors have analysed the shape and stability of droplets under the influence of electric fields. Rosenkilde et al.[127] presented a relationship between the equilibrium deformation, the strength of the electric field, the drop dimensions and the surface tension for incompressible dielectric drops. The results of Miksis and co-workers showed a critical value of the dielectric constant above which the drop developed a conical shape[128]. Reznik et al. studied

the shape evolution of small droplets under relatively strong electric fields both experimentally and numerically. They performed different experiments applying weak (subcritical) and strong (supercritical) electric fields. Their results showed that for subcritical electric fields, the droplet is stretched by the electric Maxwell stresses and acquires steady-state shapes. On the other hand, in stronger electric fields, the Maxwell stresses overcome the surface tension and jetting is initiated from the droplet tip. In this last scenario, they distinguished two situations: If the static (initial) contact angle of the droplet is $\theta s<144°$ the jet base acquires a conical shape with vertical semi-angle of 30°, which is significant smaller that of the Taylor cone. If the contact angle of the drop is in the range $144°< \theta s<180°$, there is no jetting and almost the whole drop jumps off[127]. Most recently, Di Marco et al.[120] also obtained this elongated shape of ethanol droplets subjected to an electric field of 13.3 kV/cm; the contact angle and the curvature at the apex of the drop increase with increasing the electric field.

As far as the contact angle change is concerned, distinct results have been found in different experimental studies. Vancauwenberghe et al.[120] summarized them in a table and the outcome of these works was either an increase[129,130] or decrease[131–133] of the contact angle, both as a result of increasing the magnitude electric field applied which varies from 1 to 25 kV/cm depending on the experiment.

Reviewing the mentioned citations, Roero et al.[133] used various substrates with different treatments to study the influence of the electric field on the shape of water drops and its contact angle which decreased with increasing the electric field. Same results regarding the contact angle change were obtained by Roux et al.[131] also using water as a liquid but mineral oil as a surrounding fluid. In contrast, Bateni et al.[134] using their new methodology (ADSA-EF) to study the drop shape and surface tension under external electric field, observed an increase in the contact angles; they suggested that this fact is due to a bulk effect rather than an interfacial effect[129].

- *Influence on the evaporation rate of a drop*

Seeing that the effect of an electric field is a phenomenon of considerable interest in a wide range of industrial applications such as coating, electro-spraying, cooling, drying in food industry[135], particle manipulation[136], printing, DNA mapping, heat exchange, etc., the enhancement of the heat transfer in the evaporation process may be useful to improve the evaporation rate taken into account that the generation of an electric field is a cost-effective solution because of its low power consumption. Even if the enhancement of heat transfer due to the application of an electric field is already well understood, that which concerns the evaporation of droplets remains a subject with little research. Hashinaga (1995) studied the

evaporation of water under the influence of an electric field. They found that water liquid evaporation rate could be enhanced thanks to the electric field. Takano et al.[137] investigated evaporation of several liquid drops under a voltage applied varying from 0V to 2000V. In their experiments, the substrate temperature was 300°C for both ethanol and cyclohexane drops and 400°C for water. Although all the liquids showed an improvement of the evaporation rate on hot solid surfaces, the time needed for a single drop of ethanol to evaporate completely when 300V are applied, reduced to one-twentieth of that for evaporation without an electric field, which means a high enhancement. Moreover, they showed that for ethanol and R113 with a maximum voltage applied of 250V and 2000V, respectively, the highest enhancement ratios of the evaporation heat transfer were 7.6 for ethanol and 2.8 for R113, corresponding both to the highest applied voltage. Takano et al.[137] suggested that the effect of the electric field may be less notable for non-polar liquids due to its high charge relaxation time. In their followed study[138], they measured the critical voltages and response times necessary for which the surface of the liquid starts to be unstable and finally a thin column of liquid rises from the tip of the cusp up to the upper electrode; they conclude that even in the case of non-polar liquids such as R113, surface instability may occur at a certain critical voltage and at a response time shorter than the electrical relaxation time.

1.2.2. Applications of Taylor cone

Such a phenomenon is the basis of electrospinning, electrospraying and hydrodynamic spray processes from which a jet of charged particles emanates above a threshold voltage.

Electrospinning is a process that creates nanofibers by means of an electrically charged jet of polymer solution or melt. This technique is capable of spinning fibers in a variety of shapes and sizes with a wide range of properties to be used in a broad range of biomedical and industrial applications[139].

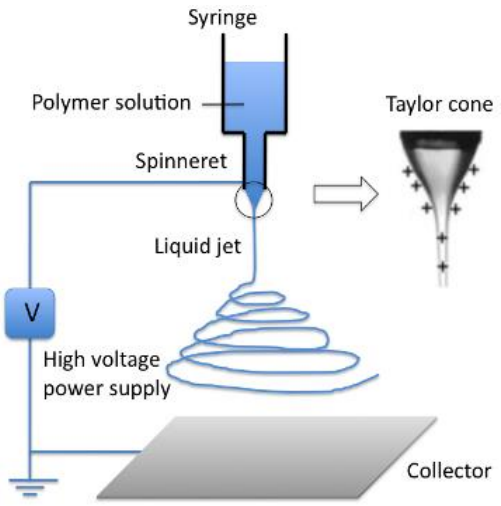

Figure 22 Electrospinning representation from Ref. Li et al[4].

Matthews et al.[140] described how electrospinning can be adapted to produce tissue-engineering scaffolds composed of collagen nanofibers. Their experiments demonstrate that it is possible to tailor subtle mechanical properties into a matrix by controlling fiber orientation. The structural, material, and biological properties of electrospun collagen suggest that this material may represent a nearly ideal tissue engineering scaffold.

The stream can be optimized by adjusting the composition of the solution and the configuration of the electrospinning apparatus, thus optimizing the alignment and morphology of the fibers being produced. Leach et at.[141] presented a procedure for setting up a basic electrospinning apparatus, empirically approximating the critical entanglement concentration of a polymer solution and optimizing the electrospinning process.

On the other hand, electrospray is one of the most versatile ionization techniques for the investigation of macromolecules, i.e. Electrospray Mass Spectrometry (ESMS) is a widely used technique in biological, biochemical, pharmaceutical and medical research. Wilm and Mann presented a study in which a theoretical description of the electrostatic dispersion in electrospray was reported. They introduced a theory which predicts the size of the zone at the tip of the Taylor cone from which the liquid is ejected. In order to minimize this emission zone, a modified electrospray ion source, called the micro electrospray, has been constructed.

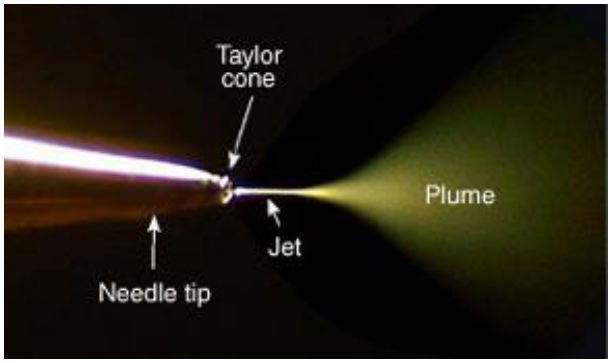

Figure 23 Electrospray picture taken from www.newobjective.com

Tan[142] studied mechanisms involved in the electrospray of biological macromolecules which may cause spraying instabilities. Hyaluronan (HA) has been studied for its biological significance. HA solutions with different concentrations and molecular sizes were investigated. Experimental results demonstrated that the molecular size and solution concentration of macro-molecules are critical factors affecting the spraying process. A concentration reduction of HA molecules happened during the electrospray process, and a hypothesis on partial reflection of HA molecules inside the Taylor-cone was presented in his study.

A part from these mentioned applications, the Taylor cone is also used in FEEP where electric force and surface tension generates surface instabilities which give rise to Taylor cones on the

liquid surface. Field Emission Electric Propulsion (FEEP) and colloid thrusters are high performance devices designed to satisfy the most demanding requirements for very low thrust, high-accuracy applications. Originally developed for science missions, FEEP is an enabling technology for precision formation flying and accurate pointing applications[143].

1.3. Objectives of the present work

The fact that an electric field can modify the drop shape and its contact angle has been of great interest from both practical and theoretical points of view. Contact angle phenomena under electric fields have been studied by many researchers for a long time. The majority of the recent work focused on the electrowetting effect considering a configuration in which the electric field is applied inside the droplet by means of a wire-electrode. These studies have shown how electric field reduces the contact angle using the aforementioned configuration. In these works, the fluid tested was generally a conductive liquid and it was characterized by a large initial contact angle – close to 180°. Most of the recent electrowetting studies and applications are carried out on hydrophobic surfaces, such as Teflon, in order to achieve this large initial contact angle. In the current study, an HFE-7500 droplet will be placed on a thin insulating surface – Parylene-C – no coated with any hydrophobic layer. The goal is clearly to investigate how dielectric and almost perfectly wetting liquids behaves in this configuration. If a similar effect is found for these liquids, another goal is to examine with more precise measurement techniques if really the contact angle is modified or just the region in its neighbourhood.

On the other hand, many researchers have also studied the shape and stability of drops under electric fields. The configurations used for these investigations have mainly consisted of a droplet deposited onto a substrate – which is usually grounded – and an electrode placed at a certain distance of the drop. Previous works have shown how the droplet elongates in the electric field direction forming a conical shape known as a Taylor cone. However, not every liquid can form a Taylor cone. Moreover, depending on the initial contact angle of the droplet – as well as on its volume - , the electric field that is required to elongate the droplet varies. The open questions are again related to the use of almost perfectly wetting dielectric liquids. With the goal of observing where is the change in shape originating and if a Taylor cone can still form using these liquids, as well as finding out the electric field influence on the contact angle, a second configuration based on those employed in previous works will be designed and put into practice.

Chapter II: Experimental Methods and Materials

2.1. Two ways to establish the electric field

The majority of the recent work considers a way to establish the electric field which is based on applying the voltage only to the solid-liquid interface (*Figure 24 (A)*), which means that the electric field is created directly inside the droplet. To do so, one electrode is placed in contact with the drop and the other one is grounded. The studies based on this setup have shown that using such configuration the electric field deforms the drop and reduces the contact angle usually by applying a potential of several hundred volts. As we have been seeing along this study, many applications use this setup in order to execute their purposes; however, the fact that the electrodes must be in contact with the liquid, such applications require a proper variation of the experimental setup and may not be convenient for large processes[120,129].

On the other hand, the electric field can also be established between two parallel plates with no drop-electrode contact (*Figure 24 (B)*). This configuration, which requires a larger applied voltage, creates an electric field within the range from 1 to 10 kV/cm. Besides, this setup may be the most appropriate for evaporation applications[120].

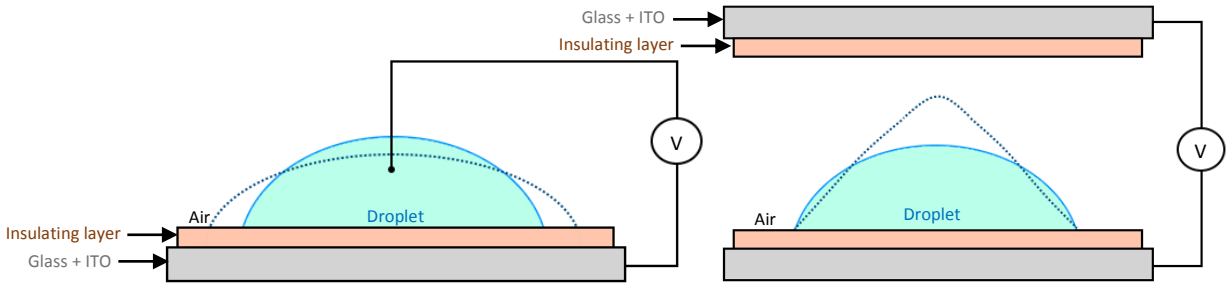

Figure 24 Schematic of two different ways to establish the electric field. The figure on the left (A) show how to establish the electric field inside the droplet and the one on the right (B) represents the setup where the electric field is applied outside the drop.

The experiments were conducted using HFE-7500 droplets surrounded by air on glass plates (diameter of 5 cm) covered on one side with a conductive coating (indium tin oxide, ITO). Parylene-C is used as insulating layer with a thickness between 8.8 and 9.3 µm (see *Figure 24*). Parylene-C was chosen as insulating material due to its remarkable electrical and chemical properties.

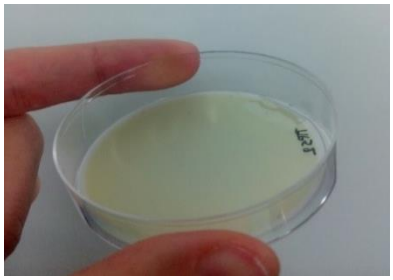

Figure 25 Glass plate covered with ITO and Parylene-C placed on his protective case.

Pieter Gijsenbergh, KUL in the framework of Belspo-PAI collaboration 'MicroMast' made the wafer; the deposition process of the ITO and the Parylene-C layer is contained in Annex A. No hydrophobic film was used due to the fact that HFE-7500 is a highly-wetting liquid which reaches very low contact angles even on Teflon surfaces.

The second setup consists of two parallel discs made of plastic. In each disc we placed one of the wafers. The upper disc of the capacitor is connected to a high-voltage power supply and the lower disc is grounded and a distance of 20 mm is initially chosen between the two plates. All experiments were conducted at ambient temperature, i.e., 22.5 ± 0.5°C, and a relative humidity of about 45 ± 5%.

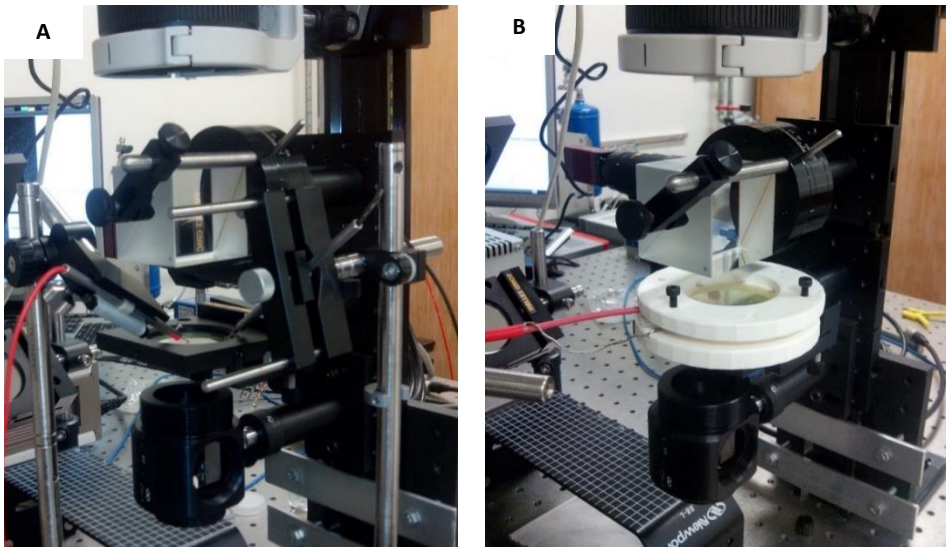

Figure 26 Pictures of the first (A) and second setup (B).

2.1.1. Features of the Electrowetting configuration

The present experimental setup is illustrated in *Figure 27*. In the case of this configuration, one of the wafers is placed on a plate which holds it. The wire that is grounded is connected through a small part of the plate directly to the ITO layer. The other wire is placed on the centre of the plate where the drop will be manually deposited with the help of a syringe. Due to the fact that this configuration is limited because of the mirror and camera positions, the wire is not mounted completely facing the drop (*Figure 26 (A)).* The cable is remarkably tilted due to this limitation which may influence the measurement results.

A sinusoidal AC signal is generated by a function generator and then it is amplified by an amplifier which allows us to go up to 300 V. Then, the amplified electrical signal is applied to the HFE-7500 droplet. An initial frequency of 100 Hz and a voltage of 300 V are chosen. All the experiments are finished within a few minutes which corresponds to the end of the drop evaporation.

It should be noted that the thickness of the wire which is in contact with the drop is less than 1 mm.

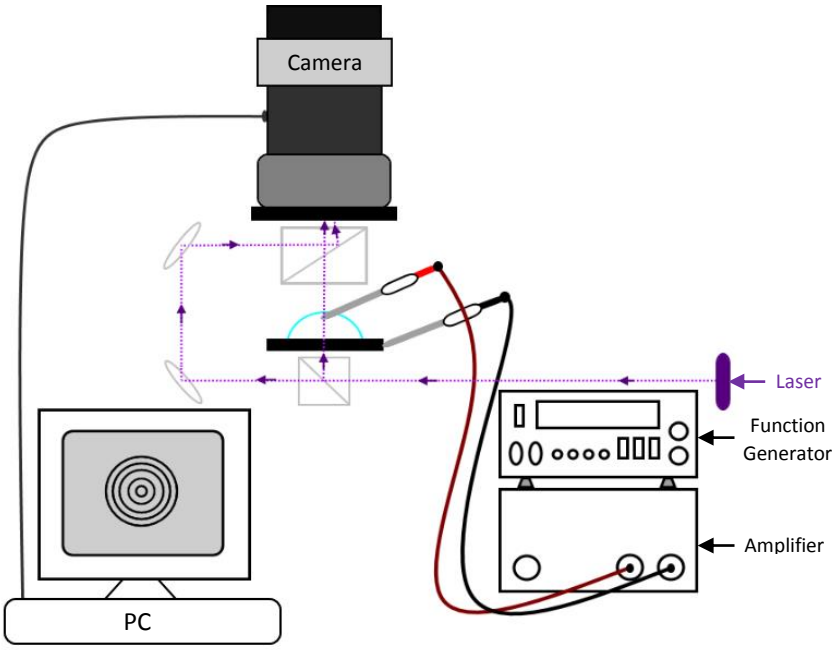

Figure 27 Schematic representing the electrowetting experimental setup

2.1.2. Design of the Taylor cone configuration

Having reviewed in the previous chapter some of the studies based on the Taylor cone configuration that have been reported so far, let us now provide further details about our specific design and the most important considerations that we must take into account before starting with the experimental results.

In this configuration, there is no drop-electrode contact. The droplet is deposited onto the bottom plate and the upper plate is placed at a certain distance of the drop. The voltage we need to apply depends on the distance between these parallel plates which determines the strength of the electric field. In such configuration the applied voltage must be higher to reach significant changes on the drop. As already said, in previous studies the electric field varied within the range of 1 to 25 kV/cm. High voltages cannot be achieved using the AC generator and its corresponding amplifier that we use for the most of the experiments of the first configuration. Instead, the DC setup introduced before was used in this section.

The distance between the parallel discs has been observed in literature to be within the range of 6 to 10 mm. Achieving these short distances has been quite difficult for us due to the limitations of the design. Besides, the magnitude of the electric field is also limited by the dielectric strength of the materials we are treating, especially those with respect to the insulating layer and the liquid droplet. Very high voltages can destabilize the drop and make it

disintegrate. Moreover, dielectric breakdown of the insulating layer should be avoided in order to ensure that next experiments will be possible to be performed.

2.1.2.1. Parallel discs design

With the aim of holding the ITO plates, two supports have been designed. The upper holder must be made of an insulating material since it is connected to high voltages. On the other hand, the bottom plate could be made of a conductive material as it is grounded - it would be welcomed that the grounded surface could be as large as possible.

Another aspect to take into account is the thickness of the holders. The separation between the plates has to be considerably small, as we have already said. However, since we need to connect the electrodes to the generator via two wires with a certain thickness, and those wires must be well attached to the support, the thickness of the holders is also constrained by the wires. Moreover, we need to put a thin plate that insulates those wires the maximum attainable. This also involves a certain thickness that we have to take into account.

It should be noted that the drop needs to be deposited onto the substrate by means of a syringe which also has a specified thickness. We need to introduce such needle through the space between the parallel discs, which means that the separation is also limited by the thickness of the syringe.

Taking all of this into account, the design that results implies an initial separation of about 20 mm. Previous works that performed similar experiments but using a separation of 10 mm applied electric fields of about 10 kV/cm, which means a potential of 10 kV. To achieve the same electric field magnitude, we might take voltages of about 20 kV. Although our amplifier allows us to go up to 20 kV, we need to be careful and see if such high voltages could be applied without negative consequences.

Since the holders have been made with the help of a 3D printer, the material used for both discs was PLA. Therefore, no conductive material have been finally used for the grounded bottom plate. The following images show the final design of the supports. Further details of the design are included in Annex F.

Once we had the holders constructed, the next step was to glue the electrode-plates to the supports and the wires to the ITO surface. First of all, the electrode-plates were glued to the support applying a silicone adhesive. Then, that small part which is not covered by Parylene-C is connected to the corresponding wire by means of a conductive glue.

After several hours waiting for everything to be well glued, we could place the whole setup onto another support which is situated below the camera in the precise position. Thanks to some

positioning screws the upper plate could be accurately fixed above the bottom plate (see Figure 28), preserving the parallelism. These screws also allow us to easily regulate the separation between plates.

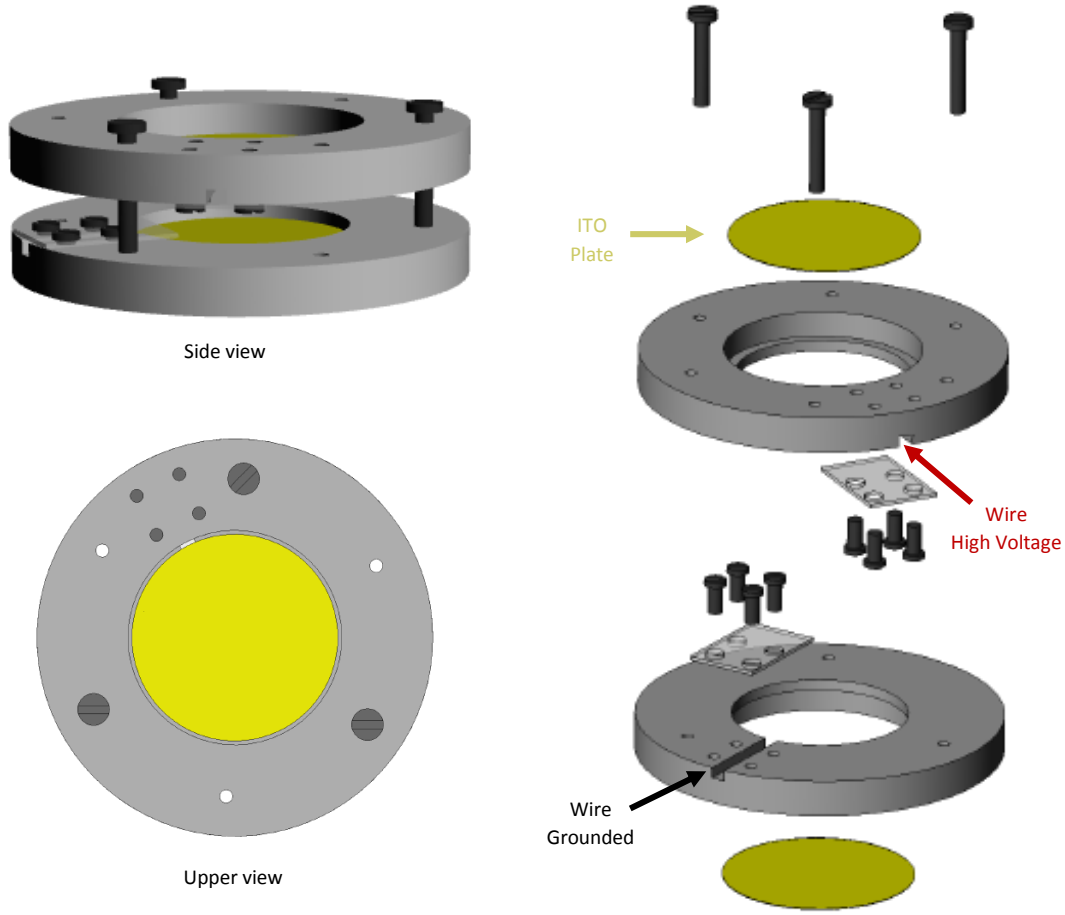

Figure 28 Second setup design (Solid Works)

2.1.2.2. Electrical breakdown

Several tests have to be conducted throughout this study. To fulfil such purposes we need to take care of our setup, thereby we can ensure that next experiment will be possible to be performed. Through information that is provided by different authors which have studied similar configurations we can get an idea of the electric field magnitude that our setup could tolerate.

Looking back to the work of Roero[133], one can distinguish many different scenarios. Demineralized water was used to carry out experiments using surfaces made of different materials: hydrophobic, hydrophilic and untreated coatings. Choosing a distance of 1 cm between plates, it has been shown that the voltage at which instability is reached - resulting in ejection of a fine jet of water with increasing electric field - depends strongly on the initial shape of the water drop and thus on the contact angle which, in turn, is controlled by the surface properties. Their work demonstrated how the instability voltage was roughly doubled if the

surface conditions changed from hydrophobic to hydrophilic. Since HFE-7500 has very low contact angles, we might expect that similar voltages to those Roero needed to apply to the cases in which the surface was hydrophilic and thus the initial contact angle (without applying any electric field) was very low, will be required also in our experiments.

Dielectric strength or breakdown voltage define the voltage at which current begins to flow through a dielectric material. Most polymeric materials exhibit values for breakdown voltage of about 10^6 V/cm. We found in the study reported by Welter et al.[28] Parylene C to be a very useful coating material because of its high dielectric strength of about 200 V/µm (breakdown voltage of Parylene C and N is plotted in *Figure 29* as a function of the polymer film thickness). However, in their experiments, the maximum voltage applied was 300 V for thin Parylene C films used as insulating coatings within the range of 6 to 10 µm. Focusing on our experiments, as already said, the voltage applied will be of almost 20 kV, much higher than those last mentioned potentials.

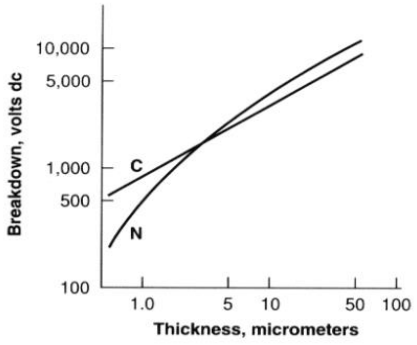

Figure 29 Breakdown voltage of Parylene C and N vs Polymer film thickness

When the electric field exceeds the critical value at which the electrical breakdown takes place, a spark leaps into the vacuum or the dielectric gets burned. In order to calculate at which voltage one of the dielectrics could break, we must find the electric field value of each layer. To simplify calculations we will study this configuration without the liquid drop. That way, we have three dielectric layers between the electrodes: Parylene-C, air and Parylene-C (see *Figure 30*).

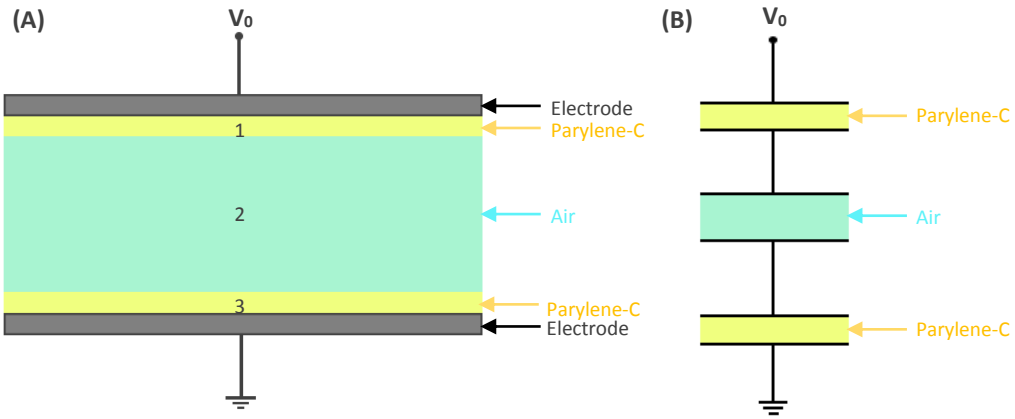

Figure 30 (A) Schematic of a simplication of the second setup and its (B) Equivalent circuit.

This problem can be completely solved assuming all the materials to be perfect dielectrics. Here we will see the solutions working with the electric field and the electric displacement field. In any case, it will be also shown how to solve the problem by means of an equivalent circuit.

If one neglects the edge effects, the electric field is assumed to be perpendicular to the plates. Thus, in each layer, the electric field will be defined as following:

$$\boldsymbol{E_i} = E_i \boldsymbol{u_z} \qquad i = 1, 2, 3 \tag{9}$$

Where 1 is the upper Parylene-C layer, 2 is the air gap and 3 is the bottom Parylene-C layer.

As they are linear media,

$$\boldsymbol{D_i} = \varepsilon_i \boldsymbol{E_i} = (\varepsilon_i E_i)\boldsymbol{u_z} = D_i \boldsymbol{u_z} \qquad i = 1, 2, 3 \tag{10}$$

Both electric field and the displacement have a single non-zero component. The condition that the electrostatic field is irrotational leads to - in each region -,

$$0 = \nabla \times E_i = \begin{vmatrix} u_x & u_y & u_z \\ \dfrac{\partial}{\partial x} & \dfrac{\partial}{\partial y} & \dfrac{\partial}{\partial z} \\ 0 & 0 & E_i \end{vmatrix} = \frac{\partial E_i}{\partial y} u_x - \frac{\partial E_i}{\partial x} u_y \tag{11}$$

Thus,

$$\frac{\partial E_i}{\partial y} = \frac{\partial E_i}{\partial x} = 0 \tag{12}$$

The electric field in each region is independent of the *x* and *y* coordinates. Then, the electric field would depend – only if it does – on the z coordinate. On the other hand, the Gauss law for every medium establishes that:

$$\nabla \cdot D_i = \frac{\partial D_i}{\partial z} = \rho_l = 0 \tag{13}$$

Which means that D_i does not depend on z. The fact that $\mathcal{E}_i$ is uniform, E_i does not depend on z either. Moreover, the displacement has the same value for each layer.

$$D_1 = D_2 = D_3 \equiv D_0 \quad D_i = D_0 u_z \;\Rightarrow\; E_i = \frac{D_0}{\varepsilon_i} u_z \tag{14}$$

Then, in each dielectric layer, the electric field is uniform and is directed in the direction of the z axis:

$$E = \begin{cases} E_1 u_z & 0 < z < b \\ E_2 u_z & b < z < b + a \\ E_3 u_z & b + a < z < 2b + a \end{cases} \tag{15}$$

The potential difference between electrodes is known, which means that we can calculate the value of D_0:

$$V_0 = \int_0^b E_1 dz + \int_b^{b+a} E_2 dz + \int_{b+a}^{2b+a} E_3 dz = D_0 b \left(\frac{1}{\varepsilon_1} + \frac{a/b}{\varepsilon_2} + \frac{1}{\varepsilon_3} \right) \tag{16}$$

$$D_0 = \frac{V_0}{b \left(\frac{\varepsilon_2 \varepsilon_3 + a/b \, \varepsilon_1 \varepsilon_3 + \varepsilon_1 \varepsilon_2}{\varepsilon_1 \varepsilon_2 \varepsilon_3} \right)} \tag{17}$$

Thus, the electric field in each layer is:

$$E_1 = \frac{V_0 \varepsilon_2 \varepsilon_3}{b\left(\varepsilon_2 \varepsilon_3 + a/b \, \varepsilon_1 \varepsilon_3 + \varepsilon_1 \varepsilon_2 \right)} \quad E_2 = \frac{V_0 \varepsilon_1 \varepsilon_3}{b\left(\varepsilon_2 \varepsilon_3 + a/b \, \varepsilon_1 \varepsilon_3 + \varepsilon_1 \varepsilon_2 \right)}$$

$$E_3 = \frac{V_0 \varepsilon_1 \varepsilon_2}{b\left(\varepsilon_2 \varepsilon_3 + a/b \, \varepsilon_1 \varepsilon_3 + \varepsilon_1 \varepsilon_2 \right)} \tag{18}$$

For a given potential difference, the electric field is more intensive within the air layer because $\varepsilon_1 = \varepsilon_3 > \varepsilon_2$, where the breakdown is also smaller. Having determined all these expressions, the maximum voltage that could be applied would be:

$$\Delta V_{max} = \frac{E_{breakdown\_air} \cdot b \cdot \left(\varepsilon_2 \varepsilon_3 + a/b \, \varepsilon_1 \varepsilon_3 + \varepsilon_1 \varepsilon_2 \right)}{\varepsilon_1 \varepsilon_2} = 135 \; kV \tag{19}$$

Where the $E_{breakdown\_air}$ is 3 kV/mm, a and b are the air and Parylene-C thicknesses respectively (a=1.5 cm and b=8.8 μm, which are the minimum values we could find[3]). ΔV_{max} is the maximum voltage the air layer could tolerate and $\varepsilon_1 = 3 \cdot \varepsilon_0$, $\varepsilon_2 = 1 \cdot \varepsilon_0$, $\varepsilon_3 = 3 \cdot \varepsilon_0$ are the dielectric constants of each layer ($\varepsilon_0 = 8.8541878176 \cdot 10^{-12}$ F/m).

The maximum voltage that the setup could handle is far from the maximum voltage that our power supply can provide. Thereby, the breakdown of the insulating layer made of Parylene C (thickness of about 8.8-9.3 μm) is not expected, nor does the breakdown of the air gap.

As said, the problem could be solved by means of an equivalent circuit (*Figure 30 B*). Each dielectric layer can be modelled as a capacitor whose capacity would be described:

[3] The thickness of the Parylene-C (d) layer of our plates varies between 8.8 and 9.3 μm (Further details included in Annex A). The separation between plates (a) varies between 1.5 and 2 cm. In order to calculate the voltage at which the air gap would break, we must take the minimum values of these variables which refer to the weaker parts of each layer.

$$C_i = \frac{\varepsilon_i S}{d} \tag{20}$$

Where S is the cross-section area of each layer and d its thickness. The three capacitors are connected in series. Then,

$$\frac{1}{C_T} = \frac{1}{C_1} + \frac{1}{C_2} + \frac{1}{C_3} \Rightarrow C_T = \frac{S\varepsilon_1\varepsilon_2\varepsilon_3}{b(\varepsilon_2\varepsilon_3 + {}^{a}/_{b}\,\varepsilon_1\varepsilon_3 + \varepsilon_1\varepsilon_2)} \tag{21}$$

The electric field in each region is obtained as following:

$$\boldsymbol{E_i} = \frac{\Delta V_i}{d}\boldsymbol{u_z} = \frac{C_T \Delta V_T}{C_i d}\boldsymbol{u_z} \tag{22}$$

Replacing the corresponding values, we obtain the same expressions of the electric fields we got before.

Talking about the liquid droplet, the dielectric constant of HFE-7500 is 5.8 and its dielectric strength is 35 kV, 0.1'' gap – which is equivalent to 138 kV/cm. The geometry of the second setup with the droplet deposited onto the substrate cannot be easily extrapolated to an equivalent circuit. In this case, the assumption of considering that the electric field is uniform in each layer would be an excessive simplification.

Conductive and non-conductive liquids are reacting differently under the influence of an electrostatic field. When the liquid is conductive, the intrinsic charge ρ is null because every charges are only present within the interface[4] and the electric field is normal to the drop. On the other hand, in the presence of a non-conductive droplet, the electric field is not homogeneous - near the droplet interface the field lines become non-uniform. Although the assumption of considering that the electric field is uniform within the air gap would be an accurately approximation, this would not apply for the dielectric droplet. A numerical simulation must be done in order to determine the electric field lines near and within the drop.

As reported in other works like those of Yarin el al.[126], the average electric field in the absence of a jet is assumed to be the electrical potential difference divided by the gap distance, which is a good approximation near the collector. However, the electric field within a distance commensurate with the radius of curvature of the tip of a Taylor cone before the jet appeared, is much higher. Since we are treating a liquid which is almost completely wetting, the assumption mentioned below would be a good approximation in this case. However, this shall

[4] Further information included in Annex G.

not apply when the drop would result in a conical shape. Having said that, the breakdown of the HFE-7500 droplet is not expected either.

2.2. Liquid: HFE-7500

HFE-7500 belong to the Hydrofluoroether family and they are considered as pure liquids, odourless, inert, with low toxic levels and with dielectric properties. Its low surface tension assures the possibility of achieving completely or almost wetting situations on the majority of substrates (even on hydrophobic surfaces such as Teflon)[5]. HFE-7500 has lower volatility than the others liquids of its family, i.e. HFE-7300, HFE-7200 or HFE-7100. Yet, it evaporates really fast if we compare it to another liquids that have been used in the study of fluids under electric fields. Although the liquid is considered as pure, we must pay attention to the way it is deposited to the destination. Plastic syringes cannot be used, otherwise the liquid may dissolve the elastomer losing its purity. Thus, glass syringe will be used to deliver the liquid to the substrate. Some of its physicochemical properties are listed below:

HFE-7500 Properties	
Molecular Weight (*g/mol*)	414
Liquid Density (kg/m^3)	1614
Surface Tension (*mN/m*)	16.2
Dielectric Strength *(kV, 0.1'' gap)*	35
Dielectric Constant	5.8

Table 1 HFE-7500 physicochemical properties.

2.3. Digital interferometry methodology

To achieve truly accurate and reliable results in contact angle measurements, the quality of the solid substrate, the purity of the test liquids and the skill of the experimenter must be taken into account. But apart from these considerations, the methodology used also plays an important role[129].

Different techniques have been used with the aim of obtaining contact angle values. Yuan and Lee[70] reported some of the most extensively methods used over the years. These techniques can be classified into two main groups: direct optical method and indirect force method. They present and discuss from the most widely used methods such as the direct measurement by Telescope-Goniometer or the Wilhelmy Balance to the most up-to-date contact angle measurement techniques such as Axisymmetric Drop Shape Analysis (ADSA) or Contact Angle Measurement of Ultrasmall Droplets.

For the current study, top interferometry will be applied. This technique has been already used in fields dealing with fluid flows, particularly related to evaporation[5,144]. Likewise, interferometry has been used by Theisen and Davoust[145,146] to measure evaporation rate in a multi-drop microsystem using electrowetting.

Since we are using a liquid with very low contact angles, this technique allows to accurately measure them unlike others methodologies which can become unreliable below 10°. Furthermore, interferometry offers the possibility of having the full drop in the field of view and extract the contact angle for each profile all along the periphery of the drop. However, as far as larger contact angles are concerned, interferometry is limited. Notwithstanding this limitation, it is sufficient to study completely or almost wetting liquids[5].

Theisen and Davoust[145,146] developed a kind of Michelson interferometer to detect surface motion at the apex of the sessile drop. Nevertheless, we are going to perform our experiments using another configuration: Mach-Zehnder Interferometer. Both of them, together with the double-beam interferometer, belong to the amplitude-splitting group of interferometers; a beam coming out of a source is separated into two waves of lower amplitude than the original one, and these two resulting beams follow a different optical path to finally be recombined at a later stage (for more details about these three interferometers and a comparison between them, get in-depth information here[5]).

In the case of Mach-Zehnder interferometry configuration (see *Figure 31*), the laser light first enters the beamsplitter O_1 and then it is divided into the reference beam b_1 and the measurement beam b_2. As we have already mentioned, the two beams recombine with each other in beamspliter O_2.

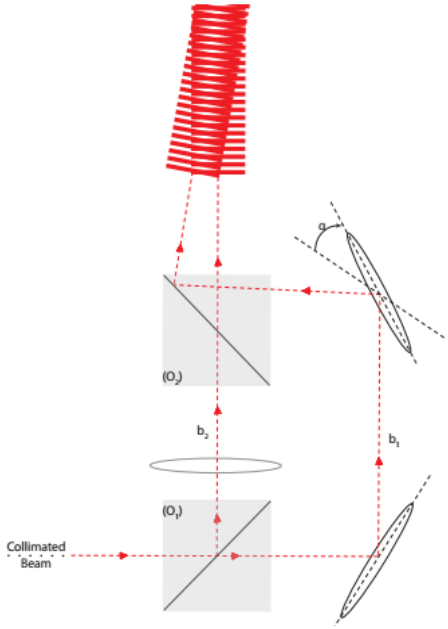

Figure 31 Side view of the Mach – Zehnder interferometer, Taken from Tsoumpas[5]

Once the interferogram is obtained, in order to analize it, a signal processing algorithm (2D-CWT algorithm[144,147–149] followed by an unwrapping algorithm[144,150]) is used to determine the phase map of the fringe pattern which allow us to obtain the thickness distribution of the drop. Tsoumpas[5] used 10 wavelets which does not allow to measure local angle maps. Recently, Dehaeck[151] reported the use of two 2D Fan wavelets to analyse closed-fringe images which allows to extract not only local phase but also local frequency information.

This algorithm is applied for every captured frame, from the moment of droplet deposition until the liquid vanishes completely. The stage of the post-processing that concerns the segmentation of the drop from the background is especially important because with it we will obtain the contact line which will allow us to determine the radius of the drop and consequently estimate the apparent contact angle (located at a distance equal to the contact radius of the profile), averaging the angles extracted from different profiles of a single drop. Unlike in the study presented by Tsoumpas[5], now we can extract the height profile and local slope as shown in the following images:

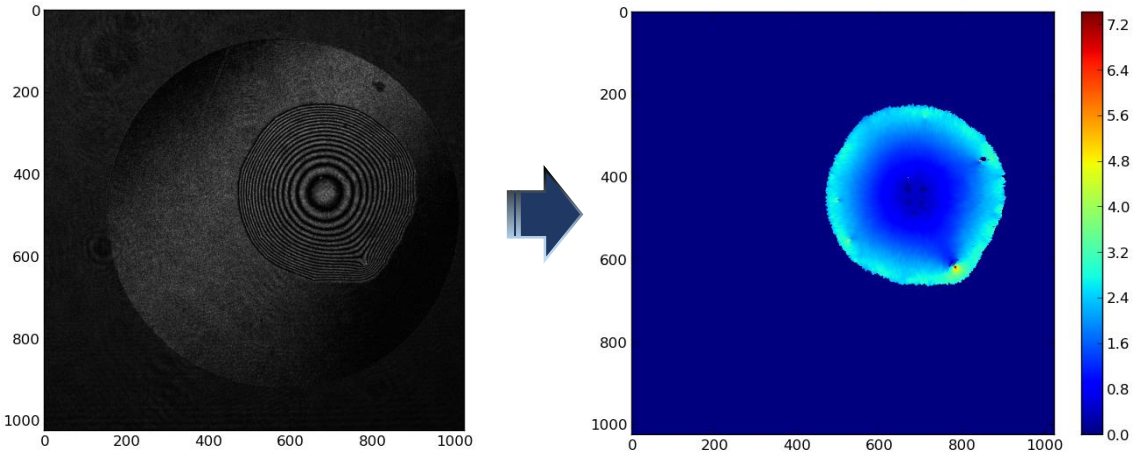

Figure 32 (A) Fringe pattern obtained when an HFE-7500 droplet is deposited onto the substrate. (B) Local slope map extracted from the fringe pattern.

The colour bar shows the range of colours which represent the local angles. As can be noted, these angles are larger close to the contact line whereas they decrease as they approach to the apex of the drop.

Chapter III: Experimental results on Electrowetting configuration

This section presents the results of the experimental study using the first configuration (conventional setup for electrowetting) described in Chapter I using AC voltage. Since preliminary tests with HFE-7100, HFE-7200 and HFE-7500 showed similar results, next measurements have been focused on HFE-7500 due to the fact that it is the least volatile and therefore allows us to draw more comparable and precise conclusions. All the results included in this first part have been conducted at ambient temperature, i.e. 22.5 ± 0.5°, relative humidity of 45 ± 5 %. Besides, we should mention that all the recorded experiments regarding the first setup are obtained with a recording rate of 5 frames per second[5].

3.1. Experiment I: Comparison between three different cases

Manually deposited drops with different initial radii - of about 2 mm - are generated per experiment. Each round of these experiments are carried out under the following conditions:

- *Case A* → 300 V - Electric Field On (with the wire inside the droplet)
- *Case B* → 0 V - Electric Field Off (with the wire inside the droplet)
- *Case C* → 0 V - Theoretical evaporation of a sessile HFE-7500 drop (Without the wire)

These three cases have been chosen with the goal of comparing their different results. Mainly, the cases A and B are chosen so that one can compare whether the electric field is causing any effect on contact angle measurements and also on the evaporation rate. On the other hand, the case C is chosen in order to prove if there is any distortion caused by the wire itself.

At each run, a small drop of about 0.5 mm^3 is manually deposited onto the substrate. The camera is previously focused and the calibration is extracted in order to analyse the obtained results afterwards.

In the cases A and B, the drop is deposited in such a way that the wire tip remains at the centre of the drop. An initial frequency of 100 Hz and a voltage of 300 V are chosen. All the experiments are finished within a few minutes which corresponds to the end of the drop evaporation.

3.1.1. Analysis of Contact Angle

Since the drop deposition cannot be accurately controlled by the experimenter, each drop has a different initial volume and consequently a different lifetime. This means that if we want to compare the contact angle using time as a reference, we cannot do so because for a specific time

[5] Except for the experiment presented in section *3.1* (test A), in which the recording rate was of 10 frames per second.

frame the volume of the drop will not be the same for each case. In order to avoid this problem, we compare the contact angle and the evaporation rate as a function of the radius which can be well extracted.

In these experiments, pinning of the contact line could occur occasionally (as can be easily observed on *Figure 33 (A)* and *(B)*) due to small dust particles present on the substrate. In any case, pinning is only local and it usually lasts less than one second near the contact line. Moreover, since we calculate the apparent contact angle at a considerable amount of points which are averaged later, no significant effect on the plotted results is thus considered.

The wire placed into the liquid drop causes a dark circle in the centre of the drop (*Figure 33 (A)* and *(B)*) which tends to increase when the voltage is applied. Looking at the fringes near the contact line, they seem to slightly expand when we apply the electric field. However, this should be accurately analysed to confirm that there is actually a significant change.

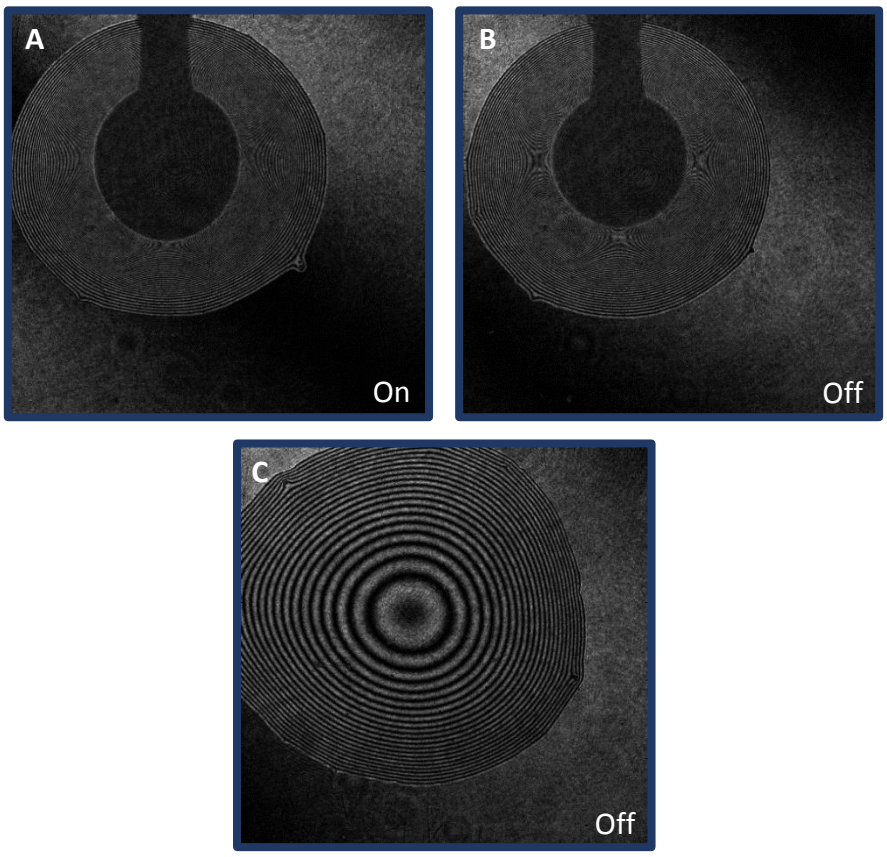

Figure 33 Interferogram (A) Case A, (B) Case B and (C) Case C. On, Off and Theoretical evaporation respectively.

On the other hand, the fringes of the case C become more expanded as we get closer to the drop centre. As one could expected, the apex is the flattest region of a freely receding drop.

The drop spreads immediately after it is deposited on the substrate. This spreading, however, only lasts few seconds (~5 s). In the cases A and C, this regime is part of the treated data, as we

can see on the contained in Annex B, where the radius is plotted as a function of time. Herein, we can clearly observe how the drop is still spreading when we start to record the images.

The following plot shows the evolution of the contact angle versus the radius for each case. As Tsoumpas[5] performed experiments of freely evaporation HFE droplets and the methodology used to measure the contact angle was the same we are employing here, we must start by comparing our freely evaporating HFE-7500 droplet with its results.

The line drawn by small red points plotted in *Figure 34* follows the same distribution as those experiments conducted on his dissertation, where the contact angle remains constant along the evaporation. However, the value of the contact angle reported in his study is about 3.4 ± 0.5 for HFE-7500 while here is about 2.8 ± 0.5[6]. This variation could be due to a different thermal conductivity of the substrate and also a matter of calibration[7].

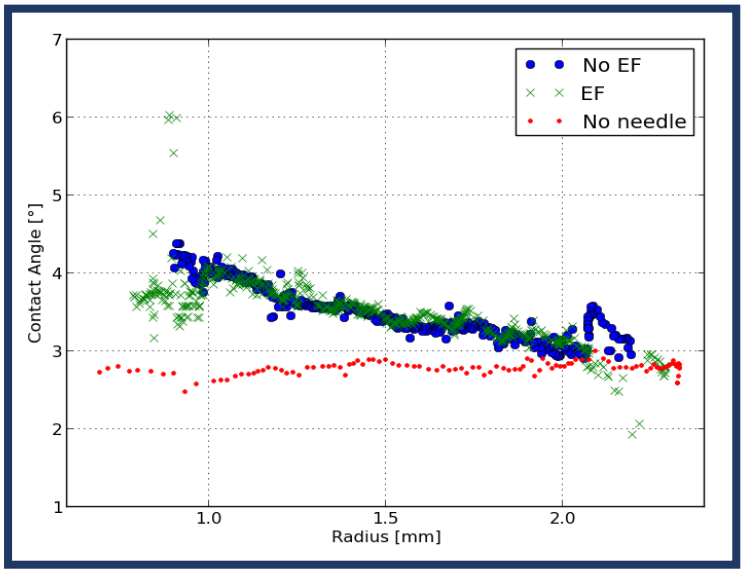

Figure 34 Apparent contact angle versus radius for A (EF), B (No EF) and C (No needle).

As can be noted, there is no difference between applying the electric field or not. Nevertheless, we can observe that there is a remarkable difference regarding the experiment without wire. This may indicate that actually the change of the contact angle is mainly due to a geometric change instead of an electrical effect.

For those cases in which the wire was placed into the drop, the contact angle seems to increase for smaller radii, which might be because the wire pulls the drop upward with a peculiar shape.

[6] The variation in the measurements of the contact angle for each cross-section of the drop with a 95 % confidence interval, i.e. twice the standard deviation, is about 1 degree.

[7] Calibration: Every time the camera is properly focused, a fringe pattern picture must be extracted in order to obtain an accurate calibration. As the refocusing is done manually by the experimenter, this may influence the value of calibration.

Such a distortion of the drop could be the reason why the contact angle increases as the radii become smaller.

3.1.2. Analysis of Evaporation Rate

Another factor that could be affected by the electric field is the evaporation rate. In order to prove this, the evaporation rate is calculated as follows:

$$Evaporation = {(Vol_i - Vol_{i+1})}/{(Time_i - Time_{i+1})} \tag{23}$$

Once again, there seems to be no sign of significant difference between the cases A and B. The theoretical evaporation (case C) shows a slightly larger value which agrees to those of Tsoumpas[5]. Therefore, the small variation between the evaporation rate of the cases A and B and the case C is also due to its geometry.

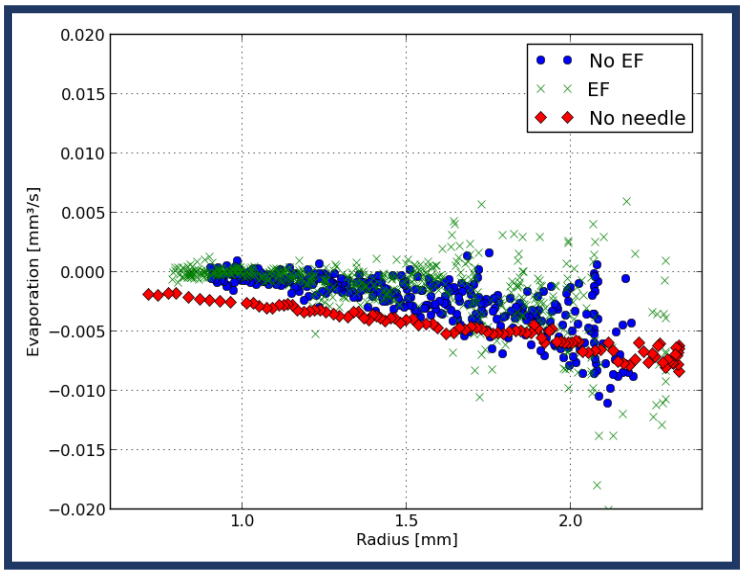

Figure 35 Evaporation rate versus radius for A (EF), B (No EF) and C (No needle).

Finally, we could say that the results do not show a significant change of the contact angle when the electric field is applied, nor does the evaporation rate. However, additional experiments are required to support such statements.

3.2. Experiment II: Electric Field On and Off on the same drop

3.2.1. Small Drop

Focusing on a single drop with an initial volume of about 0.15 mm^3, the main purpose of this experiment is to investigate if any effect is found when we switch the voltage On and Off. Every state - On or Off - only takes about 8 seconds, and we repeat this sequence until the end of the evaporation.

Using the same voltage as before (300 V) and the same frequency (100 Hz), a small HFE-7500 droplet is deposited on the substrate. The following images show the change of the fringes close to the contact line between Off (*Figure 36 (A)*), the first time we detect On (*Figure 36 (B)*) and after several images we detect On (*Figure 36 (B')*). The effect tends to become more homogeneous along the periphery of the drop after few tenths of second.

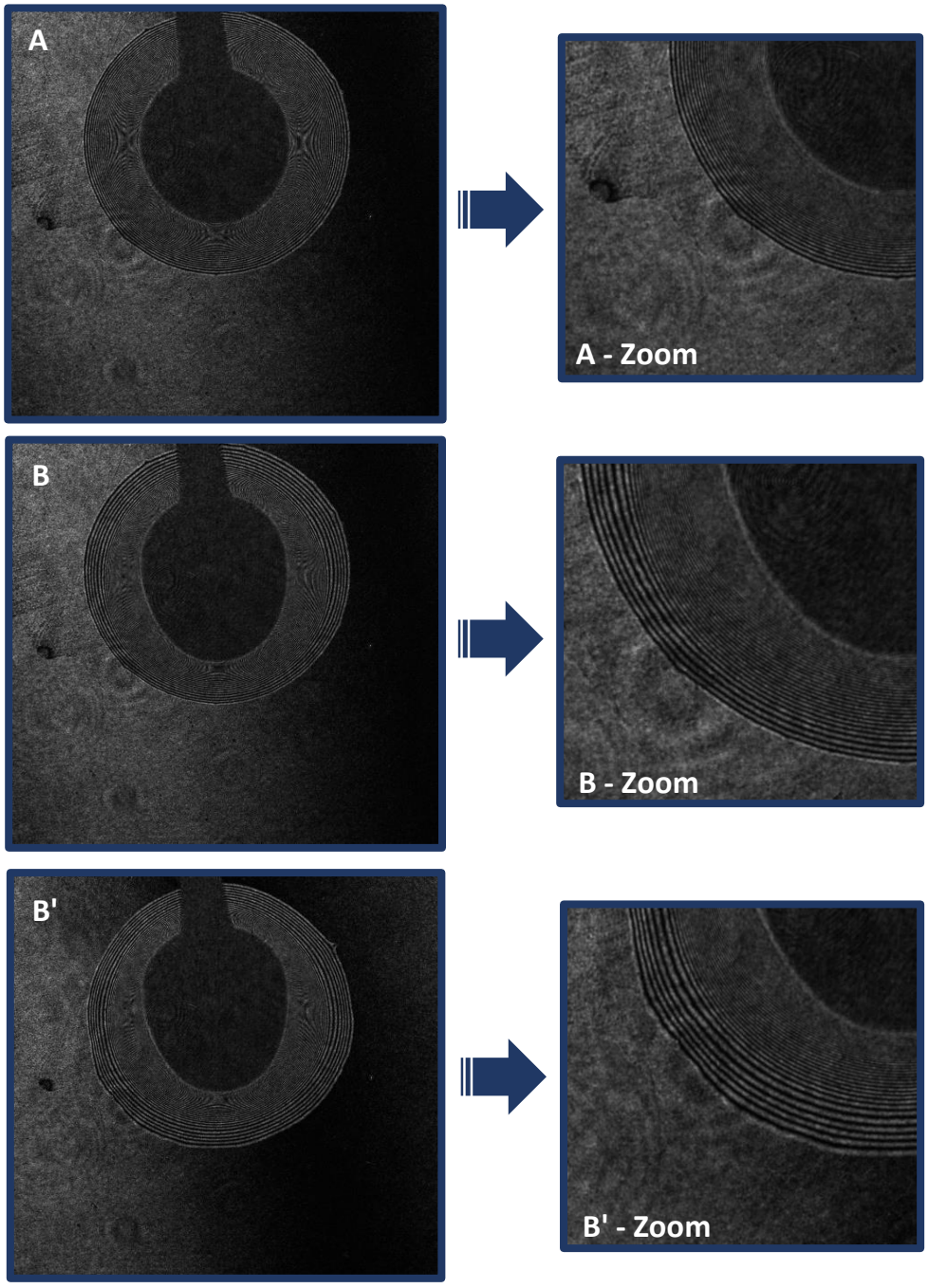

Figure 36 Fringe pattern obtained when the voltage is (A) Off, (A) first image where the effect of the electric field is detected and (C) after several images we detect On.

3.2.1.1. Analysis of Contact Angle

The next figure plots the contact angle versus time. Now there is no need to represent it as a function of the radius because we are treating the same drop all the time.

Although at first glance it seems to be quite difficult to ascertain when the electric field is On and when is Off, the graph contained in Annex C where the volume is plotted as a function of time helps to clearly determine when the electric field is Off and when it turns On[8] (represented in *Figure 37* as dashed grey lines).

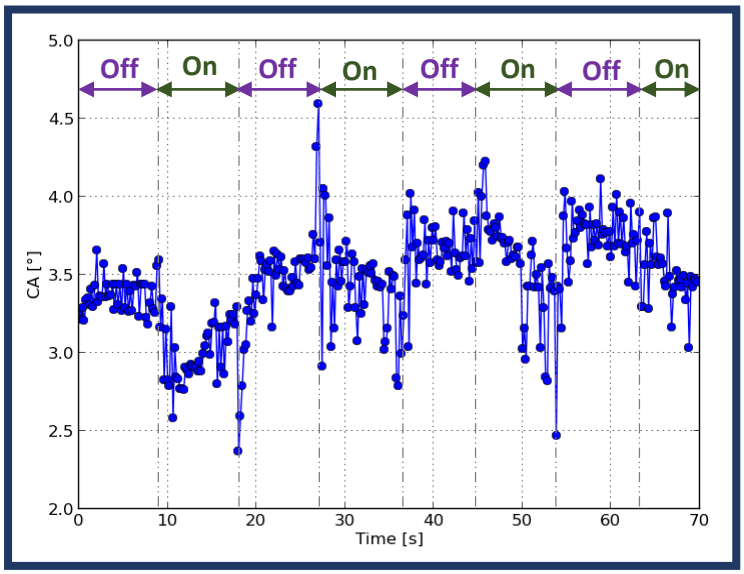

Figure 37 Apparent contact angle versus time for a small HFE-7500 drop

At the beginning, no voltage is applied, consequently the contact angle remains more or less constant. Once the voltage is applied, the contact angle tends to decrease but quickly it starts to go back to the resting value. In spite of this first observation (first time we switch on), coming measurements (from the first 'On' on) do not follow the same behaviour as we can see from *Figure 37.* Apart from this first observation that resembles a sort of transient, we cannot firmly state that a clear decrease or increase of the contact angle is found as cause of the electric field. Nonetheless, an average value of the contact angle is extracted in order to compare the two different states.

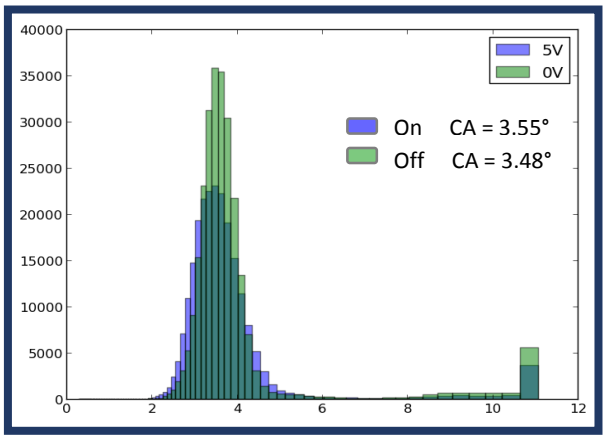

Figure 38 Histogram of all the contact angles values obtained along the periphery

[8] This plot helps us to determine when the electric field is applied because the black region of the drop located around the wire becomes bigger when the voltage is applied and consequently the volume of the drop decrease because this part is not detected as a drop.

As said before, no significant variation of the contact angle is found. There is no enough difference between the two values to claim that the electric field is actually changing the contact angle.

3.2.1.2. Analysis of Height and Local Angle

A study concerning the profile of the drop is presented. Both height and local angle profiles are thus plotted in order to prove whether the electric field is disrupting the shape of the drop.

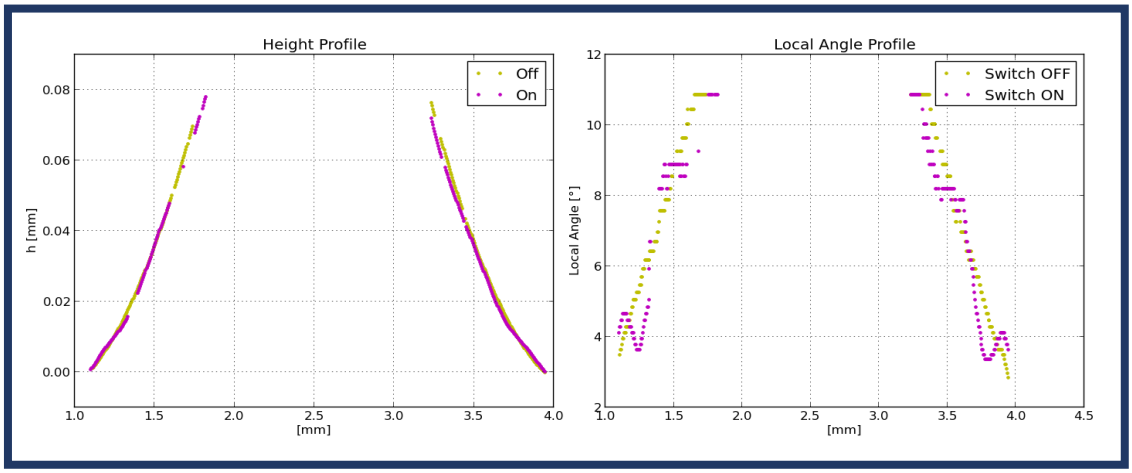

Figure 39 Height and local angle profiles regarding two different states: On and Off.

A slight variation with respect to the resting state is found when the voltage is applied, better observed on the right in *Figure 39*, which represents the local angle of the drop. This variation is essentially located quite close to the contact line but it does not significantly change the contact angle which confirms the observations from our previous experiment.

3.2.2. Large Drop

The same experiment is conducted but now injecting a drop with a larger volume (about 1.2 mm^3). Although the volume extracted is not the real one due to the fact that the central part (the area around the wire) is missing, we can estimate that the volume in this current experiment is approximately 8 times larger than before. Through this new test we could see if this little change, which in the case of a small drop is placed near the contact line, is always found at the same distance of the point where the electric field is applied.

The fringe patterns presented below show a bigger change located at a certain distance of the centre of the drop, whilst just on the contact line we can hardly perceive any difference. Moreover, *Figure 40 (B)* becomes blurred at a certain radius when we switch on the generator (shown in white in *Figure 40 (B)*). As we will see later, this blurred images will not allow to completely determine the height and local angle profiles.

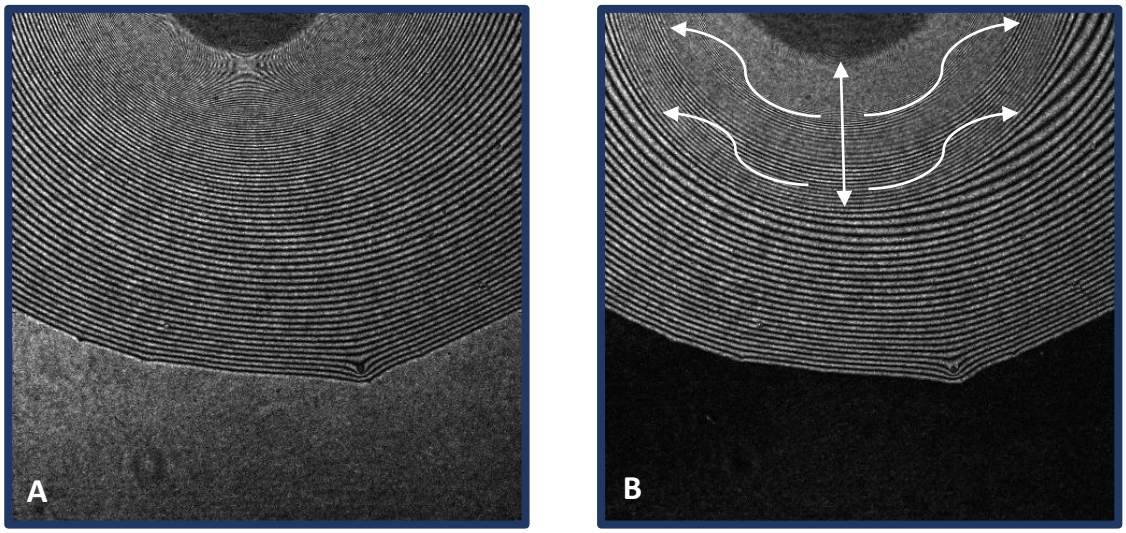

Figure 40 Fringe pattern obtained when (A) no voltage is applied and (B) the electric field is applied to the drop.

3.2.2.1. Analysis of Contact Angle

Even though, apparently, it seems that there is no change on the contact angle looking at the pictures presented above, let us now examine if this assumption is true.

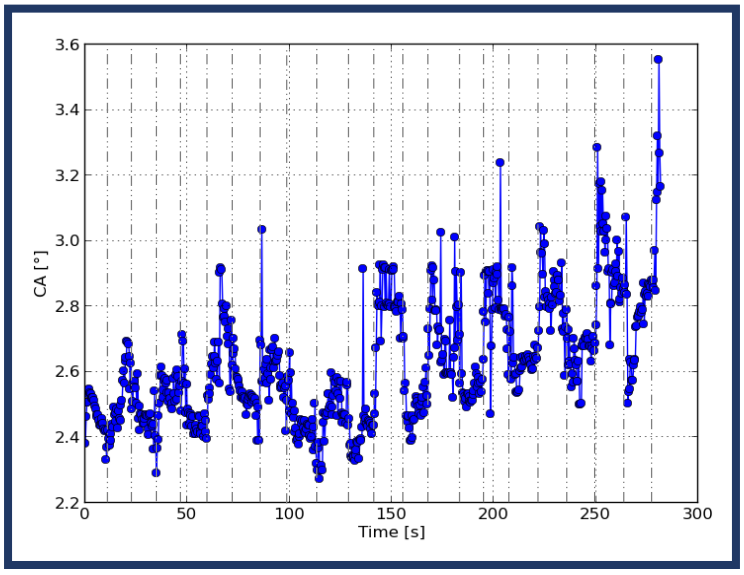

Figure 41 Apparent contact angle as a function of time for a small HFE-7500 droplet

As with the other results, the contact angle tends to increase as the radius becomes smaller due to the geometric influence of the wire. Furthermore, the contact angle seems to increase when the electric field is applied and decrease when we switch off the voltage. Nevertheless, this change remains quite small. Hence, we should calculate again the averaged value of the contact angle for each state.

Here again, no statistically significant variation has been found. Although it exists a slightly difference between the two states, one cannot confirm that the electric field is actually changing the contact angle value.

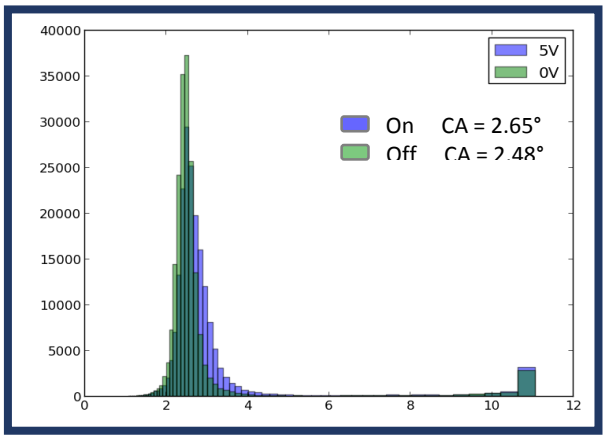

Figure 42 Histogram of all the contact angles values obtained along the periphery

3.2.2.2. Analysis of Height and Local Angle

As done previously, the local angle and height profiles are plotted in order to see if the electric field is affecting the drop shape. Moreover, we can compare if the latter deviations observed in *Figure 39* are located always at the same distance of the wire or they change their positions depending on the drop volume.

As already predicted from *Figure 42*, there is no statistically relevant change on the contact angle. However, at a certain distance of the centre, there is again this noteworthy change on the drop shape. The plot of the local angle presented in *Figure 43* shows that the main change is located between 1.5 and 2 mm from the centre of the drop, for both small and large drop scenarios (see the plot on the right of *Figure 43*, where 1st On represents the large drop and 8th On the small).

It should be mentioned that both '1st' and '8th' instants belong to the same drop (see Figure 43). The '1st' represents the first time the switch turned on and the '8th' refers at later instant of the evaporation in which the drop has already become small (similar size of droplets represented in section *3.2.1*.

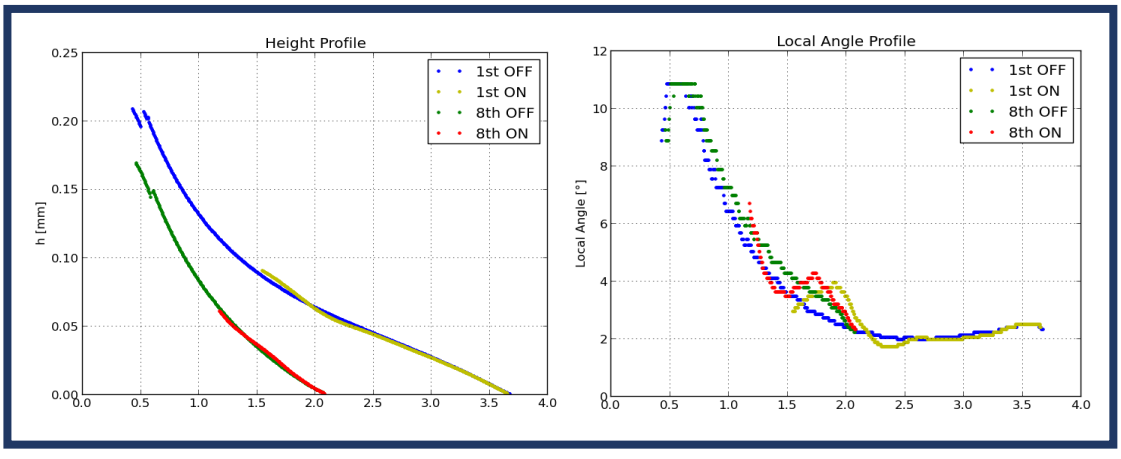

Figure 43 Height and local angle profiles regarding two different states: On and Off.

Unfortunately, at a certain point we cannot access to the data since the image becomes blurred. Therefore, it is not possible to know what happens from this point on. The fact that the significant deviation of the shape remains at the same location for both small and large drop cases, we could expect that another part with a smaller but significant change of the local angle may be found close to the wire as also had been observed in the previous case.

Besides, it should be noted that the blur disappeared in next experiments conducted with the aim of proving whether this blurred parts depended on the AC frequency. Therein, we did not find any dependence since the blur was almost completely gone in all the cases tested, which were 50 Hz, 100 Hz, 250 Hz, 500 Hz, 750 Hz, 1 kHz and 5 kHz (see Annex D). The reason why this happened remains still unknown.

3.3. Experiment III: Frequency dependence

3.3.1. AC frequency comparison

Turning our attention to the influence of the AC frequency on the contact angle and shape of the drop, now we chose different frequencies at which different tests are going to be conducted in order to prove whether the experimental results exhibit a correlation between the frequency applied and the effects observed.

The frequencies chosen are: 50 Hz, 100 Hz, 250 Hz, 500 Hz, 750 Hz, 1 kHz, 5 kHz and 10 kHz. In this section, we show experimentally that for HFE-7500 there exists a certain influence of the frequency on the shape of the droplet. However, no change has been found regarding the contact angle.

Tests have been performed with a finite voltage value of 300 V - for all frequencies - and 0 V for the Off case. The initial value of the volume of the droplet is about 1.2 mm^3.

First of all, a study comparative using all the frequencies mentioned above will be presented and discussed. Then, the same experiment introduced in paragraph *3.2.2*, which consisted of switching the voltage on and off on the same drop, will be also performed for a frequency of 1 kHz.

3.3.1.1. Analysis of Contact Angle

As far as the evaporation time is concerned, we should note again that it varies strongly depending on the manual injection of the drop. Therefore, once again the elapsed time cannot be used to compare the contact angle of different drops since every initial volume would be different for each drop. Then, in order to compare the results more properly, the drop radius is again chosen to do so.

The results are plotted in *Figure 44* and no remarkable differences are found with respect to the change of the frequency.

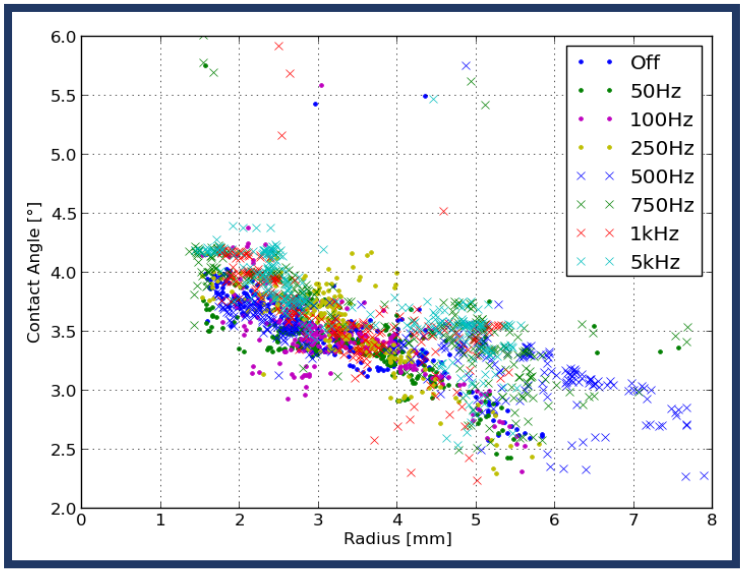

Figure 44 Apparent contact angle versus radius for different frequencies.

As shown before, the contact angle increases over time and there is no change between On and Off – due to the same reason stated before. Moreover, we see that there is no difference changing the frequency either.

3.3.1.2. Analysis of Height and Local Angle

If we turn our attention to the height and local angle profiles, we see in Figure 44 and 45 that the effect varies for each applied frequency.

These two plots illustrated in Figure 45 are not combined because this way one can more clearly observe each line which represent each frequency tested. Also, we have separated them in such a way that those cases in which the effect is more prominent are plotted together. The same applies for Figure 46. Moreover, in every plot of both figures is plotted the 0 V case in order to compare the different frequencies with the resting situation.

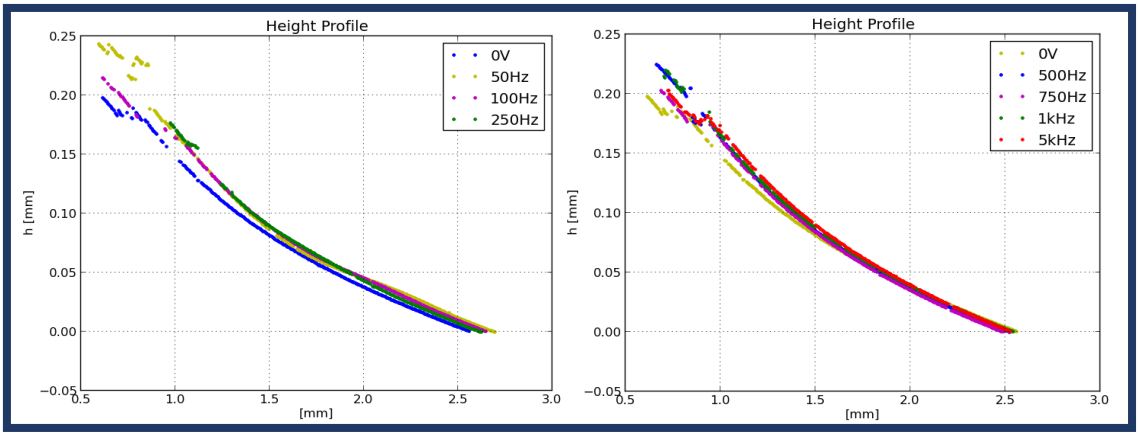

Figure 45 Height profiles for different frequencies.

Although looking at *Figure 45* we cannot clearly see the change, if we take a look at *Figure 46* which represents the local angle profile, then one can observe that the change between On and Off becomes less remarkable for higher frequencies, especially on that point where the effect is more prominent (around 2 mm).

Finally, one can state that for the same voltage applied but changing the frequency, the shape of the drop takes different profiles for each one, being less noticeable for those frequencies that are higher. In this particular case, for frequencies above 250 Hz the difference between them is almost imperceptible (see the plot on the right of *Figure 46*).

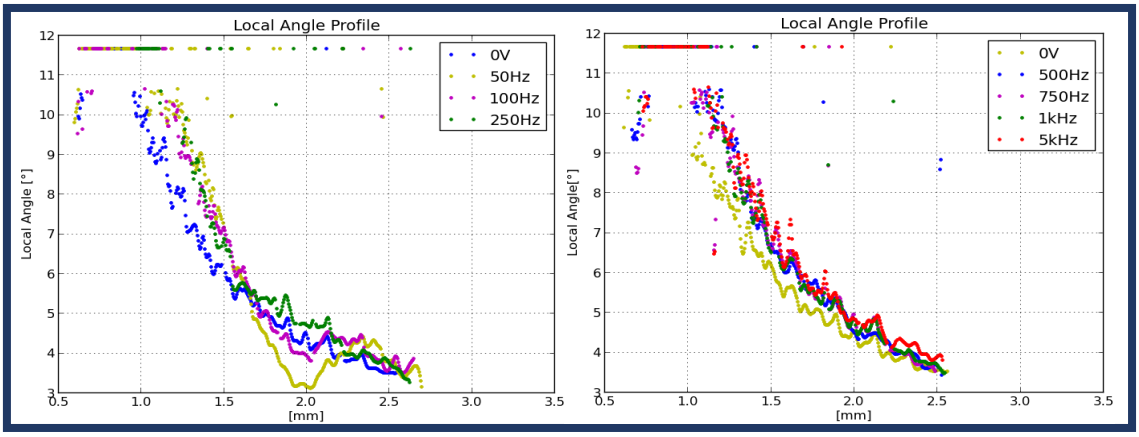

Figure 46 Local angle profiles for different frequencies.

The fact that higher frequencies lead to smaller shape deviations might be due to a threshold frequency at which the liquid starts to behave as an insulator. As introduced in paragraph *1.1.5.1*, below a certain frequency the liquids acts as a conductor and above that frequency the liquid behaves as an insulator. We mentioned in section 1.1.3.1 the study of Kumar et al. in which they determined how low liquid conductivity and high frequencies of the applied AC voltage can make decrease the effect of the contact angle reduction. Perhaps, as it happens with the contact angle reduction, the fact that for low frequencies HFE-7500 behaves as a conductive liquid also leads to these more prominent deviations of the droplet shape. In order to demonstrate this hypothesis could be accepted, we will replace the corresponding values of this present case in equation (7). Thus, the critical frequency would be:

$$f_c \sim \frac{\sigma_d + \sigma_l \frac{d}{R}}{\varepsilon_0 \left(\varepsilon_d + \varepsilon_l \frac{d}{R}\right)} \approx 130\ Hz \tag{24}$$

Where $\sigma_d = 6 \cdot 10^{-16}\ \Omega^{-1}cm^{-1}$ and $\sigma_l = 10^{-8}\ \Omega^{-1}cm^{-1}$ are the electrical conductivities of Parylene-C and HFE-7500 respectively, d[9] $= 9 \cdot 10^{-4}$ cm and R=0.25 cm are the Parylene-C thickness and the drop

[9] The Parylene-C thickness value is found between 8.8 and 9.3 µm. We decided to take 9 µm as an average value within this range.

radius and ε_0=8.8541878176·10^{-14} F·cm^{-1}, ε_d=3 and ε_l=5.8 are the vacuum, Parylene-C and HFE-7500 dielectric constants.

Apparently, it seems to be that the onset of shape deviations is linked to smaller frequencies, precisely for frequencies smaller than 250 Hz, which, in turn, more or less corresponds to the value at which the liquids starts to behave as a conductor (130 Hz). As reported by Renaudot et al.[152], when the liquids behaves as a conductor EWOD forces are predominant. On the contrary, the liquid is mainly affected by dielectrophoretic forces when it behaves as an insulator. According to the current configuration, EWOD forces seems to be the responsible of the shape deviations since they only appear when the droplet behaves as a conductor.

3.3.2. Electric field On and Off on the same drop

The same experiment conducted in paragraph *3.2.2* is now presented here but applying a frequency of 1 kHz. Tests performed in the previous paragraph have shown differences on the shape between different frequencies but no changes on the contact angle. This current experiment aims to prove that for higher frequencies, the difference on the shape of the drop is indeed less evident.

Since once again no change has been found on the contact angle, we are going to present just the results concerning the height and local angle profiles[10].

3.3.2.1. Analysis of Height and Local Angle

As shown before, the local angle tends to change less between On and Off as the frequency comes higher.

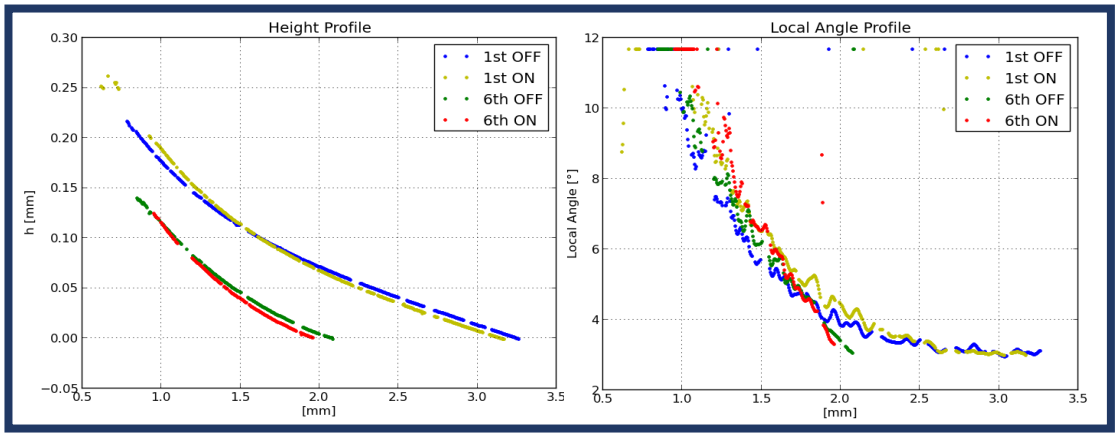

Figure 47 Height and local angle profiles regarding two different states: On and Off.

In *Figure 47* one can see that the same effect occurs for both small and large drop volume; a very little change on the slope of the droplet can be seen when we switch on the voltage.

[10] The contact angle results are included in Annex E.

However, we could not state that there exists a statistically significant change in contrast to lower frequencies.

Also here, the 6th instant refers to a later stage. '1st' and '6th' do not belong to different droplets.

3.4. Experiment IV: DC voltage

Before starting with the experimental tests using the second setup, let us now introduce the last round of experiments using the first configuration. Yet, in contrast with the previous experiments where we used an AC power supply, now we will apply DC voltage. The new generator allows us to go up to 20 kV, which means that we can verify whether voltages higher than 300 V are able to significant change the contact angle of HFE-7500 droplets.

An experimental comparison between the effect caused applying different DC voltages is presented. It should be noted that the wire used in this current case is not the same that we used before. Since another power supply and amplifier are required to generate a DC signal, another wire had to be used because the connections were different. Now, the thickness of the needle is bigger than before and the contact with the drop is thus different. Consequently, there is no point in directly comparing the AC results obtained using the other wire with the DC results obtained in the present experiments because the shape of the drop would not be the same, which means that the distortion caused by the wire is different for each wire model.

3.4.1. DC Comparison

To compare the contact angle obtained applying different electric fields, the voltages used were 0, 300, 1480 and 3000 V. Here we show the results regarding contact angle, evaporation rate, height and local angle profiles for each finite voltage. Once again, the comparison is done taking as a reference the radius, because each drop has a different initial volume and thus a different lifetime, as already discussed.

3.4.1.1. Analysis of Contact Angle and Evaporation Rate

Even for high voltages like 3000 V, the contact angle seems to not show any variance. Nor does the evaporation rate. Moreover, we should underline that the noise observed in the 3000 V case regarding the evaporation rate was very large compared to the other voltages.

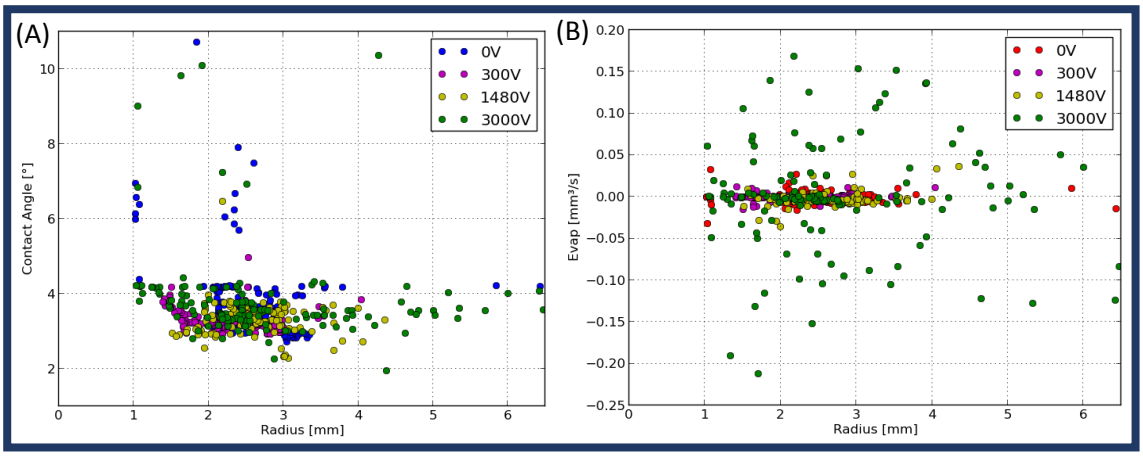

Figure 48 (A) Apparent contact angle for different DC voltages. (B) Evaporation rate as a function of radius.

3.4.1.2. Analysis of Height and Local Angle

The noteworthy changes found in the experiments conducted applying AC voltages with low frequencies have not been observed using DC. DC results showed similar results to those observed using AC voltages at high frequencies which was not expected to occur.

As can be seen from *Figure 49*, no perceivable changes are found. The local angle and height present almost the same curvature for every case.

As explained in paragraph *1.1.5.1*, there are the Ohmic current which is proportional to σE and the displacement current which is proportional to jƐωE. At low frequencies, the Ohmic current dominates and then the system behaves as if is a DC-system. Then, we would have expected the DC case to follow the AC behaviour at low frequencies. We could attribute such unexpected results to the difference of the setup employed. The wire used for the DC case was much bigger than that used for the AC experiments. It seems to be that electrowetting in dielectric liquids are very sensitive to the employed configuration.

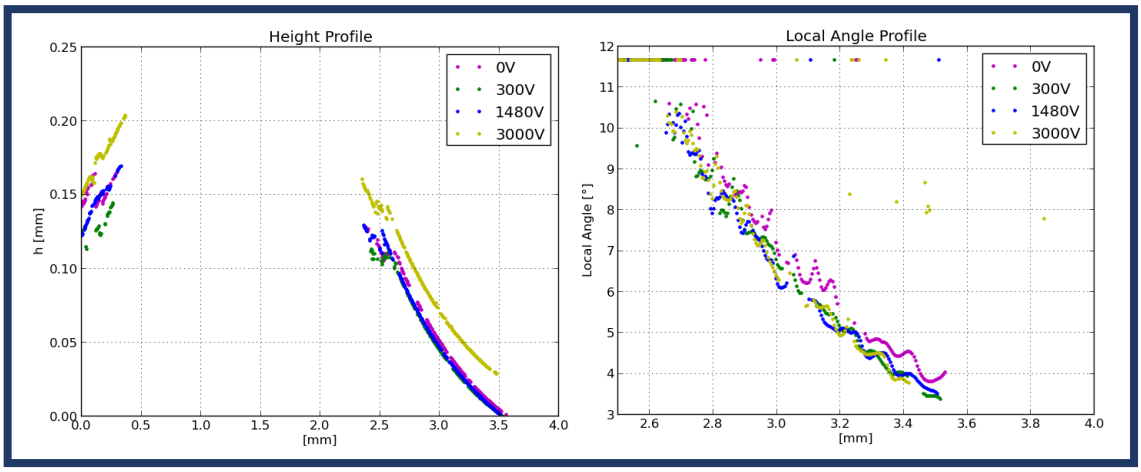

Figure 49 Height and local angle profile for different DC voltages

3.5. Conclusions

Finally, it is clear from what has been shown in those previous paragraphs that the experimental contact angle and evaporation rate do not change when an AC voltage of 300 V is applied to an HFE-7500 droplet. Moreover, regarding the contact angle, no effect have been found changing the frequency either. Consequently, we could say that significant changes are difficult to achieve using non-conductive liquids with very low contact angles, or at least that is what occurs applying an AC voltage of 300 V., in contrast with those results obtained by several researchers using conductive liquids with initial contact angles usually within the range of 40 - 160° where the difference between On and Off is actually significant. In addition, their results are remarkable even applying voltages below that we used.

However, focusing now on the effect of the electric field on the shape of an HFE-7500 droplet, it should be noted that some significant changes have been seen with respect to the height and local slope profiles. Furthermore, it has been proved that these changes are more meaningful as the frequency comes lower, whereas for AC voltages with high frequencies they do not show any change. This might be explained by the different behaviour of the drop at low and high frequencies respectively: up to a certain frequency, the liquid behaves as a dielectric and therefore dielectrophoretic forces become more important in comparison with EWOD forces. By contrast, at low frequencies the liquid behaves as a conductor. As the results showed bigger changes for those cases in which the AC frequency was lower than that the critical frequency (f_c), we could say that EWOD forces are the responsible of these deviations on the shape of the drop.

Also, no remarkable changes have been found either using DC voltages, even for 3000 V. Moreover, DC results are contradictory with what we were expecting to happen. However, due to the fact that the thickness of the wire used for the DC experiments was much bigger than that used for the AC tests, different electric field – specially locally – is thus created and perhaps we should have not expected that similar results to those obtained using AC voltage at low frequencies were supposed to happen using the DC power supply.

In the following section we will start the experimentation using the second setup which will allow to go up to higher voltages. Thus, we will see whether significant changes on contact angle can be achieved applying stronger electric fields on HFE-7500 droplets.

Chapter IV: Experimental results on Taylor cone configuration

As we have already introduced in paragraph *2.1* how the second configuration works, the main considerations that we must take into account and the description of its particular design, let us now present and discuss the experimental results with respect to this configuration[11]. Although the main setup used here is that one presented in section *2.1.2*, some unexpected results and side effects have forced us to use variations thereof. Therefore, experiments using water and HFE-7500 will be firstly shown. Then, other setups in which HFE-7500 liquid droplets have been tested, will be presented.

4.1. Experiment I: HFE-7500 – Two parallel plates

First of all, HFE-7500 was used. We deposited a large drop between the parallel plates and right after the voltage was applied. However, no effect have been observed on the computer screen. We could not apply voltages above 14000 V because little electric arcs were found around the periphery of the ITO plate. This might have been avoided by coating the entire ITO plate. The plates we have been using were not coated with Parylene-C all around, near the periphery there was a circle with a diameter of 1 mm which was not coated. Moreover, impurities and dust that are found in the air could create a path for unwanted electric currents, allowing the electric arc discharge.

Similarly as did in section *2.1.2.2*, we now calculate the maximum voltage at which the air between plates would break in absence of Parylene-C in order to justify why these electric arcs appear near the periphery of the ITO plate.

The problem becomes rather simple since we only have air as a dielectric layer. Then, the calculation is summarized as follows:

$$\Delta V_{max} = E_{breakdown\_air} \cdot a = 3\frac{kV}{mm} \cdot 15mm = 45\ kV \tag{25}$$

Taking 15 mm as the separation between plates – shorter separation we achieved which implies the most critical value – the air gap would theoretically break at 45 kV. However, this voltage will never be applied since our power supply only allows us to go up to 20 kV. As said, impurities and dust may be the responsible of the air breakdown, but actually in this case also the presence of drops could be the reason of the appearance of those arcs.

[11] It should be noted that the distance between plates could be shorter than 2 cm, in contrast to what have been expected at the beginning. Distances of about 1.5 cm could be reached.

In the end, applying voltages up to 14000 V resulted in no significant effects on HFE-7500 droplets. Therefore, we made the decision to use water instead of HFE-7500 with the aim to prove the setup worked properly.

4.2. Experiment II: Water – Two parallel plates

The main problem with using water with some salt as liquid is its contact angle. The initial contact angle of water droplets is higher than 12°, which is the maximum value that our interferometer can measure. Hence, we cannot detect if the contact angle is increasing or decreasing. However, since the shape of the drop is expected to be elongated, this can be nicely observed by taking a look at the apex of the drop which has low local angles and thus possible to be measured.

During preliminary experiments using water, the coating at the top window detached (see *Figure 50*). However, as it continued to function correctly (but with non-uniform spacing between the two electrodes) and the upper plate does not actually require an insulating layer since the drop is not in contact with the electrode, two tests at 13 and 14 kV were performed to get a qualitative picture.

In the following paragraph we present these two tests using water droplets on the second configuration. Unfortunately, as already said, voltages higher than 14 kV were not possible to apply due to the presence of electric arcs.

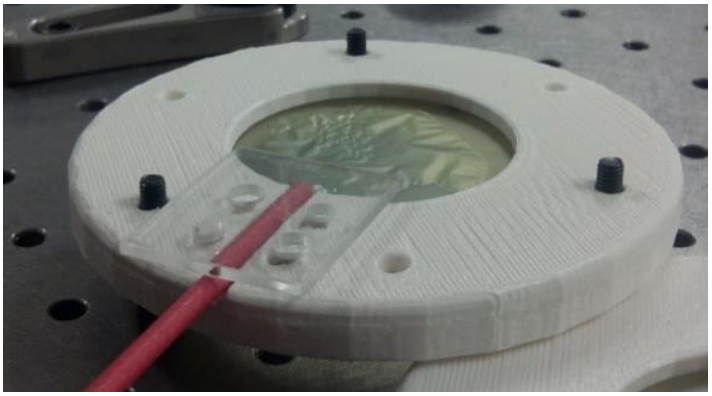

Figure 50 Picture of the upper plate after its breakdown.

4.2.1. Water Drop – 13000 V

A large water drop was deposited onto the substrate. It was observed that by means of applying a voltage of 13000 V, the interferometric image showed some changes. Therefore, let us now analyse these effects in order to prove that they were indeed significant.

Figure 51 shows how we see the droplet on the computer screen. As said, we do not focus on the contact angle, therefore it is not crucial to see the contact line of the drop on the screen. The apex of the drop is indicated by the white circumference in order to not confuse with the other

similar fringes which just are visual effects. We can also see how the fringes near the contact line are indistinguishable due to the high values of the contact angle. In *Figure 52* is plotted the height and local angle profiles for 0 V and 13000 V, in two different temporal instants. Despite the noise observed on the local angle profile, it is clear that there is an effect when the voltage is applied. The droplet elongates significantly in the field direction. *Figure 52* shows how local slopes become larger as soon as the electric field is applied. Moreover, the pointy top observed when the voltages turns on probably links at locally higher interface.

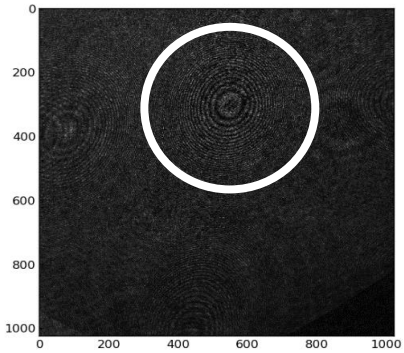

Figure 51 Water droplet fringes.

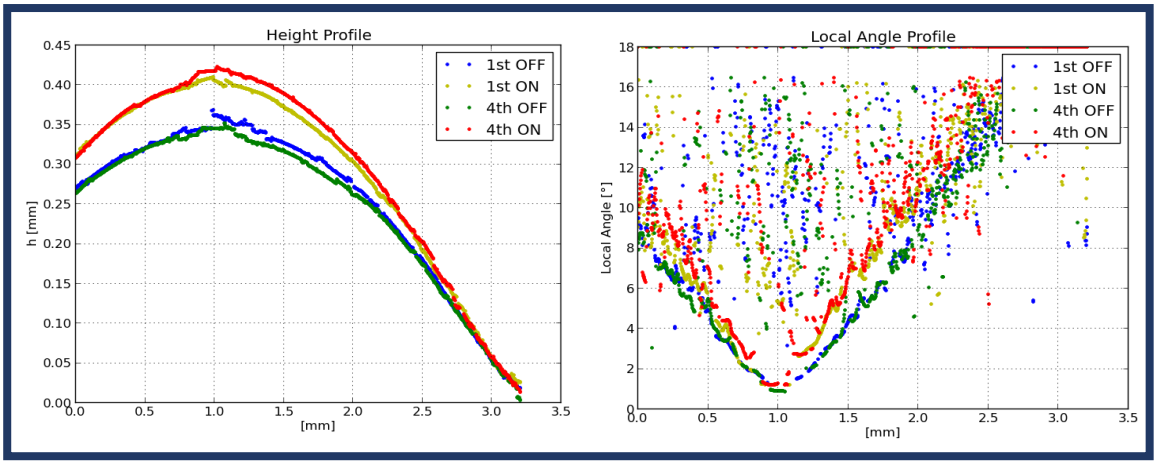

Figure 52 Height and Local angle profiles sessile water drop

4.2.2. Water Drop – 14000 V

The same experiment was conducted applying 14000 V. The elongation of the drop was expected to be slightly more significant as the electric field becomes stronger. Yet, the effect is similar to the 13000 V test.

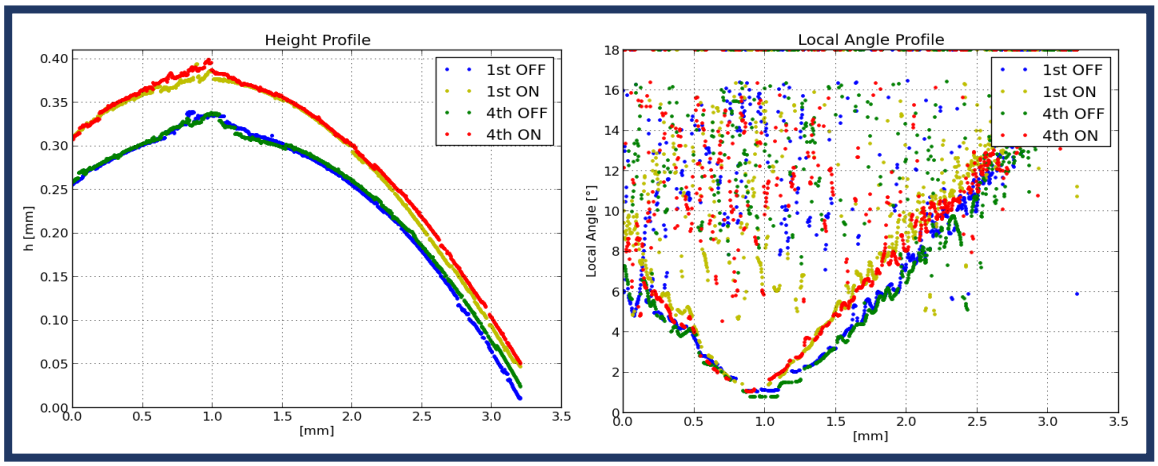

Figure 53 Height and Local angle profiles sessile water drop

4.3. Experiment III: HFE-7500 – Metal Ring

After having proved that the second setup was working as expected for water drops, we could say that unfortunately it was not accurately designed to perform experiments with HFE-7500 liquid droplets most probably due to a too large gap. Next experiments were conducted using a new variation of the second configuration in order to observe if there is any possible effect caused by the electric field on HFE-7500 drops.

The wire which was connect to the high voltage plate, was now connected to a metal ring with 17 cm of outer diameter and 6.5 cm of inner diameter (see *Figure 54*). This new design gives us better access to the centre of the bottom plate to deposit the droplet. Moreover, the ring can be placed closer to the drop which means a larger electric field strength.

Figure 54 Metal ring

Although this design includes some improvements, the main disadvantage is that we cannot see through the camera what is happening below the ring because it is not transparent. Despite the fact that we tried to deposit the droplet just in the centre of the ring, when the voltage is applied the droplet moves towards the edge and sometimes it is situated under the ring making it impossible to see what occurs from that point on. Notwithstanding, we could record several images of these experiments. Let us now analyse them.

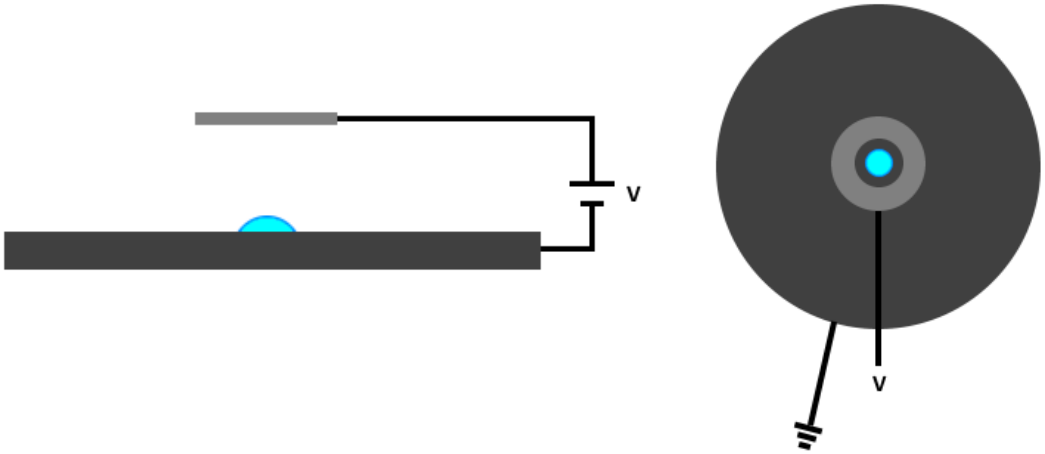

Figure 55 Metal ring configuration (A) side view and (B) upper view.

4.3.1. HFE-7500 4000 V – Attempt I

The following figures show the behaviour of the drop before applying the electric field and several images when the voltage is already applied.

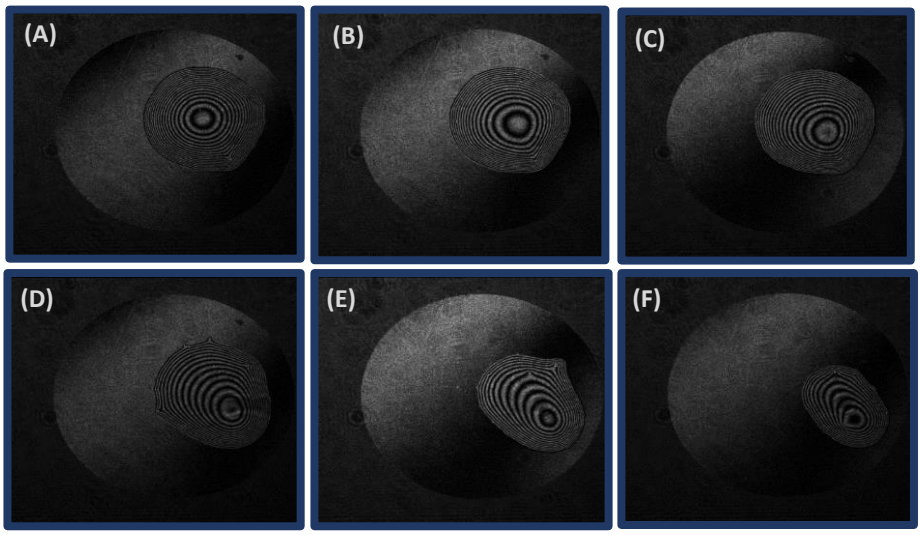

Figure 56 HFE-7500 droplet fringes using the ring setup variation

Figure 56 illustrates the sequence of images that corresponds to this experiment. Therein one can distinguish two regions: the ring is the black outer area of the image and the hole of the ring is the grey space. As shown, in this last region is where we must deposit the droplet.

As soon as the voltage is applied the droplet moves towards the ring. The apex of the drop has moved from the centre to be closer to the edge of the drop in the direction in which the droplet is directed.

The local angle homogeneously increases from the apex to the contact line when no electric field was applied (*Figure 56 (A)).* However, when the switch turns on, the input voltage influences the shape of the droplet and it varies in such a way that the region of the drop in which is moving increases its local angle as observed in the sequence illustrated in *Figure 57*. At the same time, the opposite region decreases its local angle.

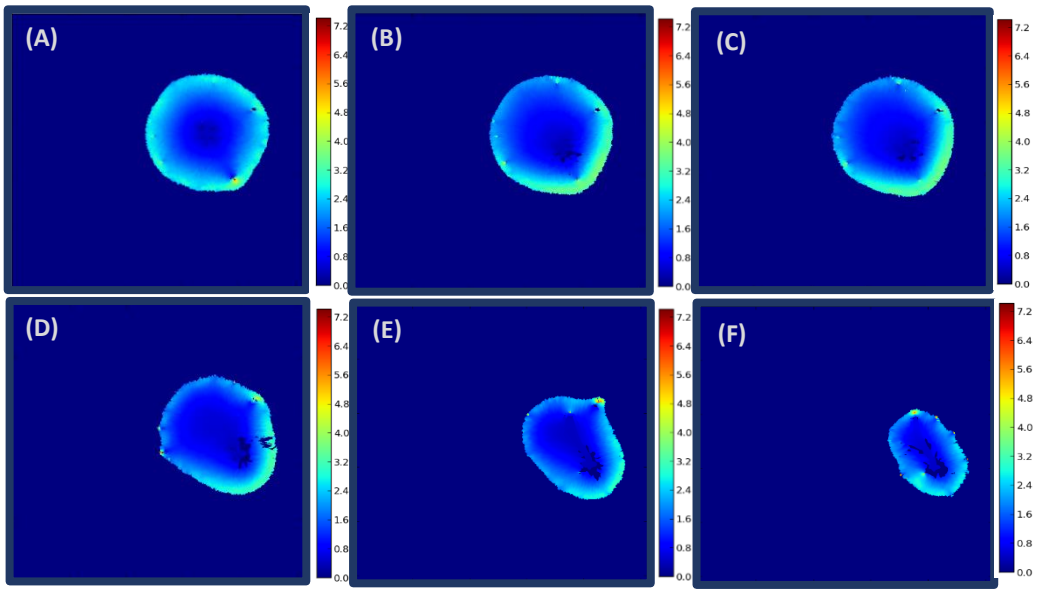

Figure 57 Local angle of HFE-7500 droplets using the ring setup variation

4.3.2. HFE-7500 4000 V – Attempt II

Once having seen how the droplet behaves when it is deposited in the centre of the plate, now we are going to present the same experiment but placing the droplet just below the ring. In this way, the droplet cannot be recorded by the camera, however, we are going to observe from the side and take some pictures of the effects that take place in this new situation.

Slightly after applying the voltage, the droplet started to eject some liquid from the apex to the ring. *Figure 58(A)* shows how the small droplet on the left takes a conical shape and ejects liquid directed to the metal ring. Another droplet placed on the centre of the image also started to eject liquid from its apex (see *Figure 58 (B)).*

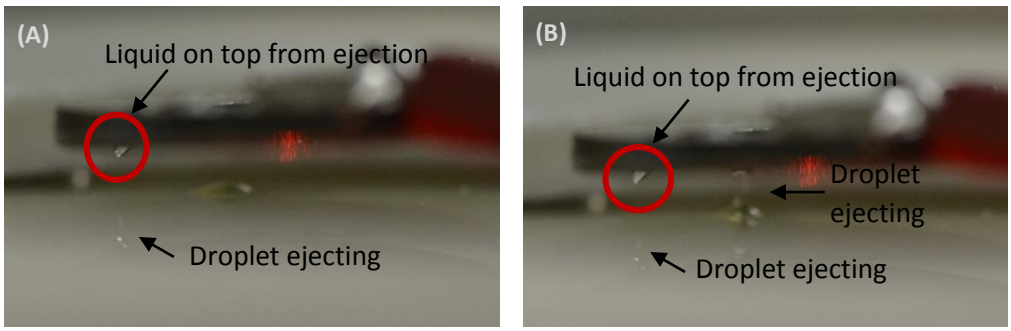

Figure 58 HFE-7500 droplet ejecting liquid in the field direction

The ejection of liquid is also demonstrated as the liquid at the top (indicated by the red circle on both images) could only come there by ejection.

4.4. Experiment IV: HFE-7500 – Needle

The main disadvantage of using the design presented in the last paragraph is that we could not follow the evolution of the contact angle over time when the voltage is applied. The droplet tends to moves towards the periphery of the ring and to be located under the metal area of the ring in which the camera cannot see the drop. Moreover, in those images in which the droplet was visible, the mask was not well extracted, and thereby the evolution of the contact angle was impossible to generate[12].

In order to avoid this, another variation of the second setup is presented. With the aim of maximizing the electric field strength, the wire which was connected to the ring is now connected to a needle and placed at a certain distance of the drop. This distance is estimated to be about 1 cm. Here, the electric field distribution is not equal as that one concerning two

[12] Sometimes, the program cannot distinguish the droplet from the background. Then, the contact angle measurements are not reliable.

parallel plates. As in the last case, neither the magnitude nor the direction of the electric field are the same at each point as it was in the first design of the second setup.

The voltages needed using this variation are much lower than those previously used. As shown in the following pictures, applying high voltages here resulted in a disintegration of the droplet.

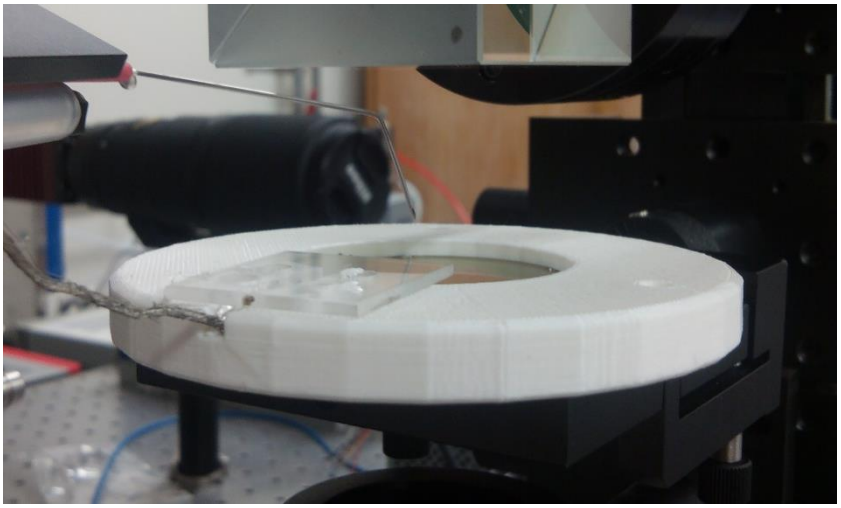

Figure 59 Needle configuration

Even for the lowest voltage allowed to apply using the DC supply and its amplifier, which was 40 V, the droplet seemed to have been broken.

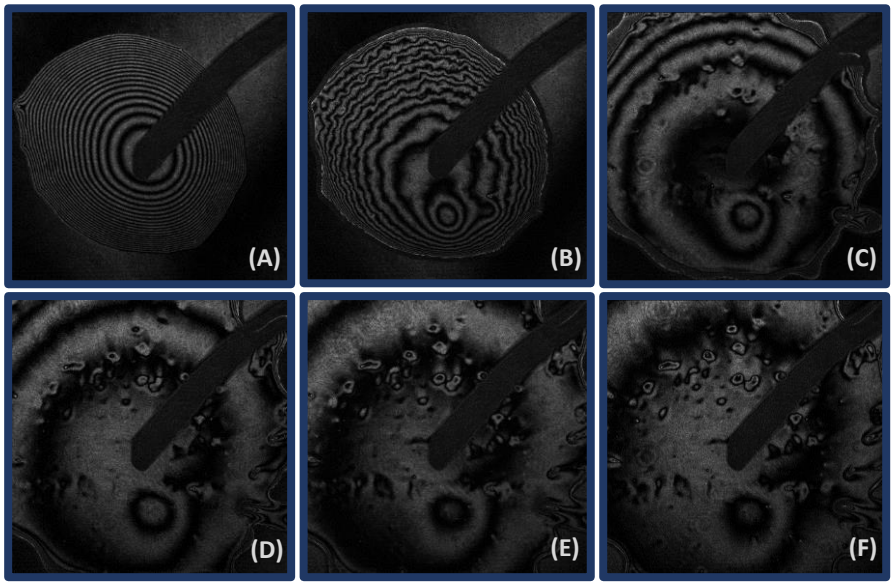

Figure 60 HFE-7500 droplet fringes using the needle setup variation

Right after applying the voltage, the droplet abruptly spreads. The fringes near the centre of the drop were suddenly separated while the fringes near the contact line brought together in such a way that we could hardly distinguish them.

The effect was so big that we could not properly analyse the evolution of the contact angle since the mask could not be well extracted – furthermore, the contact line did not lie within de camera's visual field when the voltage is applied.

It should be noted that the droplet did not return to its initial shape once the voltage was no longer applied. Due to the big disruption of the liquid when the switch turned on, we could say that the drop was not a droplet anymore. Lower voltages should be applied with the aim of proving if significant changes on the contact angle could be found but also if such effects would be reversible.

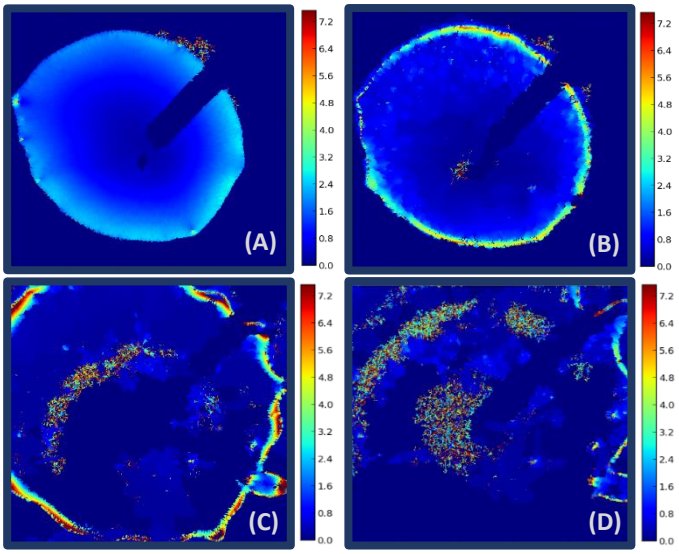

Figure 61 Local angles of HFE-7500 using the needle setup variation

Despite these problems, let us observe the local angle of the drop in the following pictures for the present experiment. As shown in Figure 60, but better observed in Figure 61, the contact angle increases in the beginning due to the fast expansion. Nevertheless, this is not necessarily expected to be larger in the equilibrium position.

4.5. Conclusions

What can be stated after having seen the behaviour of the drop when the voltage is applied is that HFE-7500 can be controlled by electric forces as many other liquids. However, its effectiveness is shown only for those situations in which the electric field is really high.

Using the first design of the second setup, the maximum electric field that has been applied was almost 10 kV/cm in the situation more favourable – 14000 V and a distance between plates of about 1.5 cm. The HFE-7500 droplet under these circumstances did not show any significant change whereas water droplets did. As already reported by Roero et al.[133], liquids with very low contact angle show less significant changes for the same magnitude of electric field applied, which means that higher electric fields are required for those liquids like HFE-7500.

Unfortunately, such high electric fields could not be achieved using the first design of the second configuration.

Nevertheless, using the two variations of the second configuration one could see how HFE-7500 can be modelled by the influence of an electric field. The metal ring setup showed how the droplet tends to be placed under the metal region when the voltage is applied. The reason could be probably the increase of the capacitance of the system, as Lambert[152] reported in his work. The last setup which used a needle as upper electrode showed that even applying low voltages (40 V) the droplet became completely deformed. Therefore, we can finally say that the effectiveness of the effect on the shape of a dielectric droplet is sharply influenced by the geometry of the setup, which in turn determines the strength of the electric field.

Chapter V: Conclusions and Outlook

In this work, we have investigated the behaviour of a highly wetting liquid under the influence of an electric field under ambient conditions. After a general review of the theoretical background and the applications of electrowetting, we presented a detailed description of the experimental apparatus developed with the aim of investigating these phenomena. In particular, two different setups have been studied: First, the most commonly used experimental configuration for electrowetting based on an ITO-coated glass with a Parylene-C layer deposited on the electrode surface as an insulating layer have been employed. Secondly, another setup which has been called Taylor cone configuration has been designed and put into practice. Therein, the voltage is applied between two parallel plates in which the droplet is not in contact with the electrode. The main goal of using this second setup is to prove whether dielectric liquids with very low contact angle can take the shape of a cone as other liquids do.

After giving details of these two effects and the corresponding explanations of their setups and experimental procedures, we continued by showing tests performed on an HFE-7500 droplet using the first setup where the electric field is created inside the droplet. Our main goal here was to measure the contact angle, the height and local angle profiles and the evaporation rate in two different scenarios: without applying the electric field and applying it. To this aim, we carried out different experiments. First, a comparison between three different situations was conducted under AC voltages: a droplet connected to a wire at 300 V, a droplet connect to a wire at 0 V and a freely evaporating droplet. Unfortunately, no significant changes were found in these first tests. Both contact angle and evaporation rate remained unaffected by the electric field. Yet, a remarkable difference was noted between the droplets attached to the wire and the freely evaporating one. For those droplets in which the wire was in contact with them, the contact angle tended to increase as the radius became smaller. On the other hand, the droplet which was freely evaporating maintained constant its contact angle as time goes on. Thus, the difference of the contact angle values was caused more by the change of the geometry than for the electric field itself. Next experiments focused on a single drop showed a slight change on the shape of the droplet when the electric field was applied. This deviation was situated always at the same distance of the centre of the drop, for both little and large liquid droplets.

In parallel with the above experiments, we also studied the influence of the AC frequency on the droplet behaviour. As the frequency came higher, less significant was the effect on the local angle. Following the explanations of Kumar et al[37]. reported in their study, we determined the frequency below which the liquid behaves as a conductor and above as a dielectric. We

observed that for those frequencies at which the droplet showed deviations in its shape corresponded to the frequencies at which the droplet behaved as a conductor.

Afterwards, the AC power supply was replaced by the DC in order to observe what happened in that case. Unlike we expected, the DC results showed surprisingly similar results regarding the local angle of those experiments using AC with high frequencies, i.e. no significant changes. The fact that the wire thickness is much larger inevitably leads to a different electric field. This creates perhaps a field which leads to shape deviations in locations where the shape cannot be measured by the interferometer. Future tests on a common configuration should be performed to elucidate this.

The main difficulty with this setup is that the electric field inside a dielectric drop is very complicated. In a conducting droplet, all interaction is limited to the solid-liquid interface and long range effects are understandable. But, in the present case, a numerical simulation is required to obtain this. Nevertheless, it can be anticipated that the electric field strength will drop off quickly with distance to the wire and therefore only local shape deviations of the droplet are understandable.

For the Taylor cone configuration, it should be mentioned that the initial parallel plate design was working correctly for water+salt droplets. However, a further reduction in separating distance is necessary to measure effects for HFE-7500 droplets. Unfortunately, due to the detachment of the coating on one wafer, such an optimalisation in our design could not be performed within the time-frame of the present work. Nevertheless, such an increase in field strength was achieved with two improvised configurations of a metal ring and a needle as a counter-electrode.

However, in these new configurations the field is not homogeneous which leads to displacement forces on the droplets. In the metal ring configuration, the droplet was displaced so as to cover as much space under the ring as possible, thus maximising the electrical capacity of the system. But, jetting could be observed in this configuration under the ring. For a needle-electrode configuration, the droplet underwent a violent spreading stage as again it wanted to maximise the electrical capacity of the system.

Appendices

A. Processing

2014-09-03 (7 man hours)

- Fabrication of stainless steel metal rings to support two-inch substrates during sputtering. (TB)
- Substrate (2 inch, glass) rinse in acetone, IPA and water
- - PVD (sputtering) ITO
  30' @ 200 W, $5 \cdot 10^{-3}$ mbar (Argon)
  Dektak XT profilemeter: **ITO = 2.2 to 2.5 µm**
- Conductivity across substrate <10 Ω
- Annealing step
  10' @ 330 °C on hot plate
- Conductivity across substrate <10 Ω

Annealing not really necessary. Substrate 1 showed many microcracks in ITO layer (wafer cleaned in HCl [1:1] and recoated with longer presputtering time). Both ITO layers have some pinholes. Thinner layer probably better.

2014-09-18 (2 man hours)

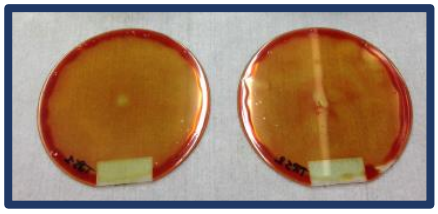

- CVD Parylene C
  10'' plasma clean @ 100 W
  0.1 ml silane adhesion promoter
  20 g Parylene C dimer
- Design (PG) & fabrication (CDE) of photoplot for Parylene pattering.

2014-09-29 (6 man hours)

- Photoresist spin coating
  Ma-P 1275 HV
  60'' @ 1000 rpm
- Soft bake procedure
  2' relaxation (to decrease edge bead, not done in first run)
  5' @ 120 °C
  15' cool down on hot plate
  10' relaxation at RT (not done in first run)
- UV exposure using photoplot
  900 $mJ \cdot cm^{-2}$ @ 365 nm
- Resist development
  8' in 351-developer [3 parts water, 1 part 351]
  Rinse and dry
- Reactive ion etching
  19' @ 200 W | 100 mTorr chamber pressure with 40 sccm O_2
- Resist stripping
  Acetone, IPA, water, dry
  Dektak XT profilometer: **Parylene C = 8.8 to 9.3 µm**

B. Radius as a function of Time (*2.1.1. Experiment I: Comparison between three different cases*)

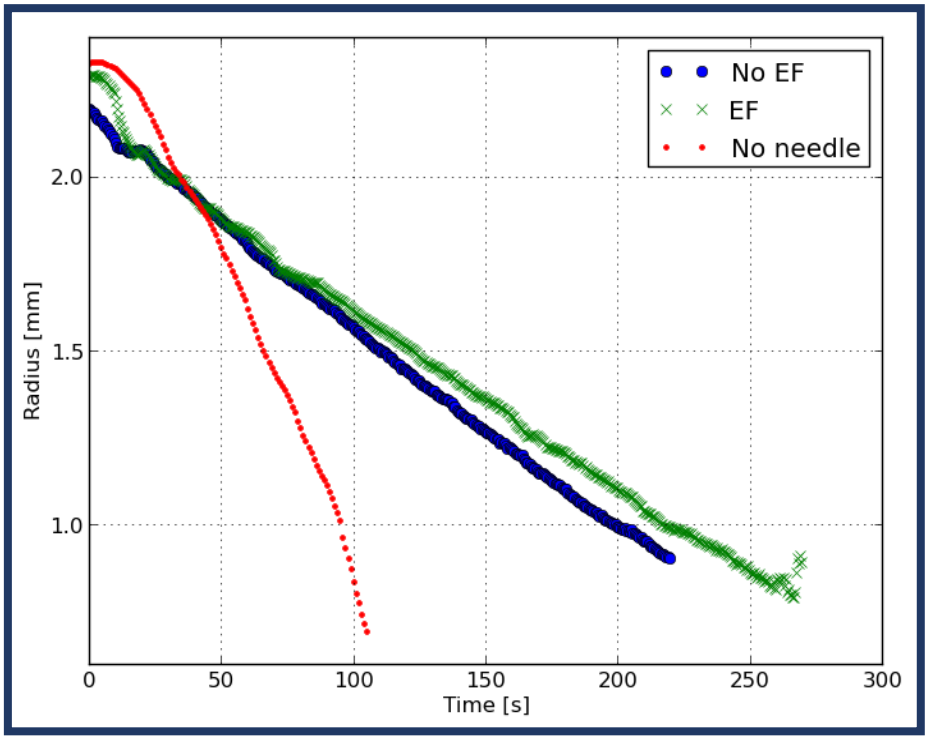

C. Volume as a function of Time (*2.1.2. Experiment II: Electric Field On and Off on the same drop*)

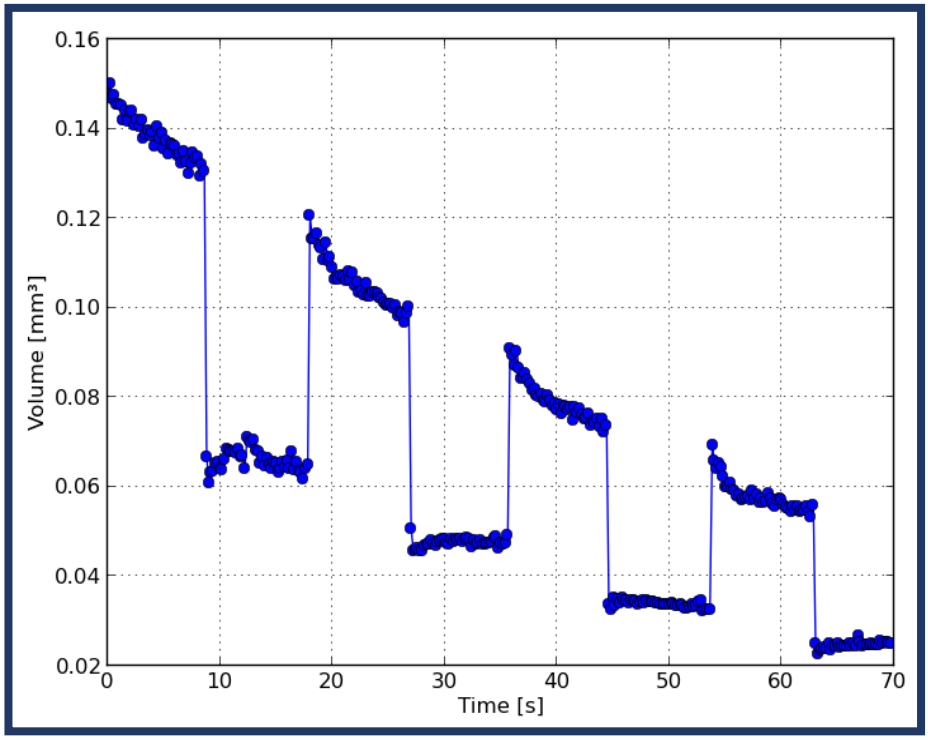

D. Blurred images (*2.1.3. Experiment III: AC frequency dependence*)

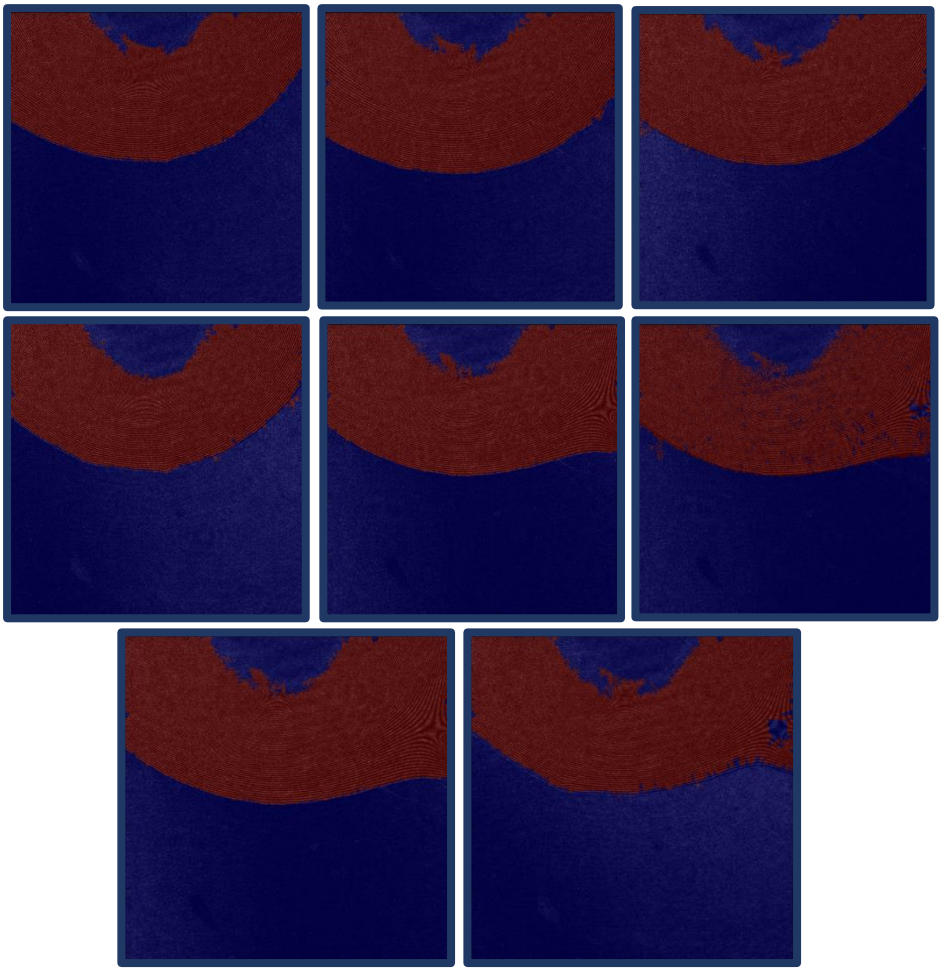

E. Contact angle results (*2.1.3. Experiment III: AC frequency dependence*)

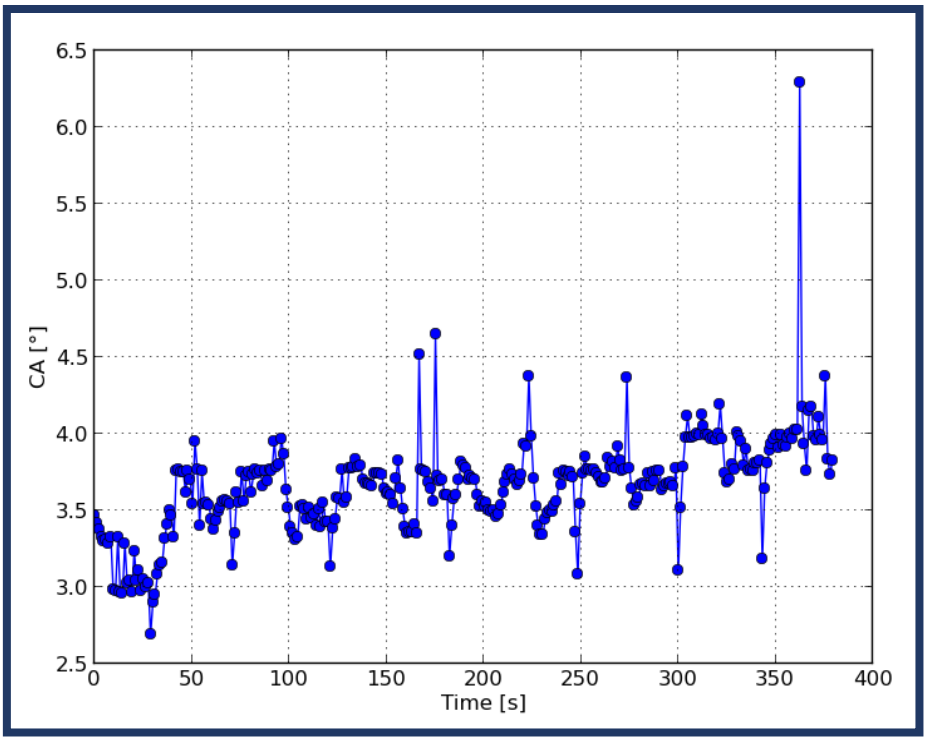

F. Design – Parallel plates (*2.2.2. Parallel discs design*)

Bottom plate

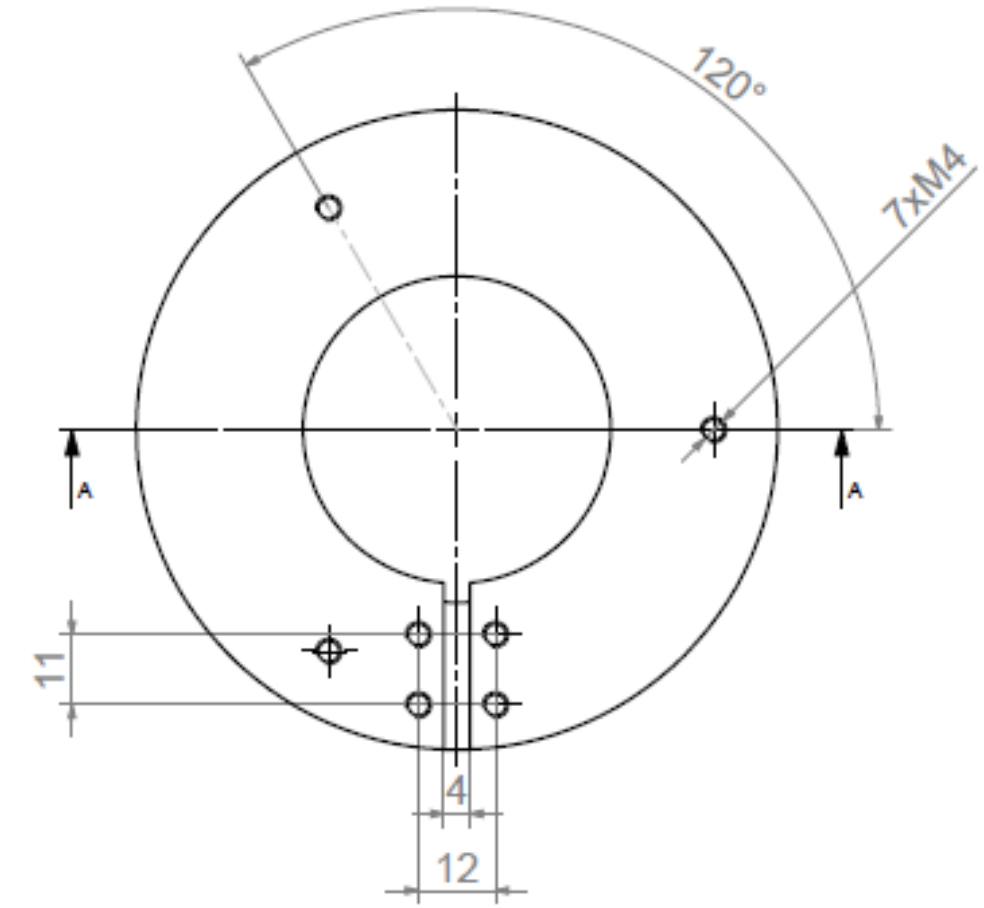

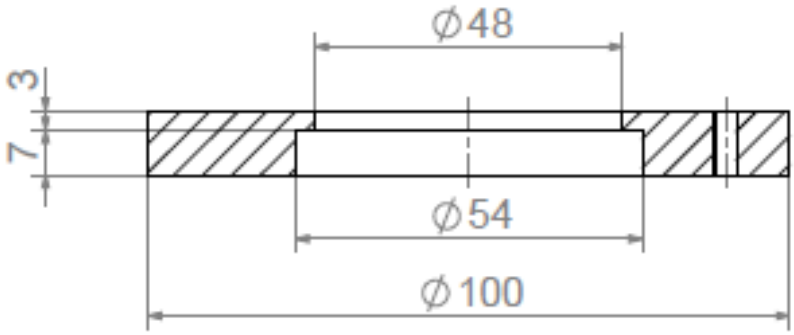

Upper plate

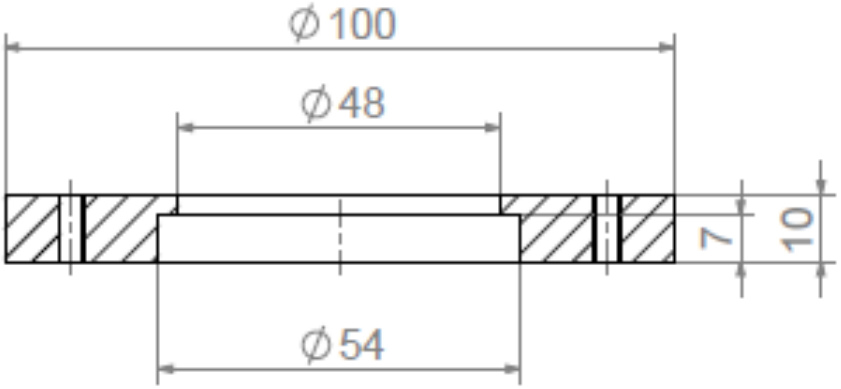

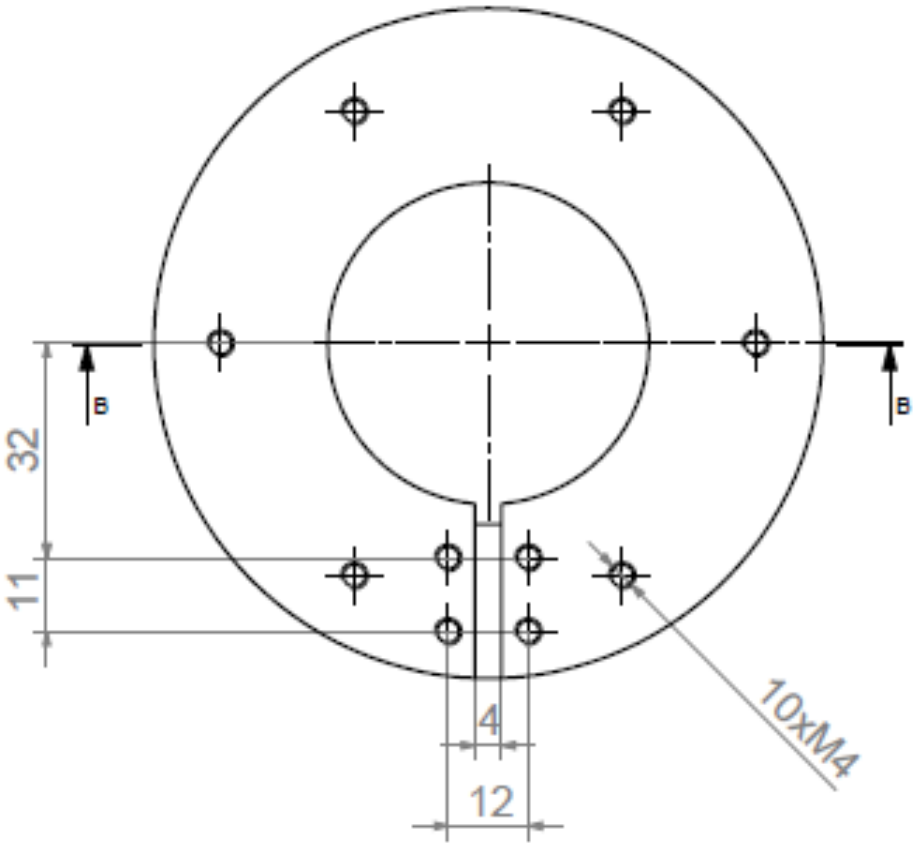

G. Electric field – Conductive droplets[153]

The force felt by a charge is directly proportional to the field strength, this force being characterized by:

$$\vec{F} = q\vec{E} \tag{26}$$

In a free space, the electric field is given by the following relation:

$$\int_S \vec{E} \cdot \overrightarrow{dS} = \int_V (\vec{\nabla} \cdot \vec{E}) dV = \int_V (div\, \vec{E}) dV \tag{27}$$

The differential form of Gauss theorem is thus obtainable,

$$div\vec{E} = \frac{\rho_0}{\varepsilon_0} \tag{28}$$

Under static conditions, the electric potential V is defined as:

$$\vec{E} = -\overrightarrow{grad}V = \frac{1}{4\pi\varepsilon_0} \sum_{i=1}^{N} \frac{q_i}{r_i} \tag{29}$$

Then,

$$div\vec{E} = div\left(-\overrightarrow{grad}V\right) = -\nabla^2 V \tag{30}$$

Combining Eq. 28 with Eq. 30, the equation ruling the shape of an electrostatic field is given by:

$$-\nabla^2 V = \Delta(V) = -\frac{\rho}{\varepsilon_0} \tag{31}$$

As said, the intrinsic charge is null because every charges are only present within the interface, then the Eq. 7 becomes:

$$\Delta(V) = 0 \tag{32}$$

Bibliography

1. Lyklema, J. *Fundamentals of Interface and Colloid Science: Solid-Liquid Interfaces*. (Academic Press, 1995).

2. Oh, J. M., Ko, S. H. & Kang, K. H. Shape Oscillation of a Drop in ac Electrowetting. 8379–8386 (2008).

3. Steckl, A. J., You, H. & Kim, D.-Y. <title>Flexible electrowetting and electrowetting on flexible substrates. **7956,** 795607–795607–6 (2011).

4. Fengyu Li, Y. Z. and Y. S. *Core-Shell Nanofibers: Nano Channel and Capsule by Coaxial Electrospinning*. (InTech, 2010). doi:10.5772/45660

5. Tsoumpas, I., Colinet, P. & Buchlin, J. Experimental Study of the Evaporation of Sessile Droplets of Perfectly-Wetting Pure Liquids. (2014).

6. Yanagisawa, T., Nakajima, A., Sakai, M., Kameshima, Y. & Okada, K. Preparation and abrasion resistance of transparent super-hydrophobic coating by combining crater-like silica films with acicular boehmite powder. *Mater. Sci. Eng. B* **161,** 36–39 (2009).

7. Perelaer, J., Hendriks, C. E., de Laat, A. W. M. & Schubert, U. S. One-step inkjet printing of conductive silver tracks on polymer substrates. *Nanotechnology* **20,** 165303 (2009).

8. Son, Y., Kim, C., Yang, D. H. & Ahn, D. J. Spreading of an inkjet droplet on a solid surface with a controlled contact angle at low Weber and Reynolds numbers. *Langmuir* **24,** 2900–7 (2008).

9. *Microsystem Technology in Chemistry and Life Science*. **194,** (Springer Berlin Heidelberg, 1998).

10. Jakeway, S. C., de Mello, A. J. & Russell, E. L. Miniaturized total analysis systems for biological analysis. *Fresenius. J. Anal. Chem.* **366,** 525–39

11. Hong, J. W. & Quake, S. R. Integrated nanoliter systems. *Nat. Biotechnol.* **21,** 1179–83 (2003).

12. Cho, S. K., Moon, H. & Kim, C.-J. Creating, transporting, cutting, and merging liquid droplets by electrowetting-based actuation for digital microfluidic circuits. *J. Microelectromechanical Syst.* **12,** 70–80 (2003).

13. Kuiper, S. & Hendriks, B. H. W. Variable-focus liquid lens for miniature cameras. *Appl. Phys. Lett.* **85,** 1128 (2004).

14. Maillard, M., Legrand, J. & Berge, B. Two Liquids Wetting and Low Hysteresis Electrowetting on Dielectric Applications. *Langmuir* **25,** 8368–8368 (2009).

15. Hao, C. *et al.* Electrowetting on liquid-infused film (EWOLF): complete reversibility and controlled droplet oscillation suppression for fast optical imaging. *Sci. Rep.* **4,** 6846 (2014).

16. Ren, H. & Wu, S.-T. *Introduction to Adaptive Lenses*. (John Wiley & Sons, 2012).

17. Beni, G. Electro-wetting displays. *Appl. Phys. Lett.* **38,** 207 (1981).

18. Hayes, R. A. *et al.* 52.1: A High Brightness Colour 160 PPI Reflective Display Technology Based on Electrowetting. *SID Symp. Dig. Tech. Pap.* **35,** 1412 (2004).

19. Hayes, R. A. & Feenstra, B. J. Video-speed electronic paper based on electrowetting. *Nature* **425,** 383–5 (2003).

20. Mugele, F. & Baret, J. Electrowetting : from basics to applications.

21. Chen, L. & Bonaccurso, E. Electrowetting -- from statics to dynamics. *Adv. Colloid Interface Sci.* **210,** 2–12 (2014).

22. Pellicer, J., García-Morales, V. & Hernández, M. J. On the demonstration of the Young-Laplace equation in introductory physics courses. *Phys. Educ.* **35,** 126–129 (2000).

23. Yoon, Y., Kim, D. & Lee, J.-B. Hierarchical micro/nano structures for super-hydrophobic surfaces and super-lyophobic surface against liquid metal. *Micro Nano Syst. Lett.* **2,** 3 (2014).

24. Prins, M. W., Welters, W. J. & Weekamp, J. W. Fluid control in multichannel structures by electrocapillary pressure. *Science* **291,** 277–80 (2001).

25. Nelson, W. C. & Kim, C.-J. 'CJ'. Droplet Actuation by Electrowetting-on-Dielectric (EWOD): A Review. *J. Adhes. Sci. Technol.*

26. Lippmann, G. Relation entre les phénomènes électriques et capillaires. 494–549

27. BERGE, B. Électrocapillarité et mouillage de films isolants par l'eau. *Comptes rendus l'Académie des Sci.* **317,** 157–163 (1993).

28. Welters, W. J. J. & Fokkink, L. G. J. Fast Electrically Switchable Capillary Effects. **7463,** 1535–1538 (1998).

29. Berthier, J. *Micro-Drops and Digital Microfluidics*. (William Andrew, 2012).

30. Raccurt, O., Berthier, J., Clementz, P., Borella, M. & Plissonnier, M. On the influence of surfactants in electrowetting systems. *J. Micromechanics Microengineering* **17,** 2217–2223 (2007).

31. Jones, T. B. On the Relationship of Dielectrophoresis and. 4437–4443 (2002).

32. Jones, T. B., Fowler, J. D., Chang, Y. S. & Kim, C.-J. Frequency-Based Relationship of Electrowetting and Dielectrophoretic Liquid Microactuation. *Langmuir* **19,** 7646–7651 (2003).

33. Masliyah, J. H. & Bhattacharjee, S. *Electrokinetic and Colloid Transport Phenomena*. (John Wiley & Sons, 2006).

34. Mugele, F. & Buehrle, J. Equilibrium drop surface profiles in electric fields. *J. Phys. Condens. Matter* **19,** 375112 (2007).

35. Jones, T. B., Wang, K.-L. & Yao, D.-J. Frequency-Dependent Electromechanics of Aqueous Liquids: Electrowetting and Dielectrophoresis. *Langmuir* **20,** 2813–2818 (2004).

36. Mugele, F., Klingner, A., Buehrle, J., Steinhauser, D. & Herminghaus, S. Electrowetting: a convenient way to switchable wettability patterns. *J. Phys. Condens. Matter* **17,** S559–S576 (2005).

37. Kumar, A., Pluntke, M., Cross, B., Baret, J.-C. & Mugele, F. Finite conductivity effects and apparent contact angle saturation in AC electrowetting. *MRS Proc.* **899,** 0899–N06–01 (2005).

38. Chevalliot, S., Heikenfeld, J., Clapp, L., Milarcik, A. & Vilner, S. Analysis of Nonaqueous Electrowetting Fluids for Displays. *J. Disp. Technol.* **7,** 649–656 (2011).

39. Bateni, A., Ababneh, A., Elliott, J. A. W., Neumann, A. W. & Amirfazli, A. Effect of gravity and electric field on shape and surface tension of drops. *Adv. Sp. Res.* **36,** 64–69 (2005).

40. Marco, P. Di, Pedretti, F., Saccone, G., Pisa, U. & Lazzarino, L. effect of an external electric field on the shape of a dielectric sessile drop t fg. (2013).

41. Kumari, N., Bahadur, V. & Garimella, S. V. Electrical actuation of electrically conducting and insulating droplets using ac and dc voltages. *J. Micromechanics Microengineering* **18,** 105015 (2008).

42. Chatterjee, D., Hetayothin, B., Wheeler, A. R., King, D. J. & Garrell, R. L. Droplet-based microfluidics with nonaqueous solvents and solutions. *Lab Chip* **6,** 199–206 (2006).

43. Jones, T. B., Gunji, M., Washizu, M. & Feldman, M. J. Dielectrophoretic liquid actuation and nanodroplet formation. *J. Appl. Phys.* **89,** 1441 (2001).

44. Bahadur, V. & Garimella, S. V. An energy-based model for electrowetting-induced droplet actuation. *J. Micromechanics Microengineering* **16,** 1494–1503 (2006).

45. Seyrat, E. & Hayes, R. A. Amorphous fluoropolymers as insulators for reversible low-voltage electrowetting. *J. Appl. Phys.* **90,** 1383 (2001).

46. Koo, B. & Kim, C.-J. Evaluation of repeated electrowetting on three different fluoropolymer top coatings. *J. Micromechanics Microengineering* **23,** 067002 (2013).

47. Saeki, F. *et al.* Electrowetting on Dielectrics (EWOD): Microfluidics. 5–6

48. Chevalliot, S., Kuiper, S. & Heikenfeld, J. Experimental Validation of the Invariance of Electrowetting Contact Angle Saturation. *J. Adhes. Sci. Technol.* **ahead-of-p,** 1–22 (2012).

49. Lin, Y.-Y. *et al.* Low Voltage Electrowetting-on-Dielectric Platform using Multi-Layer Insulators. *Sens. Actuators. B. Chem.* **150,** 465–470 (2010).

50. Cahill, B. P. *et al.* Optimization of electrowetting electrodes: Analysis of the leakage current characteristics of various dielectric layers. in *2008 11th International Biennial Baltic Electronics Conference* 79–82 (IEEE, 2008).

51. Raj, B., Smith, N. R., Christy, L., Dhindsa, M. & Heikenfeld, J. Composite Dielectrics and Surfactants for Low Voltage Electrowetting Devices. in *2008 17th Biennial University/Government/Industry Micro/Nano Symposium* 187–190 (IEEE, 2008).

52. Choi, S. *et al.* Improvement in the breakdown properties of electrowetting using polyelectrolyte ionic solution. *Langmuir* **29,** 501–9 (2013).

53. Verheijen, H. J. J. & Prins, M. W. J. Reversible Electrowetting and Trapping of Charge: Model and Experiments. *Langmuir* **15,** 6616–6620 (1999).

54. Bratko, D., Daub, C. D., Leung, K. & Luzar, A. Effect of field direction on electrowetting in a nanopore. *J. Am. Chem. Soc.* **129,** 2504–10 (2007).

55. Bratko, D., Daub, C. D. & Luzar, A. Water-mediated ordering of nanoparticles in an electric field. *Faraday Discuss.* **141,** 55 (2009).

56. Daub, C. D., Bratko, D., Leung, K. & Luzar, A. Electrowetting at the Nanoscale. *J. Phys. Chem. C* **111,** 505–509 (2007).

57. Kuo, J. S., Spicar-Mihalic, P., Rodriguez, I. & Chiu, D. T. Electrowetting-Induced Droplet Movement in an Immiscible Medium. *Langmuir* **19,** 250–255 (2003).

58. Wan, Z., Zeng, H. & Feinerman, A. Reversible Electrowetting of Liquid-Metal Droplet. *J. Fluids Eng.* **129,** 388 (2007).

59. Brassard, D., Malic, L., Normandin, F., Tabrizian, M. & Veres, T. Water-oil core-shell droplets for electrowetting-based digital microfluidic devices. *Lab Chip* **8,** 1342–9 (2008).

60. Srinivasan, V., Pamula, V. K. & Fair, R. B. An integrated digital microfluidic lab-on-a-chip for clinical diagnostics on human physiological fluids. *Lab Chip* **4,** 310–5 (2004).

61. Brassard, D., Malic, L., Normandin, F., Tabrizian, M. & Veres, T. ELECTROWETTING-BASED DIGITAL MICRO- FLUIDIC SYSTEMS BY USING WATER-OIL CORE- SHELL DROPLETS. 772–774 (2008).

62. Moon, H., Wheeler, A. R., Garrell, R. L., Loo, J. A. & Kim, C.-J. C. An integrated digital microfluidic chip for multiplexed proteomic sample preparation and analysis by MALDI-MS. *Lab Chip* **6,** 1213–9 (2006).

63. Gupta, R., Sheth, D. M., Boone, T. K., Sevilla, A. B. & Fréchette, J. Impact of pinning of the triple contact line on electrowetting performance. *Langmuir* **27,** 14923–9 (2011).

64. Li, F. & Mugele, F. How to make sticky surfaces slippery: Contact angle hysteresis in electrowetting with alternating voltage. *Appl. Phys. Lett.* **92,** 244108 (2008).

65. Nelson, W. C., Sen, P. & Kim, C.-J. C. J. Dynamic contact angles and hysteresis under electrowetting-on-dielectric. *Langmuir* **27,** 10319–26 (2011).

66. Findenegg, G. H. & Herminghaus, S. Wetting: Statics and dynamics. *Curr. Opin. Colloid Interface Sci.* **2,** 301–307 (1997).

67. Chang, J., Choi, D. Y., Han, S. & Pak, J. J. Driving characteristics of the electrowetting-on-dielectric device using atomic-layer-deposited aluminum oxide as the dielectric. *Microfluid. Nanofluidics* **8,** 269–273 (2009).

68. Pollack, M. G., Fair, R. B. & Shenderov, A. D. Electrowetting-based actuation of liquid droplets for microfluidic applications. *Appl. Phys. Lett.* **77,** 1725 (2000).

69. Kornyshev, A. A. *et al.* Ultra-Low-Voltage Electrowetting. *J. Phys. Chem. C* **114,** 14885–14890 (2010).

70. Yuan, Y. & Lee, T. R. *Surface Science Techniques*. **51,** (Springer Berlin Heidelberg, 2013).

71. Gupta, R., Boone, T., Sheth, D., Sevilla, A. & Frechette, J. Influence of contact angle hysteresis on electrowetting performance. 2–4

72. Verheijen, H. J. J. & Prins, M. W. J. Reversible Electrowetting and Trapping of Charge : 6616–6620 (1999).

73. Yang, S.-Y., Hirasaki, G. ., Basu, S. & Vaidya, R. Mechanisms for contact angle hysteresis and advancing contact angles. *J. Pet. Sci. Eng.* **24,** 63–73 (1999).

74. Peykov, V., Quinn, A. & Ralston, J. Electrowetting: a model for contact-angle saturation. *Colloid Polym. Sci.* **278,** 789–793 (2000).

75. Buehrle, J., Herminghaus, S. & Mugele, F. Interface Profiles near Three-Phase Contact Lines in Electric Fields. *Phys. Rev. Lett.* **91,** 086101 (2003).

76. Drygiannakis, A. I., Papathanasiou, A. G. & Boudouvis, A. G. On the connection between dielectric breakdown strength, trapping of charge, and contact angle saturation in electrowetting. *Langmuir* **25,** 147–52 (2009).

77. Vallet, M., Vallade, M. & Berge, B. Limiting phenomena for the spreading of water on polymer films by electrowetting. *Eur. Phys. J. B* **11,** 583–591 (1999).

78. Song, J. H., Evans, R., Lin, Y.-Y., Hsu, B.-N. & Fair, R. B. A scaling model for electrowetting-on-dielectric microfluidic actuators. *Microfluid. Nanofluidics* **7,** 75–89 (2008).

79. Bhushan, B. & Pan, Y. Role of electric field on surface wetting of polystyrene surface. *Langmuir* **27,** 9425–9 (2011).

80. Nanayakkara, Y. S. *et al.* The effect of AC frequency on the electrowetting behavior of ionic liquids. *Anal. Chem.* **82,** 3146–54 (2010).

81. Paneru, M., Priest, C., Sedev, R. & Ralston, J. Electrowetting of Aqueous Solutions of Ionic Liquid in Solid−Liquid−Liquid Systems. *J. Phys. Chem. C* **114,** 8383–8388 (2010).

82. Paneru, M., Priest, C., Sedev, R. & Ralston, J. Static and dynamic electrowetting of an ionic liquid in a solid/liquid/liquid system. *J. Am. Chem. Soc.* **132,** 8301–8 (2010).

83. Zhang, S. *et al.* Enhanced and reversible contact angle modulation of ionic liquids in oil and under AC electric field. *Chemphyschem* **11,** 2327–31 (2010).

84. Quilliet, C. & Berge, B. Electrowetting: a recent outbreak. *Curr. Opin. Colloid Interface Sci.* **6,** 34–39 (2001).

85. Vallet, M., Berge, B. & Vovelle, L. Electrowetting of water and aqueous solutions on poly(ethylene terephthalate) insulating films. *Polymer (Guildf).* **37,** 2465–2470 (1996).

86. Ko, S. H., Lee, H. & Kang, K. H. Hydrodynamic Flows in Electrowetting. 1094–1101 (2008).

87. Miraghaie, R., Sterling, J. D. & Nadim, A. Shape Oscillation and Internal Mixing in Sessile Liquid Drops Using Electrowetting-on-Dielectric (EWOD). 610–613 (2006).

88. Baret, J.-C., Decré, M. M. J. & Mugele, F. Self-excited drop oscillations in electrowetting. *Langmuir* **23,** 5173–9 (2007).

89. Srinivasan, V., Pamula, V., Pollack, M. & Fair, R. A digital microfluidic biosensor for multianalyte detection. in *The Sixteenth Annual International Conference on Micro Electro Mechanical Systems, 2003. MEMS-03 Kyoto. IEEE* 327–330 (IEEE).

90. Yoon, J.-Y. & Garrell, R. L. Preventing Biomolecular Adsorption in Electrowetting-Based Biofluidic Chips. *Anal. Chem.* **75,** 5097–5102 (2003).

91. Mugele, F., Staicu, A., Bakker, R. & van den Ende, D. Capillary Stokes drift: a new driving mechanism for mixing in AC-electrowetting. *Lab Chip* **11,** 2011–6 (2011).

92. García-Sánchez, P., Ramos, A. & Mugele, F. Electrothermally driven flows in ac electrowetting. *Phys. Rev. E* **81,** 015303 (2010).

93. Lee, H., Yun, S., Ko, S. H. & Kang, K. H. An electrohydrodynamic flow in ac electrowetting. *Biomicrofluidics* **3,** 44113 (2009).

94. Mugele, F., Baret, J.-C. & Steinhauser, D. Microfluidic mixing through electrowetting-induced droplet oscillations. *Appl. Phys. Lett.* **88,** 204106 (2006).

95. Oh, J. M., Legendre, D. & Mugele, F. Shaken not stirred —On internal flow patterns in oscillating sessile drops. *EPL (Europhysics Lett.* **98,** 34003 (2012).

96. Baret, J.-C. & Mugele, F. Electrical Discharge in Capillary Breakup: Controlling the Charge of a Droplet. *Phys. Rev. Lett.* **96,** 016106 (2006).

97. Li, X., He, G. & Zhang, X. Numerical simulation of drop oscillation in AC electrowetting. *Sci. China Physics, Mech. Astron.* **56,** 383–394 (2013).

98. Mampallil, D., Burak Eral, H., Staicu, A., Mugele, F. & van den Ende, D. Electrowetting-driven oscillating drops sandwiched between two substrates. *Phys. Rev. E* **88,** 053015 (2013).

99. Blake, T. D., Clarke, A. & Stattersfield, E. H. An Investigation of Electrostatic Assist in Dynamic Wetting. *Langmuir* **16,** 2928–2935 (2000).

100. Gabay, C., Berge, B., Dovillaire, G. & Bucourt, S. Dynamic study of a Varioptic variable focal lens. in *International Symposium on Optical Science and Technology* (eds. Fischer, R. E., Smith, W. J. & Johnson, R. B.) 159–165 (International Society for Optics and Photonics, 2002).

101. Engineering, M., Electrowetting, S., Electrowetting, D. & At, O. Electrowetting, Applications. 277–280 (2003).

102. Shamai, R., Andelman, D., Berge, B. & Hayes, R. Water, electricity, and between… On electrowetting and its applications. *Soft Matter* **4,** 38 (2008).

103. Zhao, Y. & Wang, Y. Fundamentals and Applications of Electrowetting : A Critical Review Abstract : **1,** (2013).

104. Berge, B. & Peseux, J. Variable focal lens controlled by an external voltage: An application of electrowetting. *Eur. Phys. J. E* **3,** 159–163 (2000).

105. Krupenkin, T., Yang, S. & Mach, P. Tunable liquid microlens. *Appl. Phys. Lett.* **82,** 316 (2003).

106. Krogmann, F., Mönch, W. & Zappe, H. A MEMS-based variable micro-lens system. *J. Opt. A Pure Appl. Opt.* **8,** S330–S336 (2006).

107. Bucaro, M. A. *et al.* Tunable liquid optics: electrowetting-controlled liquid mirrors based on self-assembled Janus tiles. *Langmuir* **25,** 3876–9 (2009).

108. Kang, M. & Yue, R. Variable-Focus Liquid Lens Based on EWOD. *J. Adhes. Sci. Technol.* **ahead-of-p,** 1–6 (2012).

109. Im, M. *et al.* Adhesion Force Change by Electrowetting on a Polymer Microlens Array. (2012).

110. Rogers, J. A. *et al.* Paper-like electronic displays: large-area rubber-stamped plastic sheets of electronics and microencapsulated electrophoretic inks. *Proc. Natl. Acad. Sci. U. S. A.* **98,** 4835–40 (2001).

111. You, H. & Steckl, A. J. Three-color electrowetting display device for electronic paper. *Appl. Phys. Lett.* **97,** 023514 (2010).

112. Heikenfeld, J., Drzaic, P., Yeo, J.-S. & Koch, T. Review Paper: A critical review of the present and future prospects for electronic paper. *J. Soc. Inf. Disp.* **19,** 129 (2011).

113. Kim, D. Y. & Steckl, A. J. Electrowetting on paper for electronic paper display. *ACS Appl. Mater. Interfaces* **2,** 3318–23 (2010).

114. Wheeler, A. R., Moon, H., Kim, C.-J., Loo, J. A. & Garrell, R. L. Electrowetting-based microfluidics for analysis of peptides and proteins by matrix-assisted laser desorption/ionization mass spectrometry. *Anal. Chem.* **76,** 4833–8 (2004).

115. Ratner, D. M. *et al.* Microreactor-based reaction optimization in organic chemistry--glycosylation as a challenge. *Chem. Commun. (Camb).* 578–80 (2005). doi:10.1039/b414503h

116. Karuwan, C. *et al.* Electrochemical detection on electrowetting-on-dielectric digital microfluidic chip. *Talanta* **84,** 1384–9 (2011).

117. Zhou, J. *et al.* Superhydrophobic ZnO for EWOD Digital Microfluidic Device for Application in Micro Total Analysis System (μ-TAS). (2012). at

118. Tian, H. *et al.* Evaporation Phenomenon in Micro Polymerase Chain Reaction (μPCR) System and a Possible Electrowetting Solution. (2012).

119. Cheng, J.-T. & Chen, C.-L. Active thermal management of on-chip hot spots using EWOD-driven droplet microfluidics. *Exp. Fluids* **49,** 1349–1357 (2010).

120. Vancauwenberghe, V., Di Marco, P. & Brutin, D. Wetting and evaporation of a sessile drop under an external electrical field: A review. *Colloids Surfaces A Physicochem. Eng. Asp.* **432,** 50–56 (2013).

121. Rayleigh, Lord. On the equilibrium of liquid conducting masses charged with electricity. (1882).

122. Melcher, J. R. & Taylor, G. I. Electrohydrodynamics: A Review of the Role of Interfacial Shear Stresses. *Annu. Rev. Fluid Mech.* **1,** 111–146 (1969).

123. Taylor, G. Electrically Driven Jets. *Proc. R. Soc. A Math. Phys. Eng. Sci.* **313,** 453–475 (1969).

124. Yarin, A. L. & Reneker, D. H. Taylor Cone and Jetting from Liquid Droplets in Electrospinning of Nanofibers. (2001).

125. Taylor, G. Disintegration of Water Drops in an Electric Field. *Proc. R. Soc. A Math. Phys. Eng. Sci.* **280,** 383–397 (1964).

126. Reneker, D. H. & Yarin, A. L. Electrospinning jets and polymer nanofibers. **49,** 2387–2425 (2008).

127. Rosenkilde, C. E. A Dielectric Fluid Drop an Electric Field. *Proc. R. Soc. A Math. Phys. Eng. Sci.* **312,** 473–494 (1969).

128. Miksis, M. J. Shape of a drop in an electric field. *Phys. Fluids* **24,** 1967 (1981).

129. Bateni, a *et al.* Effect of electric fields on contact angle and surface tension of drops. *J. Colloid Interface Sci.* **283,** 215–22 (2005).

130. Bateni, a., Amirfazli, a. & Neumann, a. W. Effects of an electric field on the surface tension of conducting drops. *Colloids Surfaces A Physicochem. Eng. Asp.* **289,** 25–38 (2006).

131. Roux, J. M. & Achard, J. L. Forces and charges on a slightly deformed droplet in the DC field of a plate condenser. *J. Electrostat.* **67,** 789–798 (2009).

132. Roux, J. M., Achard, J. L. & Fouillet, Y. Forces and charges on an undeformable droplet in the DC field of a plate condenser. *J. Electrostat.* **66,** 283–293 (2008).

133. Roero, C. Contact angle measurements of sessile drops deformed by a DC electric field.

134. Bateni, A., Amirfazli, A. & Neumann, A. W. Effects of an electric field on the surface tension of conducting drops. *Colloids Surfaces A Physicochem. Eng. Asp.* **289,** 25–38 (2006).

135. Ould Ahmedou, S. A., Rouaud, O. & Havet, M. Assessment of the Electrohydrodynamic Drying Process. *Food Bioprocess Technol.* **2,** 240–247 (2008).

136. Liu, Y. *et al.* Manipulation of nanoparticles and biomolecules by electric field and surface tension. *Comput. Methods Appl. Mech. Eng.* **197,** 2156–2172 (2008).

137. Takano, K., Tanasawa, I. & Nishio, S. Active enhancement of evaporation of a liquid drop on a hot solid surface using a static electric field. *Int. J. Heat Mass Transf.* **37,** 65–71 (1994).

138. Takano, K., Tanasawa, I. & Nishio, S. Enhancement of Evaporation of a Liquid Droplet using EHD Effect: Criteria for Instability of Gas-Liquid Interface Under Electric Field. *J. Enhanc. Heat Transf.* **3,** 73–81 (1996).

139. Garg, K. & Bowlin, G. L. Electrospinning jets and nanofibrous structures. *Biomicrofluidics* **5,** 13403 (2011).

140. Matthews, J. A., Wnek, G. E., Simpson, D. G. & Bowlin, G. L. Electrospinning of collagen nanofibers. *Biomacromolecules* **3,** 232–8

141. Leach, M. K., Feng, Z.-Q., Tuck, S. J. & Corey, J. M. Electrospinning fundamentals: optimizing solution and apparatus parameters. *J. Vis. Exp.* (2011). doi:10.3791/2494

142. Tan, Z. Partial Reflection of Hyaluronan Molecules Inside the Taylor-cone During Electrospray. *Engineering* **04,** 84–87 (2012).

143. Vasiljevich, I. Design and Development of a Micro - Field Emission Electric Propulsion Thruster. (2005).

144. Dehaeck, S., Rednikov, A. & Colinet, P. Vapor-based interferometric measurement of local evaporation rate and interfacial temperature of evaporating droplets. *Langmuir* **30,** 2002–8 (2014).

145. Theisen, J. & Davoust, L. Dual-frequency electrowetting : application to drop evaporation gauging within a digital microsystem . 1–23 (2011).

146. Theisen, J. & Davoust, L. Joint use of electrowetting and interferometry to measure evaporation rate in a. 9–12 (2012).

147. Gdeisat, M. A. *et al.* Spatial and temporal carrier fringe pattern demodulation using the one-dimensional continuous wavelet transform: Recent progress, challenges, and suggested developments. *Opt. Lasers Eng.* **47,** 1348–1361 (2009).

148. Zhong, J. & Weng, J. Spatial Carrier-Fringe Pattern Analysis by Means of Wavelet Transform: Wavelet Transform Profilometry. *Appl. Opt.* **43,** 4993 (2004).

149. Zaid, A. & Abid, A. Fringe Pattern Analysis using Wavelet Transforms Holy Quran Prophet Teachings. (2008).

150. Herráez, M. A., Burton, D. R., Lalor, M. J. & Gdeisat, M. A. Fast two-dimensional phase-unwrapping algorithm based on sorting by reliability following a noncontinuous path. *Appl. Opt.* **41,** 7437 (2002).

151. Dehaeck, S., Tsoumpas, Y. & Colinet, P. Analyzing closed-fringe images using two-dimensional Fan wavelets. *Appl. Opt.* **54,** 2939–52 (2015).

152. Renaudot, R. *et al.* Optimization of Liquid dielectrophoresis (LDEP) Digital Microfluidic Transduction for Biomedical Applications. *Micromachines* **2,** 258–273 (2011).

153. Pierobon, M. Theoretical and Experimental Study of an Electrospray: Corona Discharge Influence.